TOWARDS EFFICACIOUS MANAGEMENT OF MICROBIAL INFECTIONS

by

Caroline Wairimu Karanja

A Dissertation

Submitted to the Faculty of Purdue University

In Partial Fulfillment of the Requirements for the degree of

Doctor of Philosophy

Department of Chemistry

West Lafayette, Indiana

December 2020

THE PURDUE UNIVERSITY GRADUATE SCHOOL

STATEMENT OF COMMITTEE APPROVAL

Dr. Herman O. Sintim, Chair

Department of Chemistry

Dr. Ji-Xin Cheng, Co-chair

Department of Biomedical Engineering (Boston University)

Dr. Hilkka I. Kenttamaa

Department of Chemistry

Dr. Stephen Robert Byrn

Department of Industrial and Physical Pharmacy

Approved by:

Dr. Christine Hrycyna

I dedicated this work to God, my family (My father the late Benard Karanja, my dearest mother Nancy Karanja, my beloved siblings (Lillian Gitiba, Timothy Karanja, Anne Karanja, and Antony Karanja), my nephews (Leslie Karanja, and Ryan Kirika), my nieces (Kimberly Nyambura and Eden Wambui), my uncle Ben Mwangi and my Godmother Margaret Wairimu) and my dear friends (Donald Mitchel, Francis Addeah Darko, Dee Bernhardt, and the Very Reverend Theodore C. Dudzinski).

Thank you! I had the best team to cheer me on!

ACKNOWLEDGMENTS

I extend my sincere gratitude towards all personages who helped in this endeavor. Without their help, and guidance my efforts towards my studies would have been in vain.

Firstly, I would like to express my gratitude to the department of Chemistry for affording me an opportunity to do my doctoral studies at such a prestigious institution.

Prof. Ji-Xin Cheng, thank you for taking me on as your student despite my lack of background in optics. I am grateful for your patience and guidance.

Prof. Herman O. Sintim, thank you for allowing me to finish my studies in your group. By doing so, you helped me balance my familial obligations and my studies. My family and I are extremely grateful. Above all, thank you for your patience and guidance.

To the rest of my committee members Prof. Hilkka I. Kenttamaa and Prof. Stephen Robert Byrn, thank you for agreeing to be part of my journey. Thank you for always having time for me whenever I needed your help.

I would also like to express my gratitude to Professor Mohamed Seleem and Dr. Uma K. Aryal. Thank you for your time and guidance. The numerous consultations I had with you were indispensable for my research.

Dr. Weili Hong, thank you for mentoring me during my time in Prof. Ji-Xin's group.

Dr. Nimishetti Naganna, thank you for synthesizing the isoquinoline molecules for me.

TABLE OF CONTENTS

LIST OF TABLES

LIST OF FIGURES

ABSTRACT

Before the 20th century infectious ailments were a central basis for morbidity and mortality globally. The introduction of effective antimicrobial agents in the mid-20th century was a turning point in medicine. Fatal diseases such as bacterial meningitis became curable, morbidity and mortality rates associated with infectious diseases reduced and surgical procedures became safer. The success of these new antimicrobial agents led many to believe problems of dealing with infectious diseases could be eradicated. This confidence soon waned due to the upsurge of drug-resistance strains. Today, rapid emergence of drug-resistance and slow introduction of new therapies are some of the contributing factors to high morbidity and mortality rates associated with infectious diseases. Consequently, to efficaciously manage drug-resistance infections, we must exercise stewardship over available resources and promote development of new antimicrobials.

To aid in antimicrobial stewardship we sought to develop a rapid azole susceptibility testing technology for *Candida albicans*. *Candida albicans* is a prevalent cause of fungal blood stream infections associated with high mortality rates. Timely administration of the appropriate antifungal is correlated positive patient's outcome. However, timely administration is hindered by the sluggish turnovers of traditional susceptibility testing methods which take up to 72 hours. Herein, we demonstrate glucose metabolic profiling can be used as a rapid readout of fluconazole susceptibility. By probing the *de novo* lipogenesis, we could discriminate between a fluconazole-susceptible and fluconazole-resistant *Candida albicans* strain within 5 hours.

To promote development of new antimicrobial agents we conducted phenotypic screens and targeted screens in efforts to identify new chemical structures with antibacterial or antivirulence properties. From the phenotypic screen we identified alkynyl isoquinoline as Gram-positive specific antibacterial agents. In our targeted screen we identified an inhibitor of *Mycobacterium tuberculosis* phosphodiesterase (CdnP). CdnP facilitate immune evasion, hence we envision CdnP inhibitors could be developed into antivirulence agents. Lastly, to promote development of new antimicrobial agents we developed a facile technique for identifying inhibitors of cyclic dinucleotide (CDNs) metabolizing enzymes. Due the vital role of CDNs in bacterial physiology, CDNs metabolizing enzymes have been proposed as ideal target for development of new antimicrobial agents.

CHAPTER 1. INTRODUCTION

1.1 Microbial Infections

A microbial infection is the colonization of host (a living organism that harbors the microbe) by microbial agents. Microbes use the host's resources to support self-replication, which often leads to disease formation. The principle that microbes can cause diseases is referred to as the germ theory. Prior to the germ theory, miasmatic theory of disease causation was widely accepted. Miasmatic theory postulated miasmas (poisonous vapors produced by putrefying organic matter) invasion of the body lead to disease formation.[1] Germ theory started gaining gradual acceptance in Europe in the middle of the 19th century.[2] Louis Pasteur and Robert Koch scientific proofs of the germ theory propelled the acceptance .Louis Pasteur was the first to discover microbes were responsible for the putrefaction.[3,4] Robert Koch provided the first scientific proof of a link between a specific microbe and a disease.[5,6] Using a microscope, Koch observed rod-shaped structures in the blood of a cow that had died from anthrax. Koch inoculated mice with the blood of the anthrax-ridden cows and by the following day the mice had died. While conducting autopsy, Koch found the same rod-shaped structures in the spleen, blood and lymph nodes of the dead mice. Pasteur's other significant contribution to germ theory is the linkage of microorganisms as causative agent of silk worm diseases that were devastating the textile industry.[4] Two mysterious diseases (*pébrine and flacherie)* were affecting silk worms. Pasteur was able to prove two different microbes were responsible for the diseases, *pébrine* caused by a protozoa and *flacherie* by a bacteria. By selecting non-infected eggs with the aid of a microscope the diseases were contained. Today germ theory is globally accepted.

Microbes which cause diseases are referred to as pathogens. Diseases caused by pathogens are referred to as infectious diseases because they can be transmitted to other individuals. Pathogens are diverse consisting of viruses, prokaryotes, and eukaryotes. Pathogens are divided into two categories: facultative and obligate.[7] Facultative pathogens are microbes which have more than one replication niche, such microbes can colonize both environmental reservoirs and hosts. Obligate pathogens on the other hand, require a host to replicate. All viruses are obligate pathogens.

Bacterial and eukaryotic pathogens are mostly facultative pathogens with a few exceptions such as *mycobacterium tuberculosis* and *Plasmodium falciparum* which are obligate pathogens.

Table 1.1: List of some of infectious disease epidemics and pandemics that have devastated humanity throughout history. Smallpox is caused by the Variola virus. Yersinia pestis bacterium is the causative agent for bubonic plagues. Vibrio cholerae bacterium is responsible for cholera. Spanish flu was caused by the H1N1 influenza virus.

430 BC	541 AD	1347 AD	1519 AD	1817 AD	1855 AD	1918 AD	1981 AD
• Small pox • 30,000 deaths • Greece	• Justinian's Plague • First Bubonic pandemic • Byzantine Empire • Tens of Million deaths	• Black death • First Bubonic pandemic • Europe and Asia • Tens of Million deaths	• Small pox • Aztec Empire Mexico • 5-8 Million deaths	• 6th Cholera pandemic • World wide • >800,000 deaths	• Third Bubonic Pandemic • Asia, Europe, Africa, and Americas • Tens of Millions deaths	• Spanish Flu • World wide • > 50 Million deaths	• HIV • World wide • >35 Million deaths

Infectious diseases are detrimental and sometimes fatal to the host. In fact, for centuries infectious diseases have been a leading cause of death. Throughout history there have been outbreaks of infectious diseases epidemics and pandemics which have claimed millions of lives (Table 1.1).[8-12] Despite the global advance in medicine, microbial infections are still associated with high mortality rates, causing millions deaths every year.[13,14] This mainly due to poverty, emergence of novel unrecognized microbial infections, and re-emergence of recognized microbial infections. A 2016 study reported more than half of the deaths in low income countries were caused by group 1 conditions which include communicable diseases, maternal, prenatal, and nutritional conditions. [13] By contrast, in high income countries only less than 7% of the deaths were a result of group 1 conditions. This dissimilarity can be attributed to the increased exposure to risk factors (unsafe sex, poor hygiene, poor sanitation and unsafe water) and sporadic supply of drugs in low income countries.[15,16]

More than 40 new pathogens have been identified in the last the last 50 years.[17-26] A subset of these new pathogens is listed in Table 1.2. Diseases caused by newly identified pathogens are referred to as emerging diseases. Some of these diseases have been devastating to humankind. For instance, HIV pandemic which is still ongoing has killed more than 35 million people since 1980s. Nearly all of the new pathogens are of zoonotic origin. In fact, the Center for disease control and

prevention (CDC) approximates about 75% (three out of four) of emerging infectious diseases comes from animals.[27]

Table 1.2: A subset of infectious diseases and causative pathogens that have emerged in the last 50 years.

Pathogen	Disease	First identified in humans
Monkey pox virus	Monkey pox	1970
Rotavirus	Infantile Gastroenteritis	1973
Ebola Virus	Ebola	1976
Legionella pneumophila	Legionnaires	1977
Cryptosporidium sp	Cryptosporidiosis	1978
Human T-lymphotropic virus type 1 (HTLV-1)	T-cell lymphoma-leukemia	1980
HIV virus	AIDS	1983
Hepatitis C virus	Hepatitis	1989
Vibrio Cholera 0139	Cholera	1992
Sin Nombre virus	Hantavirus pulmonary syndrome	1993
H5N1 strain of avian influenza	Influenza	1997
SARS coronavirus	Severe acute respiratory syndrome (SARS)	2003
Covid-19 virus	Coronavirus disease	2019

Re-emerging microbial infections (infectious ailments which were once associated with high morbidity and mortality rates globally or in a specific region, and then declined, but are now becoming a significant cause of morbidity and mortality[28]) have also contributed significantly to the current infectious disease global burden. Some of the factors that lead to the re-emergence of an infectious ailments include emergence of antimicrobial-resistant strains, lack of immunization, ecological changes and international travel. Emergence of drug-resistant strains particularly pose a considerable threat worldwide. The World Health Organization (WHO) has raised an alarm over the increasing number of antimicrobial-resistant infections globally. Antimicrobial-resistant infectious ailments are associated with higher morbidity, death rates, and hospital expenditures compared to microbial infections caused by drug-suspectable strains. If no action is taken to curb the rise of antimicrobial resistance, common infectious diseases which are easily eradicated can turn into devastating infections. The 2014 review on antimicrobial resistance estimates annually

at least 700,000 deaths are caused by drug-resistant microbial diseases, and projects the number escalate to 10 million by 2050 if the present trend is left unchecked.[29,30] The United Nations also warns drug-resistance microbes threatens the accomplishment of the Sustainable Development Goals .[31] Sustainable Development Goals (SDGs) are blueprints adapted by the United Nations members to ensure prosperity of people and the planet. Ensuring good health for all citizens is one of the key points of SDGs.

1.2 History of antimicrobials and emergence of drug resistance

An antimicrobial is an agent that kills or stop the growth of a microbial. Antimicrobials are either extracted from nature or synthesized. Archeological evidence show human exposure to antimicrobial dates back to 350 AD.[32-34] In 1980, traces of tetracycline were detected in the bones of a Sudanese Nubian dated between AD 350 and 500. However, the widespread use of antimicrobials for management of infectious diseases did not start until the 20th century.[34,35] Prior to the widespread use of antimicrobials, the global average life expectancy was around 47 years.[36,37] Until the 20th century, diseases such as: leprosy, cholera, typhoid fever, yellow fever, and smallpox were rampant and usually they were accompanied by high mortality rates.[37,38] The widespread use of antimicrobials drastically transformed treatment of infectious diseases worldwide, culminating in increased life expectancy.[35,39] For example, the united states life expectancy increased from 47 years at the beginning of the 20th century to 77 years by the end of the century.[36] Not surprising the primary cause of mortality changed from infectious diseases to non-communicable diseases in most industrialized countries. In 1900, the three leading causes of death in the US were pneumonia, tuberculosis, and diphtheria, however by 1997 heart disease and cancer accounted for more than 50% of all deaths.[40] These successes cannot be attributed to antimicrobials alone, other factors like better hygiene and safer water also contributed to the decline of infectious diseases. The huge achievements in management of infectious diseases nurtured confidence in many that infectious diseases could be eradicated. For example, in 1962 Sir McFarland Burnett (an Australian virologist and 1960 Nobel laureate) said: “By the end of the Second World War it was possible to say that almost all of the major practical problems of dealing with infectious disease had been solved.”[38] Time would later prove this confidence to be erroneous.

Antimicrobials used to treat bacterial infections are referred to antibiotics or antibacterial agents. Antimicrobials used for fungal infections are referred to as antifungals. Agents used to treat

viral infections are referred to as antivirals and antiprotozoal are drugs used to treat protozoan infections. The scope of this work covers antibacterial and antifungal agents consequently, only these two classes of antimicrobials will be discussed further.

1.3 History of Antibiotics and Antibacterial agents development

The words Antibiotic and antibacterial agents are used interchangeably today in reference to agents that kill or stop growth of bacteria. However, the true definitions are as follows. Antibiotic is agent produced by another microorganism that kills or stop the growth of bacteria. While an antibacterial is an agent that kills or stop the growth of bacteria that is synthetic, semi-synthetic, derived from plants or animals.

Pyocyanese was the first antibiotic to be used to treat human infections. Blue pigmented substance from *Bacillus pycyaneus*, (today known as *Pseudomonas aeruginosa)* was observed to inhibit growth of other pathogenic bacteria.[34,41] Rudolf Emmerich and Oscar Löw in 1889 grew *Bacillus pycyaneus* in batches and used the supernantant (Pyocynase) to treat infections, the results were inconsistent leading to the abandonment of Pyocyanese.

Paul Ehrlich and Sir. Alexander Fleming are considered the fathers of the modern antibiotic era. Paul Ehrlich based on his observation aniline dyes stained only the bacteria which they exterminated formulated the concept of '*magische Kugel' (*magic bullets).[34,42,43] Dr. Ehrlich defined magic bullet as a compound that act only on the cells that absorbs it. In regards to infectious diseases treatment, a magic bullet is a compound that kills the disease causing pathogen without affecting the host cells. Dr. Ehrlich started screening for a magic bullet for treatment of syphilis. By this time atoxyl, an arsenical, has been reported to have activity against trypanosomes.[44] At that time spirochaete, the causative agent of syphilis, was not recognized to be a bacterium because of its corkscrew appearance under the microscope and was classified in the same group as trypanosome, a protozoa.[45] Dr. Ehrlich in collaboration with Alfred Bertheim (chemist) and Sahachiro Hata (bacteriologist) synthesized hundreds of organoarsenic derivatives and tested their potency in treating syphilis infected rabbits. By the end of 1909, they came across compound 606 which successful cured syphilis infected rabbits and was shown in clinical trials to be effective in treating syphilis patients. The drug was marketed as *Salvarsan*, and together with its derivative *Neosalvarsan* which was more soluble and less toxic than *Salvarsan* were used for syphilis treatment until they were replaced by Sir. Alexander Fleming's penicillin in 1945.[34]

Perhaps the most famous account of discovery of antimicrobials is Sir. Alexander Fleming's discovery of penicillin in 1928. A lucky break that transformed medicine. Fleming in his own words said, "*When I woke up just after dawn on September 28, 1928, I certainly didn't plan to revolutionize all medicine by discovering the world's first antibiotic, or bacteria killer. But I suppose that was exactly what I did*."[46] Fleming was sorting petri dishes after returning from a holiday when he came across a dish that was contaminated with mold.[47,48] The peculiar thing about this dish was it was dotted with bacteria colonies everywhere expect the area around the mold. Fleming postulated the mold was secreting a diffusible substance that was inhibiting bacteria growth. The mold belonged to penicillium genus. He isolated the fungus and upon further investigations, Fleming discovered the mold juice had antibiotic activity against a wide range of bacteria. Isolation of the mold juice active ingredient, penicillin, proved to be a difficult task hindering the use of penicillin as a chemotherapy for bacterial infections. For over a decade there was no progress in isolation of penicillin. Fate of penicillin was change in 1939 by a team at Oxford University. After coming across Fleming article on penicillin, Ernst Chain proposed to his supervisor Howard Florey he should try to isolate penicillin. By 1940 Florey and team had developed a method for purification of penicillin, and demonstrated the purified substance was effective against bacteria *in vitro* as well as *in vivo.*[49] In 1945 penicillin was introduced for mass use as a chemotherapy.

In 1932 a German pathologist Gerhard Domagk discovered Prontosil, an orange-red azo dye, despite lacking *in vitro* activity against bacteria portrayed *in vivo* efficacy in both animals and patients.[47,50] The prontosil paradox (lack of activity *in vitro*) was solved in 1935 when Daniele Bovet of the Pasteur Institute discovered prontosil was in fact a prodrug with sulfanilamide being the active moiety.[51] This unearthing led to the production of sulfanilamide and derivatives as chemotherapies for bacterial infections.

The discovery of Salvarsan, Prontosil and Penicillin paved way for the innovation of other antibiotic and antibacterial agents. From 1950 to 1970 there was a rapid introduction of novel antibacterial agents, seven novel classes antibacterial are introduced in this period.[34,52] This rapid advancement in antibacterial discovery led to widespread confidence bacterial infections would be eradicated.[53,54] This confidence was soon diminished by the emergence of drug resistant bacteria.

1.4 Bacteria drug-resistance

Bacteria is said to be drug-resistant when an antimicrobial agent that were once effective against the bacteria can no longer kill or halt the growth of the bacteria. Bacteria deploy different mechanisms to establish drug resistance. Some fundamental mechanisms include modifications of the antimicrobial molecule to make it ineffective, prevention of the antimicrobial from reaching the target by decreasing influx or by increasing efflux of the antimicrobial compound , mutation of antimicrobial target site and bypassing of targeted enzymes in biological processes.[55] Drug-resistance to some the antimicrobials emerged only a few years after the initial discovery. By 1960s, it was reported more than 80% of isolated staphylococcal strains were resistant to penicillin.[56] However, development and discovery of new classes of antibiotics and antibacterial agents waned the concern. In fact in 1962 Dr. Burnet (1960 Nobel prize laureate) wrote one of his famous quote: "One can think of the middle of the twentieth century as the end of one of the most important social revolutions in history, the virtual elimination of the infectious diseases as a significant factor in social life".[57,58] Yet, by 1965 there was a concern about the rise of antibiotic resistance. A group of international infectious disease experts and microbiologists met to discuss if new antibiotics were needed to deal the growing emergence of drug-resistant isolates.[59] Once again new antimicrobials were introduced which reestablished the confidence about the conquest of bacterial infections. In 1978 Robert G. Petersdorf, an infectious disease expert at the time, stated: "Even with my great personal loyalty to Infectious Disease, I cannot conceive the need for 309 more infectious disease experts unless they spend their time culturing each other".[60] Surely Robert G. Petersdorf could not have made such remark if there was a way he could have predicted the pandemics we are facing today and the widespread emergence of multidrug resistant infections. For most of us it is becoming more apparent there is no endgame with infectious diseases.

The rapid emergence of drug resistant bacterial infections poses a substantial threat to public health. The CDC approximates at least 2 million people in the US alone get infected by antibiotic resistance bacteria culminating with 23, 000 deaths annually.[61] The concern is escalated by the emergence of superbugs. Superbugs are bacterial strains that are resistant to all available antimicrobial agents. In 2016 a woman from Nevada died from an infection caused by a *Klebsiella pneumoniae* strain that was resistant to all antimicrobials available in the US.[62]

The unfortunate truth about antibiotics and antibacterial agents is that, eventually with extensive use resistant phenotypes will emerge. Which means we must continually discover new

agents to keep up with resistance evolution. An alternative approach is development of antivirulence therapies that instead of killing the bacteria, they inhibit their ability to form an infection.[63,64] Agents not detrimental to growth presents less selective pressure for generation of resistant phenotypes hence, 'true antivirulence agents' (agents that diminish bacteria pathogenicity with no effect on growth) would be less prone to development of resistance.

1.5 Novel signaling pathways mediated by cyclic dinucleotides presents new opportunities for novel antimicrobial and antivirulence agents

Cyclic dinucleotides (see Figure 1.1 for structures) are secondary messengers that play vital roles in both bacterial and mammalian cells.[65,66] Both bacterial and mammalian cyclic dinucleotide acts as pathogen-associated molecular patterns, which upon recognition by germline encoded pattern recognition receptors a signaling cascade is triggered that induce an immune response. In mammalian cells, the presence of dsDNA in the cytosol leads to the production of a noncanonical 2'3- cyclic guanosine monophosphate–adenosine monophosphate (2'3- cGAMP).[67] 2'3 -cGAMP then binds to stimulator of IFN genes (STING) to induce interferon response. Bacterial cyclic dinucleotides released in the cytosol also induce interferon response. In fact, several pathogenic bacteria including: *Listeria monocytogenes*, group B *streptococcus spp, chlamydia spp*, and *Mycobacterium tuberculosis (M. tuberculosis)* have been reported to use cyclic dinucleotides to mediate interferons production.[68-71] C-di-AMP also binds to RECON (reductase controlling NF-κB) and ERAdP (ER adaptor), resulting in production of pro-inflammatory cytokines.[72-75] *Mycobacterium tuberculosis* and group B *streptococcus spp* are reported to degrade c-di-AMP as an immune evasion strategy.[76,77]

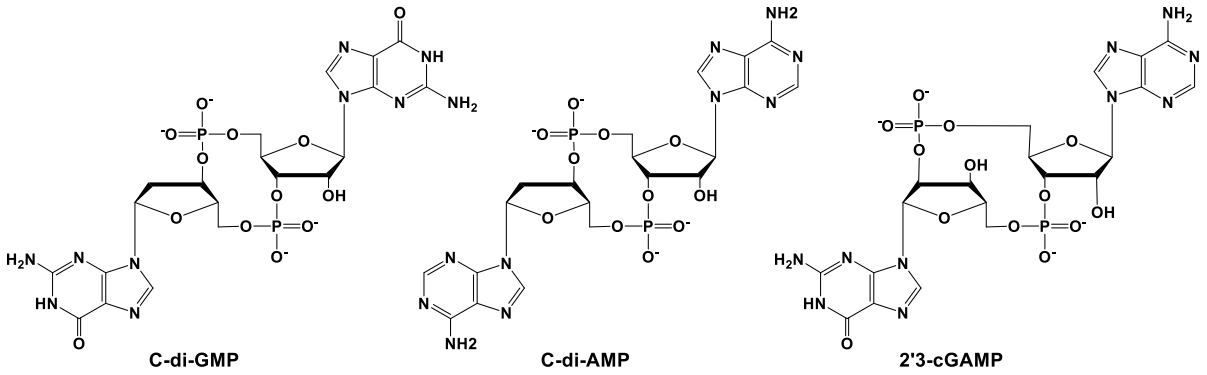

Figure 1.1: Structures of bacterial cyclic dinucleotides (c-di-GMP and c-di-AMP) and mammalian cyclic dinucleotide (2'3-cGAMP).

Cyclic dinucleotides also play pivotal roles in bacteria physiology. C-di-GMP is synthesized mainly by Gram-negative bacteria including *Pseudomonas aeruginosa, Salmonella typhimurium, Escherichia coli, Vibrio cholerae* and *Caulobacter crescentus.*[66] C-di-AMP in contrast is produced mainly by Gram-positive including *Staphylococcus aureus, Streptococcus pneumoniae, Streptococcus pyogenes* and *L. monocytogenes.*[78] C-di-GMP coordinates motility to sessility transition. In some bacteria species, increased levels of c-di-GMP in the cell correlates with sessile lifestyle whereas low c-di-GMP cellular levels correlates with planktonic lifestyle.[79] C-di-AMP is implicated in several physiological processes including cell wall and membrane homeostasis, DNA damage repair, biofilm formation, regulation of potassium ion channels, virulence and sporulation.[78,80,81] C-di-AMP homeostasis is indispensable for growth in a number of bacteria including *S. aureus, L. monocytogenes,* and *B. subtilis.*[82-84]

Due the vital roles played by bacterial cyclic dinucleotides (CDN), bacterial CDN metabolizing enzymes have been targeted for development of new antimicrobial and antivirulence agents. Several c-di-GMP synthesis inhibitors associated with reduced biofilm formation phenotype have been identified.[85,86,87] A specific *Pseudomonas aeruginosa* c-di-GMP phosphodiesterase (RocR) inhibitor was reported to inhibit swarming.[88] Several c-di-AMP synthesis inhibitors have been reported as well.[89-91] Opoku-Temeng and colleagues reported a benzylidene-indolinone derivative as c-di-AMP synthesis inhibitor that has Gram-positive antibacterial activity, reduce biofilm formation and re-sensitize methicillin-resistant *S. aureus* and vancomycin-resistant *enterococci faecalis* to methicillin and vancomycin respectively.[92] Dey and colleagues demontrated inhibition of *mycobacterium tuberculosis* c-di-AMP phosphodiesterase (CdnP) with 5'-phosphadenylyl-adenosine (pApA) analogs significantly boost IRF induction.[76]

1.6 History of antifungal development

Globally It is estimated more than 1.5 million people die annually from IFIs, with *Cryptococcus, Candida, Aspergillus,* and *Pneumocystis* being responsible for more than 90% of these deaths.[93] In fact, Invasive candidiasis is top five on the list of the most common blood stream infections in the US.[94] The nature of the microorganism has contributed to the slow development of antifungal. Fungi is a eukaryotic organism hence, the similarity with the host cells make discovery of 'magic bullets' targeting the pathogen alone a bit more challenging. Also, a lesser market for antifungal agents also attributes to the lack interest in mycosis research. In general,

there are few cases of life-threatening fungal infections compared to other pathogens. Below is a summary of discovery and development of antifungal agents for IFIs management.

At the beginning of the 20th century compounds with nonspecific mode of action, and with low potency such as saturated potassium iodide, were used to treat superficial fungal infections. The first antifungal nystatin was introduced in the 1951, which coincided with the "golden era" of antibiotics discovery.[94] Nystatin a natural product produced by *Streptomyces noursei* and *Streptococcus abbidus* has a broad spectrum activity against but its low solubility and toxicity limited it use in systemic infections.[95,96] Discovery of nystatin prompted further screening of *Streptomycete* cultures for antifungal activity. In 1953 amphotericin B a polyene just as nystatin was discovered. Characterization of amphotericin B showed it was very similar to nystatin. However, amphotericin B had more inhibitory activity than pure nystatin in *in vitro* assays. There was an uproar of excitement about amphotericin B after experimental studies showed orally administered amphotericin B was effective in treating mice with fungal infections. Amphotericin B became the first significantly effective agent for management of systemic mycoses. However, amphotericin B is far-off from the desired 'magic bullet' for mycoses. Like nystatin it is associated with high toxicity and low solubility.

Search for safer antifungal continued. In 1964 5-flucytosine was introduced as oral agent for the treatment of candidosis and cryptococcosis.[97,98] However, the rapid emergence of resistance limited its use as a monotherapy. In 1981 ketoconazole was introduced as an oral agent for treatment of systemic infections.[99,100] Ketoconazole was the only orally agent available for treatment of systemic mycoses for over a decade. The introduction of the triazoles compounds (fluconazole and itraconazole) in the 1990s presented another major advancement for systemic mycoses.[101] Both fluconazole and itraconazole have a broader activity spectrum and safer compared to ketoconazole. Itraconazole has a broader spectrum compared to fluconazole however, the later has more favorable pharmacokinetics and toxicity profile. The newest class of antifungals the echinocandins, were introduced at the beginning of the 21st century.[102] Echinocandins major advantages are their fungicidal activity and minimal toxicity. Azoles compounds and amphotericin B poses fungistatic activity. Echinocandins are limited by their low solubility, and requirement for intravenous administration. All the antifungal agents mentioned here are still used in clinic today. The fact Amphotericin B is still considered a gold standard for various IFIs despite its toxicity portrays the limited options for treatment of IFIs.

1.7 Fungal drug-resistance

Fungi is said to be drug-resistant when an antifungal agent that were once effective against the fungi can no longer kill or stop the growth of the fungi. Just in the case of bacterial resistance, emergence of resistance poses a threat in the management of fungal infections. Even though isolation of drug-resistant strains is not as prevalent in fungal infections as in bacterial infections, the arsenal of antifungal agents is limited. Resistance to almost all clinical available antifungals have been documented. [103] Multidrug resistance is uncommon in medical mycology however, new fungal species that are resistant to multiple antifungals are emerging (*Candida glabrata* and *Candida auris*).[104,105] Fungi has a higher predisposition to develop resistance against azole compounds.[106] Echinocandins are normally used to treat azole-resistant fungal infections hence the emergence of Echinocandin-resistant strains is alarming.

Known fungal drug-resistance mechanisms correlate with bacterial drug-resistance mechanisms. Fungi has been shown to development resistance by modifying the target, altering the biosynthetic pathway to bypass the target, overexpressing the target or increased drug efflux. [107,108]. As aforementioned, bacteria are known to employ similar tactics.

1.8 Factors contributing to drug-resistance development

Antimicrobial resistance is a phenomenon which occurs naturally over time following exposure of microbes to antimicrobials. This fact is attested by the report of genes encoding resistance to antibiotics used in clinic today were found in an ancient DNA sample isolated from a 30,000 years old Beringian permafrost sediment,[109] an era thousands of years before the 'golden age of antibiotic'. Antimicrobial resistance is driven by selection pressure exacted by exposure to antimicrobials. Its factual microbe's development of drug-resistance is inevitable. However, human practices have accelerated the process.[110] As early as the onset of the golden era of antibiotics, scientists warned of the dare consequences of improper use of the wonder drugs. In 1945, Sir Alexander Fleming stated, "*Penicillin is to all intents and purposes non-poisonous so there is no need to worry about giving an overdose and poisoning the patient. There may be a danger, though, in under dosage. It is not difficult to make microbes resistant to penicillin in the laboratory by exposing them to concentrations not sufficient to kill them, and the same thing has occasionally happened in the body".*[111] Today antimicrobial resistance (AMR) is rampant. A

review on AMR published in 2014 estimates at least 700,000 deaths occur annually worldwide as a result of drug-resistant infections, and projects the number could escalate to 10 million by 2050 if the current trend is left unchecked.[29,30] Factors that have been associated with the global rise of AMR include misuse or overuse of antimicrobials in humans, misuse or overuse of antimicrobials in agriculture, environmental contamination, healthcare transmission, lack of rapid diagnostics, sub-optimal dosing, and travel. [110,112,113]

Globally, antibiotics are heavily over-prescribed. In several regions of the world, antibiotics are obtainable over the counter without a doctor's prescription. This lack of regulation promotes overuse and misuse of the drugs. Another common example of misuse of antimicrobials in humans is the use of wrong antimicrobial agent following a misdiagnosis (there are numerous cases where antibacterial agents have been used to treat viral infections often following a misdiagnosis). Overuse and misuse increase the selection pressure for AMR development. Misuse of antimicrobial agents in agriculture is marked by the extensive usage of antibiotics to promote growth and prevent infections. The antimicrobials and or drug-resistant microbes are then transferred to humans when we consume the agricultural products (crops or animals) contributing to the development of AMR infections.

The extensive use of antimicrobials in humans and agriculture has also contributed to the environment pollution with antimicrobials.[114] Antimicrobials of pharmaceutical origin are found in sewages, waste water treatment plants, groundwater, freshwater and marine environments. Presence of antimicrobials in the environment results in the increase of drug-resistance microbes in the environment. These drug-resistant microbes and the antimicrobial pollutants can then trace back to humans through consumption of agricultural products or drinking of untreated water facilitating the continual emergence of AMR infections.

Hospitals are said to be epicenters for AMR development.[115] In the hospitals particularly in the intensive care unit (ICU) pressure for selection and emergence of AMR is high due to the heavy use broad-spectrum antimicrobials. Multidrug-resistant bacteremia is very common in the ICU, with the incidence rate reported to be as high as 40% in many parts of the world. [115] The lack of rapid diagnostics contributes greatly to the misdiagnosis of causative pathogen and sub-optimal dosing. Upon admission broad-spectrum antimicrobials are administered as first line therapy till the causative pathogen is determined which usually take days. Studies have shown this practice results in 30%-60% rate of inappropriate or incorrect therapy administration. Which contributes to

the development of AMR and high mortality rates. Timely administration of the correct antimicrobial agent is correlated with positive clinical outcome.[116-118] Transmission from patients to patients also account for the higher incidence rate of AMR emergence in the intensive care unit. Patient to patient transmission is normally through the contaminated hands of hospital workers, contaminated medical apparatus.[119]

We live in an era the globe has become a village. People can travel with ease to any part of the globe. Globalization is to be lauded for the positive impact on world economy, intercultural exchange etcetera. However, globalization also contributes to the spread of drug-resistant microbes. Several studies have shown travelers have a higher incidence rate of colonization with drug-resistant bacteria than non-travelers.[120,121]

CHAPTER 2. INTRODUCTION TO RAMAN SPECTROSCOPY

2.1 Discovery of Raman Effect

Raman microscopy is based on to the inelastic scattering of light by molecules, a phenomenon commonly referred to as the Raman Effect. The Raman Effect was first described by Sir Chandrasekhara Venkata Raman (C. V. Raman, 1930 Nobel Laureate) in 1928.[122-124] C. V. Raman interest in light scattering was sparked by the curiosity to understand the origin of the deep blue color of the Mediterranean Sea. He was unsatisfied by the proposed notion that the color of the sea was due to the reflection of the sky. C. V. Raman successfully proved the color of the sea was a result of the light scattering by the water molecules. C. V. Raman henceforth, unrelenting studied light scattering phenomenon. In 1921 while investigating light scattering by transparent liquids, C. V. Raman and his colleague Mr Seshagiri Rao while studying light scattering by water molecules, observed the depolarization of the transversely scattered light increased drastically following the irradiation of water molecules with a violet beam.[123] Further investigations of the phenomenon revealed the depolarization of the scattered light was a result of the presence of a 'trace of fluorescence' in the scattered beam.[123] The measured depolarization depended on whether a blue filter was placed in the path of the incident beam or the scattered light. Depolarization was smaller when the filter was placed in the scattered light path. By 1924 only polar liquids were shown to exhibit the phenomenon.

Although the phenomenon was referred to as a 'feeble fluorescence' in publications, C. V. Raman believed it was a distinct new type of secondary radiation. However, the belief the phenomenon was only exhibited by some liquids and the conjecture the 'feeble fluorescence' was unpolarized as ordinary fluorescence suppressed the idea to publish the phenomenon as a new radiation. However, early 1928 C. V. Raman had a strong motivation to continue the research after he had a conviction the effect was an optical equivalent of the X-ray scattering described by Arthur H. Compton. Prof. Compton while studying x-ray scattering observed two kinds of scattered x-rays, unmodified and modified. The unmodified x-ray had the same wavelength as the incident beam while the unmodified had a longer wavelength. The latter is referred to as the Compton Effect. The first step C. V. Raman undertook was the reexamination of the universality of the phenomenon using a powerful beam. All the liquids (over 80 in number) examined exhibited the

effect. Further investigations proved the radiation was polarized differentiating it was distinct from fluorescence which is unpolarized.

The striking analogy to Compton Effect was observed in the line-spectrum of the detected light. The scattered light spectrum consisted of narrow wavelengths separated from the incident beam wide wavelengths by a dark space. These narrow wavelengths would disappear if a filter transmitting only the incident radiation was placed in the beam path. It was evident, each wavelength of the incident beam gives rise to two lines in the scattered spectrum, one unmodified and the other shifted to a longer wavelength. C. V. Raman offered partial absorption of the incident quantum of radiation by the molecule, followed by the scattering of the unabsorbed part as the probable origin of this new phenomenon. Accepting this notion meant molecules could also add quantum of their own frequencies to the incident radiation resulting modified scattering at shorter wavelength. The latter scenario was also observed in their experiments however, the former was more predominant.

2.2 Vibrational Raman Spectroscopy

As a result of inelastic scattering, molecules can experience either a vibration state shift, or a rotational state shift. Raman scattering where molecules experience a vibrational state shift is called vibrational Raman scattering. Herein two kinds of vibrational Raman techniques will be discussed, spontaneous Raman scattering and Stimulated Raman scattering.

Scattering that produces bands with the same frequency as the incident beam is referred to as Rayleigh scattering. As aforementioned light scattered via Raman Effect can have a frequency greater or smaller than the incident beam. Raman bands with frequencies smaller than the incident frequency are referred to as Stokes bands. While Anti-stokes bands refers to those bands with frequency greater than the incident beam. (Figure 2.1). The nomenclature is according to Stoke's law of fluorescence, which states the frequency of the emitted light is always smaller than that of the exciting beam. Light scattering is not a true electronic transition process, when a photon collides with a molecule it is elevated to a virtual energy state instead of a discrete state as in the case of absorption. In Stokes scattering, the molecule initial state is the ground state and after interacting with a photon it relaxes to an excited state. In Anti-Stokes scattering, initially the molecules are in the excited state, the scattering process relaxes the molecules to the ground state. Stokes scattering is stronger than Anti-Stokes scattering. This is expected as under thermal

equilibrium the occupation of the higher vibrational state will be lower compared to that of the ground state.

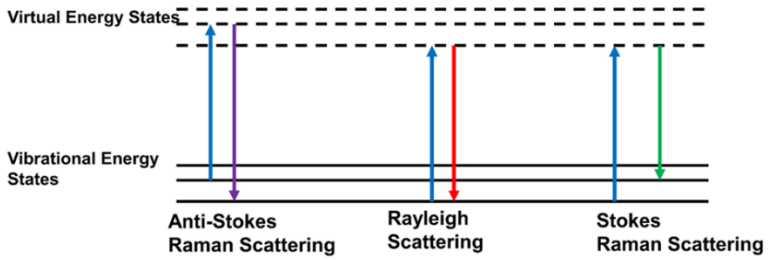

Figure 2.1: Energy level illustration of the different possibilities of light scattering. Upward arrows represent photon annihilation and downward arrows represents photon creation.

2.2.1 Spontaneous Raman Scattering

In Spontaneous Raman scattering, signal is generated just as described by C. V. Raman. Which involves exciting the sample with a laser and measuring the intensity of the inelastic scattered light (Figure. 2.2). Spectrum is obtained by plotting the intensity as a function of the Raman shift ($\Delta \tilde{V}$ R) defined as:

$$\Delta\tilde{V}R = \tilde{V}\,laser - \tilde{V}S \qquad \text{Equation 2.1}$$

Where $\tilde{V}_{laser}$ is the wave number of the laser beam, and $\tilde{V}_S$ the wavenumber of scattered light. Spontaneous Raman scattering is useful for label free analysis chemicals in biological samples.[125,126] However, the small cross-section associated with Raman scattering which results in low image contrast and slow acquisition speed limiting the use of Raman scattering in chemical mapping samples. Nonlinear Raman scattering techniques such as stimulated Raman scattering (SRS) significantly enhance the Raman signal culminating in faster imaging acquisition speeds.

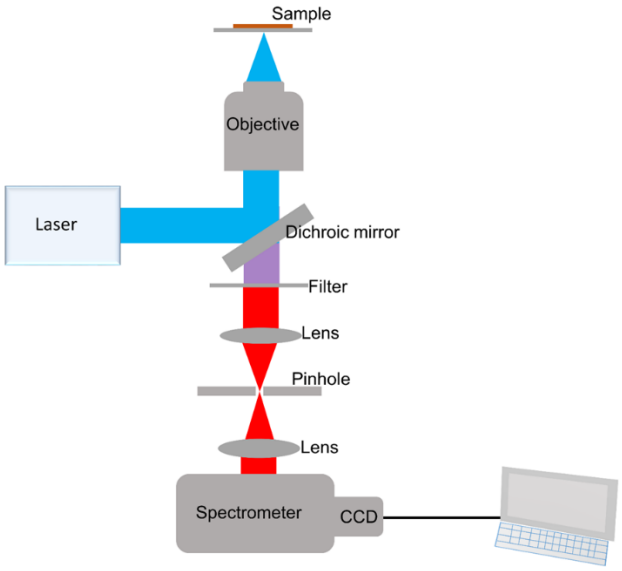

Figure 2.2 : Schematic illustration of Raman spectroscopy setup. CCD, charge-coupled device.

2.2.2 Nonlinear Raman scattering: Stimulated Raman Scattering (SRS)

Linearity of Raman signal is defined based on the dependence of the signal on the intensity of the incident radiation. Spontaneous Raman scattering is linear. SRS is an example of a nonlinear Raman process. For SRS process, the samples is excited with two laser beams (pump and probe). The energy difference for the two beams, $\Omega = \omega_{pump} - \omega_{probe}$, is matched to the energy gap of a vibrational transition.[127] As a result the rate of vibrational excitation is greatly enhanced compared to spontaneous Raman scattering. The excitation is accompanied by photons loss in the pump beam and photons gain in the probe beam (Figure 2.3). The loss of photons is referred to as stimulated Raman loss and the gain of photons is referred to as stimulated Raman gain.

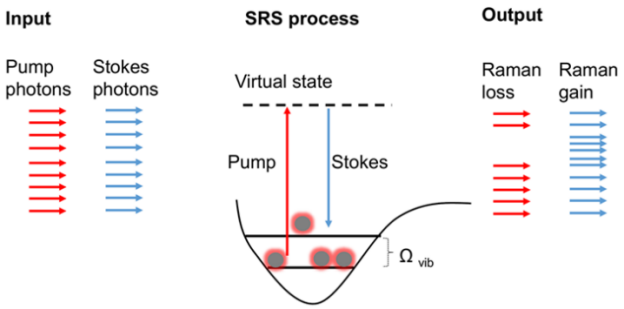

Figure 2.3: Stimulated Raman scattering (SRS) principle.

CHAPTER 3. STIMULATED RAMAN IMAGING REVEALS ABERRANT LIPOGENESIS AS A METABOLIC MARKER FOR AZOLE-RESISTANT *CANDIDA ALBICANS*

3.1 Introduction

Human fungal infections have been referred to as "hidden killers", as the impact of these diseases on human health is not highly appreciated.[93] Medical mycology research lags behind other pathogen research despite the high mortality rates associated with invasive fungal infections (IFIs)[93,128,129]. IFIs are responsible for over one and a half million deaths every year worldwide.[129] Over ninety percent of fungal-related deaths results from species that belong to the following genera: *Cryptococcus, Candida*, *Aspergillus*, and *Pneumocystis*.[93] *Candida* genus, most notably *Candida albicans* (*C. albicans*), is the fungi mostly associated with IFIs.[130-132] *C. albicans* is a benign member of the human microbiota. However, in severely immunocompromised individuals, *C. albicans* can cause blood stream infections (*Candidemia*), in time developing into disseminated invasive *Candidiasis* when the infections spread to other organs.[133,134] Unfortunately, life-saving practices such as: transplantation procedures, the use of indwelling devices, and prolonged intensive care stays have increased the occurrence of IFIs.[135] It is projected that the incidence of IFIs will continue to raise due to the prevalence of immunosuppressing diseases such as cancer, and human immunodeficiency virus (HIV).

Echinocandins and fluconazole are recommended as the first line therapy for IFIs.[136] Echinocandins targets the cell wall by inhibiting β-(1, 3)-glucan synthesis, a vital component of the cell wall. Fluconazole on the other hand affects fungal cell mem- brane integrity by inhibiting ergosterol biosynthesis, a major sterol component of the cell membrane. Fluconazole has several advantages over other antifungal drugs in terms of the cost, safety, oral bioavailability, and ability to cross the blood brain barrier.[137] Unfortunately, the widespread use of fluconazole has resulted in increased antifungal resistance to the drug among different fungal strains, especially *C. albicans.*[107,138] Establishment of resistance becomes a confounding factor that negatively impacts

patients' outcome. Determination of antifungal resistance is therefore crucial for guiding therapeutic decision making. Observational studies have described a correlation be- tween early administration of antifungal therapy and reduced mortality in critically ill patients with fungal infections.[117,118] However, antifungal susceptibility assessment by current gold standard methods is limited by slow turnaround time; usually twenty-four to forty-eight hours of incubation is required.[139] Rapid evaluation of drug susceptibility is therefore essential for facilitating early administration of appropriate antifungal.

Molecular techniques such as polymerase chain reaction (PCR) have the potential for rapid detection of certain resistance arising from genetic mutations.[138] These methods, though robust, are also technically demanding and cannot detect all resistant strains. On the other hand, metabolism is integral to pathogenicity. In fact, metabolic adaptation has been shown to affect antifungal susceptibility.[134,140] Eukaryotic pathogens such as *Candida* exhibit drug resistance by reducing intracellular concentration, drug inactivation, target modification, target overexpression, bypassing target pathway, or by sequestering the drug away from the target.[141] The cell needs energy to maintain these defense mechanisms. One way of attaining this energy is through metabolic regulation. Metabolic profiling has provided deep insight into abnormalities illness such as cancer.[142,143] Consequently, it is believed that metabolic profiles can distinguish between susceptible and resistant strains. The metabolomics field mainly relies on mass spectrometry methods to characterize metabolic profiles of biological samples owing to their high specificity and sensitivity.[144,145] A major limitation of mass spectrometry is sample preparation, where by the metabolites of interest have to be extracted from the tissue or cells.

Vibrational spectroscopy based on infrared absorption or Raman scattering offers an extraction-free analytical technique for metabolic profiling of biological samples.[146,147] Raman scattering is advantageous over infrared absorption in that it is free from water interference, making it ideal for biological samples. Raman microscopy does, however, has a major limitation; the Raman effect is extremely weak, which results in slow image acquisition speed. Fortunately, strong signals can be achieved with coherent Raman scattering modalities, which include co- herent anti-Stokes Raman scattering (CARS) and stimulated Raman scattering (SRS). CARS suffers from non-resonant background interference, complicating the signal recovery process.[148] On the other hand, SRS is non-resonant background free, which enables direct signal

interpretation.[127] Both CARS and SRS microscopy have the capability of mapping lipid droplets in yeasts[149,150] and human specimens. [151,152]

Here we demonstrate the ability of SRS microscopy to rapidly detect fluconazole susceptibility via live cell metabolic imaging. Our SRS imaging data revealed aberrant lipogenesis in fluconazole-resistant *C. albicans* strains. Furthermore, we found that exposure to fluconazole only attenuates lipogenesis in the susceptible strain. By direct imaging of lipogenesis activity, our method can discriminate the susceptible strain from the resistant strain within five hours, which is more than five-fold faster than the conventional methods that require up to forty- eight hours. These results collectively substantiate SRS microscopy as a feasible platform for rapid detection of antifungal susceptibility.

3.2 Experimental Section

3.2.1 Chemicals and Reagents

Yeast extract peptone dextrose (YPD), Yeast Nitrogen Base (YNB), Yeast extract, 2-deoxy-D-glucose (2-DG), Thiazolyl Blue Tetrazolium Blue (MTT), and Oleic acid-d34 were purchased from Sigma-Aldrich (St. Louis, MO, USA). Yeast extract peptone (YP) was prepared by adding twenty grams of bacteriological peptone (Becton Dixon. Franklin, NJ) and ten grams of yeast extract in one liter of distilled water. Glucose-d7, and 2-deoxy-2-[(7-nitro-2,1,3-benzoxadia-zol-4-yl) amino]-D-glucose (2NBDG) were purchased from Cayman Chemical (Ann Arbor, MI). Phosphate-buffered Sa- line (PBS), and fluconazole were purchased from ThermoFisher Scientific (Waltham, MA). Ultrapure Agarose purchased from Invitrogen (Carlsbad, CA).

3.2.2 *C. albicans* Culture

Cells were cultured at 37^{o}C in an incubating orbital shaker (VMR, model 3500I). *C. albicans* cells were grown overnight in YPD, pelleted, and washed three times with 1x PBS. Approximately, 1x 107 cells/ mL were resus- pended in fresh YPD, and grown to exponential phase (five- hour incubation). For glucose depletion study, cells in exponential phase were cultured in YPD and YP overnight. For glycolysis inhibition assay, cells in exponential phase were cultivated in YPD and YPD supplemented with 0.2M 2-DG overnight. For the glucose-d7 uptake

assay, cells in exponential phase were incubated overnight in YNB medium supplemented with 2% glucose-d7. Fatty acid uptake assay was performed by incubating cells in exponential phase with YNB medium supplemented with 0.1% Oleic acid-d34 for six hours. For 2NBDG uptake assay, cells were first exposed to fluconazole for 3 hours, and then incubated with 100µM 2NBDG for thirty minutes.

3.2.3 Glycolysis inhibition toxicity test

Cells were grown over- night in YPD. Cells were then washed three times in PBS and optical density (OD) adjusted to 0.5 at 600nm. The cells were then inoculated in YPD supplemented with 1M 2-DG. 200 µl of the cells and YPD 1M 2-DG mixture were seeded to the first row of a 96-well plate. A two-fold serial dilution to a final con- centration of 0.2 M 2-DG was performed. The cells were then incubated at 37ºC for 3 hours. Cell viability was measured with MTT colorimetric assay.

3.2.4 Clinical isolates and antifungal susceptibility testing

A total of twenty-six *C. albicans* clinical isolates (Table 3.1) were screened against fluconazole, following the Clinical and Laboratory Standards Institute (CLSI) M27-A3 guidelines for yeast and molds. All experiments were carried out in triplicates and repeated at least twice.

Table 3.1: *Candida albicans* strains used in the study

***Candida albicans* strains**	**Strain ID and designation**	**Description**	**Fluconazole minimum inhibitory concentration µg/ml**
C4	NR 29436 (P34048)	Bloodstream isolate from a person with a bloodstream infection collected in Istanbul, Turkey in 2001.	1
C5	NR 29435(P57072)	Bloodstream isolate from a person with a bloodstream infection collected in Iowa City, Iowa, USA, in 2000.	0.25

Table 3.1 continued

C7	NR 29437 (P75010)	Bloodstream isolate from a person with a bloodstream infection collected in Brussels, Belgium in 2000.	>128
C9	NR 29453 (P87)	Oral isolate from an HIV+ person collected in Pretoria, South Africa.	0.5
C10	NR 29438 (P75016)	Bloodstream isolate from a person with a bloodstream infection, collected in Tel-Hashomer, Israel, in 2000	0.5
C12	ATCC 90028 (NCCLS 11)	Bloodstream isolate, Iowa, USA.	0.25
C14	ATCC 26790 (H-29)	Pulmonary isolate	>128
C32	NR 29351 (18M)	Human isolate collected in China	0.25
C34	NR 29353 (18K)	Human isolate collected in China	0.25
C35	NR 29354 (18E)	Human isolate collected in China.	0.25
C39	NR 29358 (28H)	Human isolate that was obtained from China	>128
C41	NR 29360 (22O) .	Human isolate that was obtained from China	0.5
C43	NR 29362 (11C)	Human isolate that was obtained from China	0.5
C47	NR 29366 (28I)	Human isolate that was obtained from China	>128
C48	NR 29367 (28A)	Human isolate that was obtained from China	>128
C49	NR 29368 (28C)	Human isolate that was obtained from China	>128
C53	NR 29446 (P94015)	Bloodstream isolate from a person with a bloodstream infection collected in Utah, USA.	>128
C55	NR 29448 (P60002)	Bloodstream infection, collected in Arizona, USA	>128
C56	NR 29450 (P37037)	Oral isolate from a healthy person collected in Melwak, Wisconsin, USA, in 1999	0.5

Table 3.1 continued

C62	ATCC MYA 573 (M4)	Bloodstream isolate from a patient with AIDS, Germany	>128
C63	ATCC 64124 (Darlington)	Mouth swab isolate	>128
C64	ATCC 90029 (NCCLS 67)	Bloodstream isolate, Iowa, USA	0.5
ERG11	10B1A3A	Homozygous mutation in ERG11.	4
UPC2	11A8A2A	Homozygous activating mutation in UPC2	2
TAC1	SCTAC1R34A	Homozygous activating mutation in TAC1 (Cdr1 and Cdr2 hyper expression)	4
MRR1	SCMRR1R34A	Homozygous activating mutation in MRR1 (Mdr1 hyper expression)	4

3.2.5 Specimen preparation for imaging

Agarose gel were used for live cell imaging. To prepare the gel, ten microliters of melted 2% (w/v) agarose solution (agarose solution prepared by dissolving agarose in distilled water) was pipetted on a cover-glass (VMR), then immediately covered with another cover-glass. After the gel solidified the top slide was removed by sliding it toward one end of the other slide. Strips of double-sided tape were mounted around the gel to help with the sealing after the sample was mounted on the gel. Cells were pelleted, washed three times with 1x PBS. Two microliters of the cells were transferred to the agarose gel and covered with another cover- glass. Slight amount of pressure was applied to ensure the sample was completely sealed.

3.2.6 Stimulated Raman loss microscopy and Two-photon fluorescence microscopy

An ultrafast laser system with dual output (Newport, InSight DeepSee) supplied the excitation sources. The tunable output with a pulse duration of 120 fs was used as the pump beam. For C-H vibrational imaging the pump beam was tuned to 802nm, and 847nm for C-D vibrational im- aging. The second output centered at 1040 nm with a pulse duration of 220 fs was used as the Stokes beam. Stokes beam was modulated at 4.9MHz by an acousto-optic modulator. The pump and stokes were then overlapped before being focused into the sample using a 60x water immersion

objective lens (NA = 1.2, UPlanApo/IR, Olympus). An oil condenser (NA = 1.4, U-AAC, Olympus) was used to collect the signal. Since we detect the stimulated Raman loss (SRL), the stokes beam was blocked using bandpass filters (HQ825/150m, Chroma). SRL signal was detected using a Si photodiode integrated with a resonant circuit used in our previous paper [153]. The signal was sent to a lock-in amplifier (Zurich instruments, HF2LI). A schematic showing SRS principle and SRS setup can be found in figure 2.3 and figure 2.4.

Two-photon fluorescence microscopy was performed on the same set up; the signal was detected using a photomultiplier tube.

3.2.7 Raman Spectroscopy

A 5-ps laser (Tsunami, Spectra- Physics, Mountain View, CA) tuned to 707 nm was used as the pump beam. More details can be found in a previous study [126]. Each spectrum was acquired in twenty seconds. Pump power was maintained at 74 mW.

3.2.8 Data analysis

Quantification of lipid droplets was performed with ImageJ software particle analysis function. Integral density was used to represent the amount of lipid in a lipid droplet. LD integral density refers to the area of the LD multiplied by the mean gray scale of LD. Mean gray scale correlates with the SRS intensity.

3.3 Results and Discussion

3.3.1 SRS imaging of fluconazole-susceptible and -resistant *C. albicans*

To test the metabolic characteristic of fluconazole-resistant *C. albicans*, we obtained C-H frequency (2850 cm-1) SRS images of two randomly selected *C. albicans* clinical isolates, one susceptible and one resistant. The SRS phenomenon has a linear dependence on the concentration of the molecule being probed, therefore we can use the intensity of the signal to quantify the metabolite of interest [150,154]. SRS images of the two randomly selected strains unveiled more lipids accumulation in the fluconazole-resistant *C. albicans* (Figure 3.1a-b). To test if this phenomenon

holds for other fluconazole-resistant *C. albicans*, we carried out a blinded study of twenty-two *C. albicans* clinical isolates (twelve fluconazole-susceptible and ten fluconazole-resistant) (Table 3.1). Interestingly, we saw a huge variation in the susceptible sub-population, some strains did not accumulate any lipids at all, and others possessed as much lipids as the resistant strains. On the other hand, all resistant strains accumulated a substantial amount of lipid (Figure 3.2). For statistical comparison of the two sub-population, we performed Mann Whitney U test since our data does not assume a normal distribution (Figure 3.1c-d). Our analysis showed the two distribution were statistically different (P-value =5.01 E-5). These data suggest fluconazole-resistant *C. albicans* accumulate more lipids than fluconazole-susceptible *C. albicans*.

Our SRS imaging data showed increased lipid accumulation in fluconazole-resistant *C. albicans.* This is not surprising as several studies have shown that lipids indirectly contribute to antifungal tolerance. Azole-resistant *C. albicans* encodes drug efflux proteins belonging to the ATP binding cassette (ABC) family, which prefer membrane rafts for localization within the plasma membrane.[155-157] Protein kinase C signaling, a protein activated by diacylglycerols (DAGs) in the presence of phosphatidylserine (PS) as a cofactor has been shown to contribute to antifungal tolerance in *C. albicans*.[158-160] These studies together with our observation reveal the importance of lipids in establishment of azole resistance.

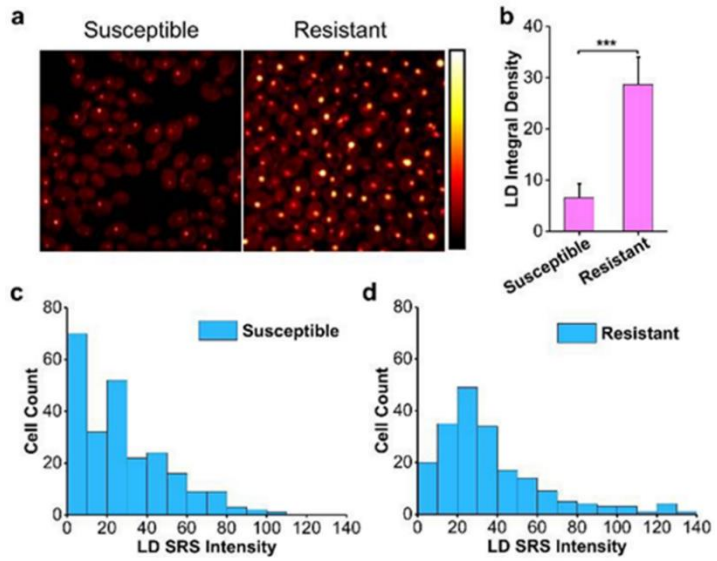

Figure 3.1: SRS imaging of fluconazole-susceptible and –resistant *C. albicans*. (a) C-H frequency (2850 cm-1) SRS images of fluconazole-susceptible and -resistant *C. albicans*. (b) Quantification of lipid signal from both fluconazole-susceptible and -resistant *C. albicans* strains. Student's t-test was used for statistical analysis. *** p< 0.001. (c) Histogram showing lipid storage distribution of a fluconazole-susceptible *C. albicans* subgroup. (d) Histogram showing lipid storage distribution of a fluconazole-resistant *C. albicans* sub-group. Twelve strains were sampled for the susceptible subgroup, and ten for the resistant subgroup. Twenty cells were analyzed for each strain. * Data collected incorporation with Hong, W.

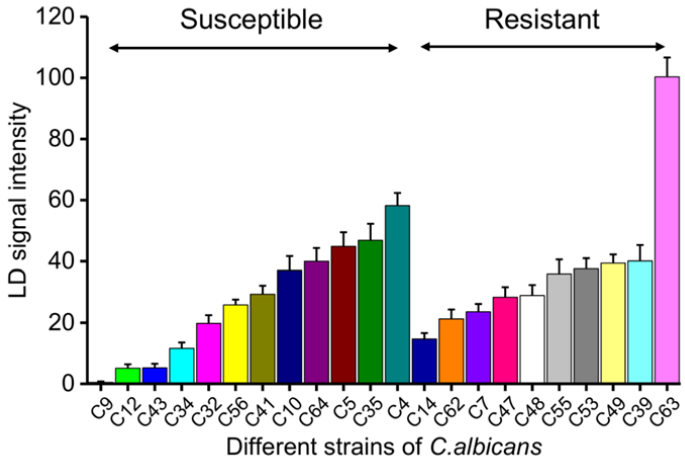

Figure 3.2: Quantification of lipid droplets from twenty-two different strains of *C. albicans*. SRS images taken at C-H frequency. Twenty cells were analyzed and averaged for each strain. Our study revealed a huge variation in the susceptible sub-group lipid accumulation, some strains barely showed any lipid accumulation while the others accumulate as much as the resistant strains. On the contrary, all resistant strains accumulated a substantial amount of lipid. * Data collected incorporation with Hong, W.

3.3.2 Aberrant lipid accumulation in fluconazole-resistant *C. albicans* arises mostly from de novo lipogenesis.

Eukaryotic cells have two sources for lipids: *de novo* biosynthesis and exogenous uptake. Excessive lipids from both sources are stored in lipid droplets (Figure 3.3a).[143] Thus, we endeavored to determine which of the two sources was responsible for the increased lipid storage in fluconazole-resistant *C. albicans*. Cytosolic acetyl-CoA is an essential building block for lipid biosynthesis.[161] Different carbon metabolism pathways such as: glycolysis, β- oxidation, and glyoxylate cycle converge on acetyl-CoA as the central metabolic intermediate.[162] However, glucose is a ubiquitous carbon source, which is universally used as the preferred carbon source by most cells.[163] To probe the contribution of *de novo* lipid biosynthesis to the increased lipid accumulation in fluconazole-resistant *C. albicans*, we examined the effects of glycolysis on lipids storage. Cells were grown to stationary phase, since yeast cells accumulate more lipids in the stationary phase.[164] First we cultivated fluconazole-susceptible and -resistant strains both in glucose supplemented YPD medium and glucose deficient YP medium. We took C-H frequency (2850 cm-1) SRS images of cells grown in both mediums and quantified SRS signal from the LDs (Figure 3.3b and 3.3d). We found a significant decrease in LD SRS signal from both susceptible and resistant cells (Figure 3.3 d). However, the ΔI for the LD was higher in the resistant strain (ΔIsusceptible=21.16, ΔIresistant=129.23), indicating glycolysis was a major contributor of the accumulated lipids. Next, we used 2-Deoxy-D-glucose (2DG), a glycolysis inhibitor, to further confirm that *de novo* biosynthesis was a major donor to the elevated lipid storage in fluconazole-resistant *C. albicans*. 2DG is a glucose analog which is avidly taken up by the cells, but cannot undergo further glycolysis since the 2-hydroxyl group in glucose mole cule is replaced by a hydrogen.[165] To assess the effects of 2DG on lipid storage, we took C-H frequency (2850 cm-1) SRS images of cells cultivated in YPD medium supplement with 2DG and cells cultivated in normal YPD medium, and compared the intensity of the LDs signal (Figure 3.3c and 3.3e). Again we observed a significant decrease in both strains. Nevertheless, ΔI for the LD signal was still higher in the resistant strain (ΔIsusceptible=9.41, ΔIresistant=23.73). Our results so far indicated glycolysis inhibition was more detrimental to the resistant strain. To further confirm this, we performed a cell viability assay, unquestionably the resistant strain had a lower half maximal inhibitory concentration (IC50) (Figure 3.3f). To track *de novo* lipogenesis in the cell, we used deuterium labelled glucose (glucose-d7). Remarkably, C-D vibrational frequency is located in a

cell-silent region, where no other Raman signal exists (Figure 3.4), thus enabling detection of newly synthesized molecules with high specificity and sensitivity. We cultivated both strains to stationary phase in YNB medium supplemented with glucose-d7 and detected C-D vibrational signal as an indicator of newly synthesized lipid droplets. Perfect colocalization of LDs from C-D (2120 cm-1) and C-H (2850 cm-1) vibration frequencies confirmed glucose- d7 was utilized by the cells to synthesize lipids Figure 3.5a). Quantification of C-D signal from the LDs indicated the resistant strain had a higher *de novo* lipogenesis rate than the susceptible strain Figure 3.5b-c).

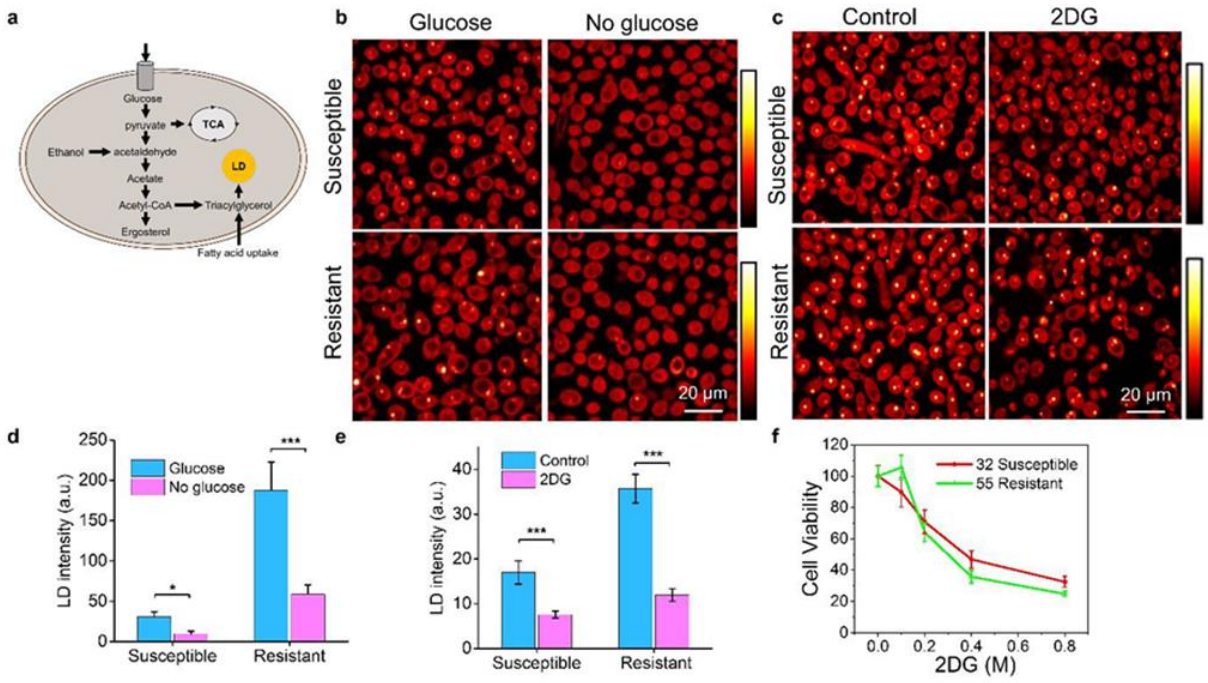

Figure 3.3: De novo lipogenesis contributes substantially to lipid accumulation in *C. albicans*. (a) Schematic illustration of lipid sources in a *C. albicans* cell. (b) Glucose depletion attenuates lipid accumulation in both fluconazole-susceptible and -resistant *C. albicans* strains. (c) Glycolysis inhibition significantly reduces lipid storage. (d) Quantification of effects of glucose depletion on lipid accumulation. Twenty cells analyzed for each group (e) Quantification of effects of glycolysis inhibition on lipid accumulation. Twenty cells analyzed for each group. (f) Glycolysis inhibition is more detrimental to the resistant strain. All SRS images taken at C-H vibrational frequency (2850 cm-1). Student's t-test was used for statistical analysis. * $p < 0.05$, *** $p < 0.001$. * Data collected incorporation with Hong, W.

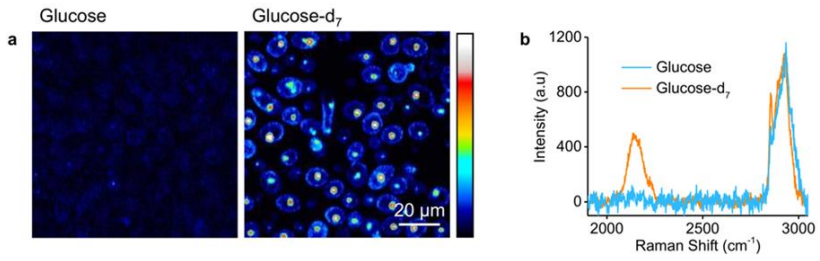

Figure 3.4 : Visualization of *de novo* lipogenesis using deuterated glucose, glucose-d_7. (a) C-D frequency SRS images (2120 cm^{-1}) of cells cultivated with normal glucose and cells cultivated with deuterated glucose. (b) Raman spectra of lipid droplets from cells cultivated with normal glucose and cells cultivated with deuterated glucose. Cells cultivated in the presence of deuterated glucose have a peak around 2120 cm^{-1}, an otherwise Raman silent region. Imaging at this frequency offers both specificity and selectivity. * Data collected incorporation with Hong, W.

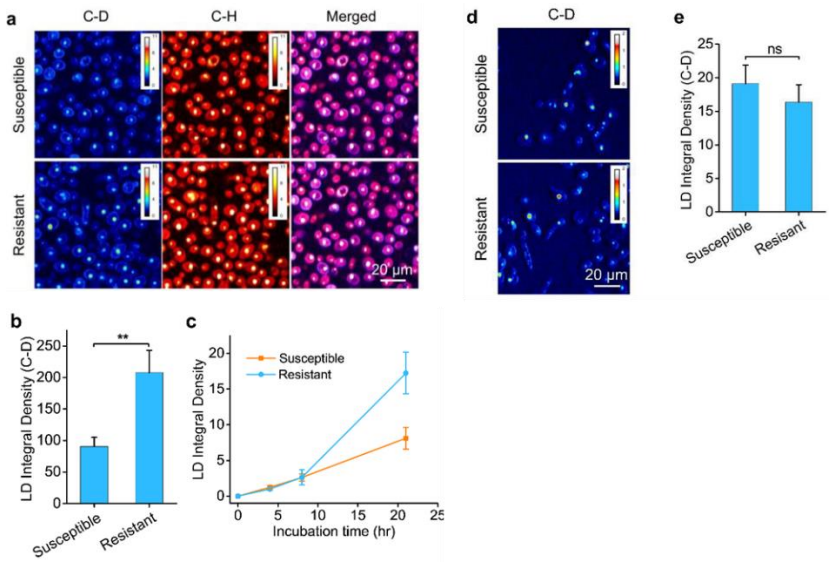

Figure 3.5: Tracking the source of increased lipid storage in fluconazole-resistant *C. albicans*. (a) Visualization of *de novo* lipogenesis via C-D frequency imaging. C-D and C-H SRS images were taken for colocalization of newly synthesized lipid with accumulated li- pids. (b) Quantification of lipid droplets C-D signal shows *de novo* lipogenesis is higher in the fluconazole-resistant strain. (c) Quantification of *de novo* lipogenesis variation with time for both fluconazole-susceptible and -resistant *C. albicans* strains. Twenty cells analyzed at each time point. (d) Visualization of fatty acid uptake by fluconazole-susceptible and -resistant *C. albicans* strains via C- D frequency (2120 cm-1) SRS imaging. (e) Quantification of fatty acid up take by fluconazole-susceptible and -resistant *C. albicans* strains. Twenty cells analyzed for each strain. Student's t-test was used for statistical analysis. ** $p < 0.01$. ns (not significant). * Data collected incorporation with Hong, W.

Our data so far suggested that increased lipid biosynthesis is responsible for the aberrant lipid accumulation in fluconazole- resistant strain. To confirm this, we compared the rate of fatty acid uptake of both strains. In order to trace cellular uptake of fatty acids, we cultivated cells in medium supplemented with deuterated oleic acid for six hours, and detected C-D signal as a measurement of exogenous fatty acid uptake. Fatty acid uptake by the susceptible and the resistant strain was not significantly different (Figure 3.5d-e). These data collectively indicate the aberrant lipid accumulation in fluconazole-resistant *C. albicans* is mainly from increased lipid biosynthesis.

3.3.3 *De novo* lipogenesis as a signature for antimicrobial susceptibility

As witnessed in the blind study (Figure 3.2) we cannot differentiate fluconazole-susceptible and resistant *C. albicans* solely based on their lipid accumulations, we wondered if fluconazole treated induced any metabolic reprogramming and if this change could be used to discriminate a susceptible strain from a resistant strain. Next, we tested whether glucose-based metabolic activity can be used to discern between a fluconazole- susceptible and -resistant strain. Fluconazole is a fungistatic drug, meaning that it inhibits cell growth rather than killing the cell (Figure 3.6). Inhibiting growth slows down metabolic activity and this alteration can be probed with SRS microscopy. To validate metabolic reprogramming induced by fluconazole, we compared the uptake of a fluorescent glucose analog (2NBDG) [166] by cells cultivated both in the presence and absence of fluconazole. In the presence fluconazole, 2NBDG uptake was significantly reduced in the susceptible cells (Figure 3.7a-b). On the contrary, fluconazole treatment upregulated 2NBDG up- take in the resistant cells (Figure 3.7a-b). To further confirm the contrasting metabolic reprogramming in fluconazole-susceptible and -resistant cells, we used Raman spectroscopy to quantify the effects of fluconazole on glucose-d7 uptake. Fluconazole treatment resulted in substantial reduction of C-D signal in the LDs of the susceptible cells (Figure 3.8a-b), but no significant change was detected in the resistant cells (Figure 3.8c-d). These data together affirmed that fluconazole exposure induced diverging metabolic adaptions in susceptible and resistant strains.

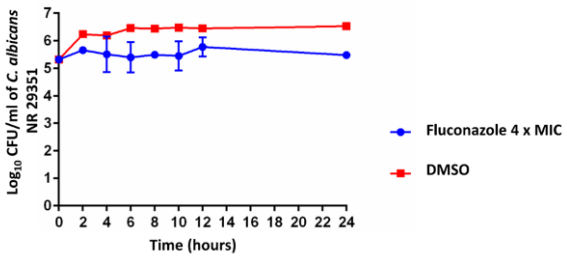

Figure 3.6: Time kill curves for fluconazole and dimethyl sulfoxide (DMSO) against *C. albicans* NR 29351. This curve shows fluconazole antifungal mechanism is not fungicidal.* data produced by Eldesouky, H. E.

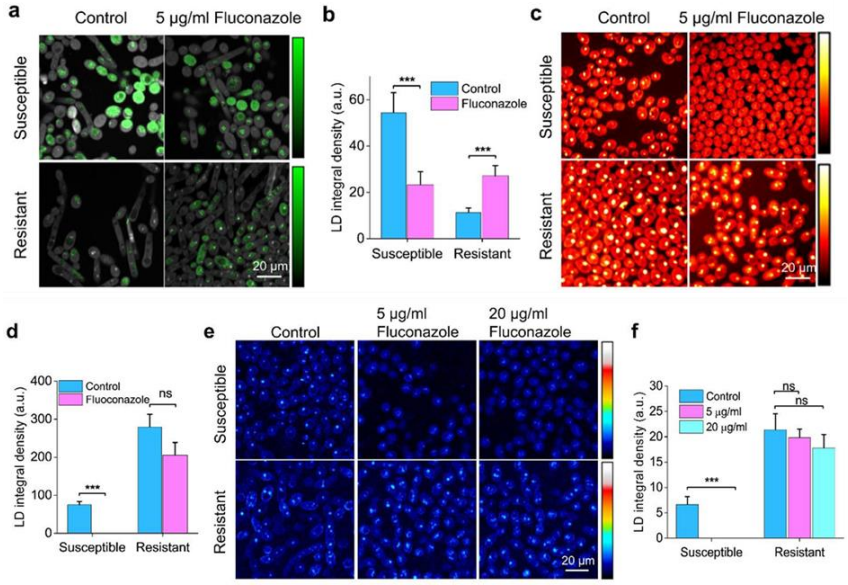

Figure 3.7: Fluconazole exposure has contrasting effects on metabolism in fluconazole-susceptible and -resistant *C. albicans* strains. (a) Exposure to fluconazole downregulates 2NBDG (glucose analog) uptake in fluconazole-susceptible strain, while it upregulates 2NBDG uptake in the fluconazole-resistant strain. (b) Quantification of 2NBDG uptake alteration induced by fluconazole treatment in fluconazole-susceptible and -resistant *C. albicans* strains. (c) C-H frequency SRS imaging reveals exposure to fluconazole attenuates lipid accumulation in the susceptible strain, and no significant change in the resistant strain. (d) Quantification of lipid accumulation alteration induced by fluconazole treatment in fluconazole-susceptible and -resistant *C. albicans* strains. (e) Visualization of d*e novo* lipogenesis via C-D frequency SRS imaging reveals *de novo* lipogenesis is attenuated by fluconazole treatment in the susceptible strain, on the contrary, the lipogenesis rate is relatively the same in the absence and presence of fluconazole in the resistant strain. (f) Quantification of *de novo* lipogenesis alteration induced by fluconazole treatment in both fluconazole-susceptible and -resistant *C. albicans* strains. Student's t-test used for statistical analysis. *** p< 0.001. ns (not significant). * Data collected incorporation with Hong, W.

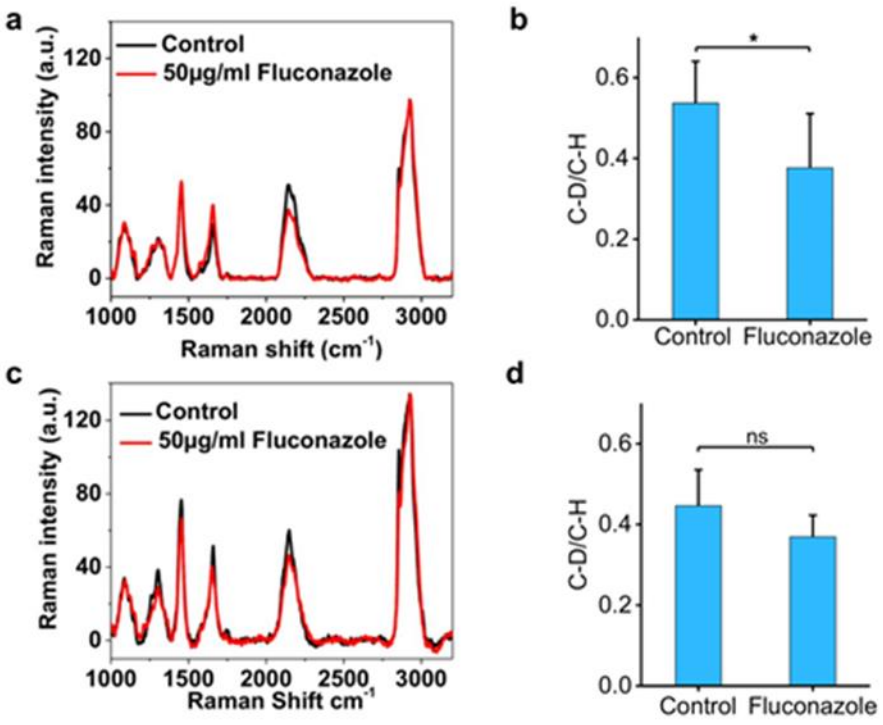

Figure 3.8: Fluconazole exposure induce metabolic adaptation in susceptible *C. albicans*. (a) Raman spectra of lipid droplets of susceptible cells cultivated in the absence and presence of fluconazole. (b) Quantification of glucose incorporation in the lipid droplets of susceptible cells cultivated in the absence and presence of fluconazole. (c) Raman spectra of lipid droplets of resistant cells cultivated in the absence and presence of fluconazole. (d) Quantification of glucose incorporation in the lipid droplets of resistant cells cultivated in the absence and presence of fluconazole. *C. albicans* cells were exposure to fluconazole for 2 hours. Student's t-test used for statistical analysis. * Data collected incorporation with Hong, W.

Our blinded study showed that some fluconazole-susceptible strains accumulate as much lipids as the resistant strains (Figure 3.2). To validate that lipid accumulation attenuation upon exposure to fluconazole was an indicator of fluconazole susceptibility, we repeated the same experiment with a fluconazole-susceptible strain (C4 strain) that possess high lipid accumulation (In our blinded study C4 was the susceptible strain with the highest lipid accumulation). Similar to the susceptible strain used earlier, fluconazole treatment resulted in a drastic reduction of lipid accumulation in the C4 strain (Figure 3.9a-b).

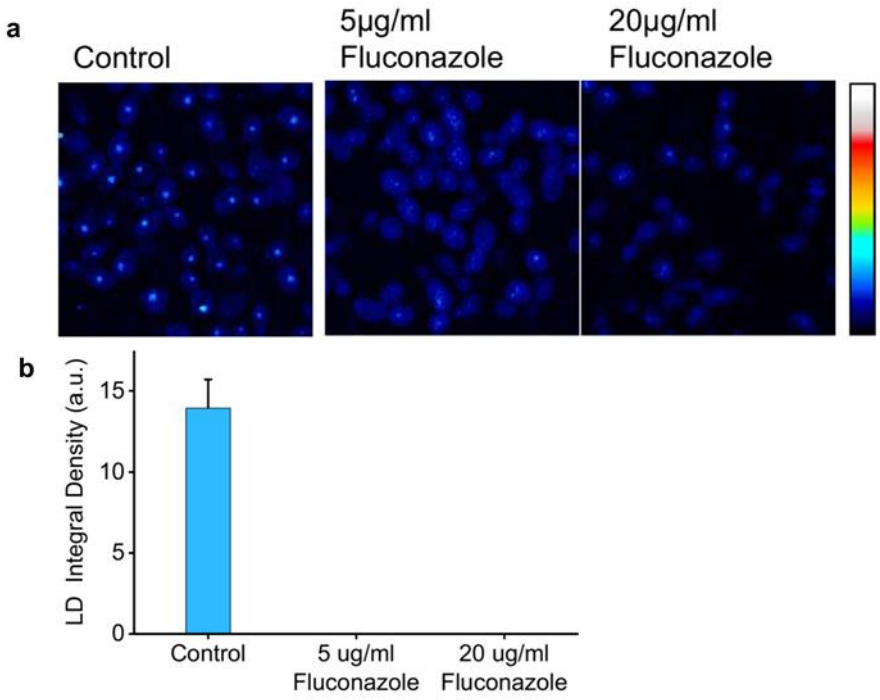

Figure 3.9: Fluconazole treatment attenuates lipogenesis in fluconazole-susceptible *C. albicans*. (a) C-D frequency SRS images of fluconazole-susceptible cells from a strain that accumulates high levels of lipids (C4). Lipogenesis was greatly attenuated in this strain as well, indicating attenuation of lipid accumulation was a sign of fluconazole susceptibility. (b) Quantification of lipid accumulation by C4 strain in the presence and absence of fluconazole. *C. albicans* cells were incubated overnight at 37°C. * Data collected incorporation with Hong, W.

We then asked what would be the shortest incubation time required to comfortably distinguish a susceptible strain from a resistant strain. Cells were incubated in glucose-d7 medium for three, five and seven hours in the presence and absence of fluconazole. C-D frequency (2120 cm-1) SRS images were then taken, and signals of the control, and treated groups were compared. Signal from the three-hour incubation was too weak (data not shown), however, we saw a significant difference in the five-hour incubation for the fluconazole-susceptible strain (Figure 3.10a). The difference in lipogenesis was more significant in the seven-hour group (Figure 3.10a). In contrast, no significant change in lipogenesis was evident in the fluconazole-resistant strain for both five-hour and seven-hour groups (Figure 3.10b). Therefore, we can discriminate between the two strains within five hours, which is more than five-fold faster than the conventional methods that require up to forty-eight hours. These studies demonstrate the robustness of metabolic imaging for rapid detection antimicrobial susceptibility.

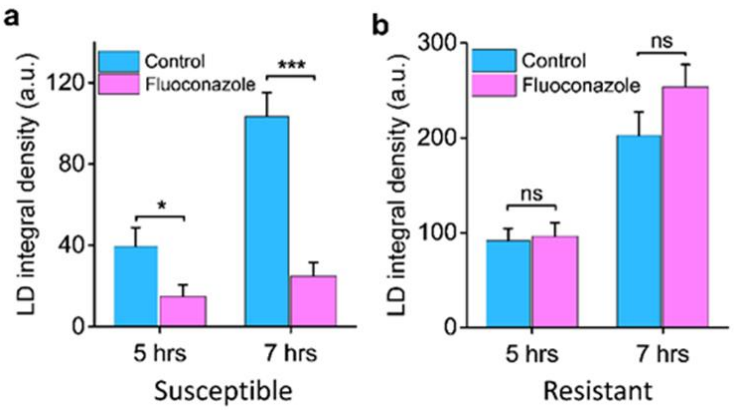

Figure 3.10: Metabolic imaging has a potential for rapid detection of antimicrobial susceptibility testing. (a) *De novo* lipogenesis alteration induced by fluconazole treatment in fluconazole-susceptible *C. albicans* is detectable with in five hours. (b) *De novo* lipogenesis alteration is not seen in fluconazole-resistant *C. albicans* under the same conditions. Student's t-test used for statistical analysis. * $p < 0.05$, *** $p < 0.001$, ns (not significant). * Data collected incorporation with Hong, W.

Molecular techniques require pre-knowledge of the target gene being probed. This makes it challenging to detect resistance arising from unknown mutations or non-genetic processes. To demonstrate our technique could easily detect resistant *C. albicans* regardless of mechanism of resistance, we repeated the experiment with four fluconazole-resistant *C. albicans* strains which varied in mechanism of resistance and compared them to the susceptible strain. Two of the mutants have an overexpression of the drug target (ERG11 and UPC2), and the other two have upregulated efflux proteins (MRR1 and TAC1). Upon exposure to fluconazole lipid biosynthesis was significantly attenuated in the fluconazole-susceptible (Figure 3.11), however, *de novo* lipogenesis rate remained unchanged in all the mutants (Figure 3.11). These results demonstrate the relentless ability of our technique to detect fluconazole resistance regardless of the genetic background, which is not achievable with molecular techniques

Rodaki and colleagues independently showed glucose increases *C. albicans* resistance to fluconazole antifungal.[167] Unfortunately, we cannot directly differentiate between fluconazole-susceptible and -resistant based on their lipogenesis profiles since some susceptible strains tend to have a lipogenesis rate similar to the resistant strains (Figure 3.2). Nevertheless, we showed that by probing the metabolic alteration induced upon exposure to fluconazole, we can distinguish between susceptible and resistant strains. Furthermore, we illustrated that this method allows for rapid detection of fluconazole susceptibility; with only five hours of incubation we were able to

discriminate susceptible strain from the resistant strain. A major improvement to the twenty-four to forty-eight hours needed for the conventional methods. A major limitation of our method is sensitivity. In a previous study, our group showed the detection limit for glucose-d7 by SRS is in the mM range.[154] Fortunately, such sensitivity is sufficient for us to see the difference between the susceptible and resistant strains.

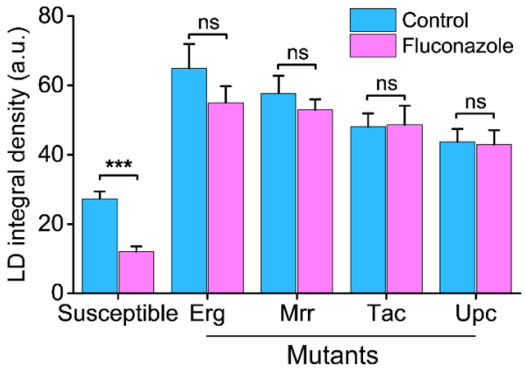

Figure 3.11: Rapid detection of resistance via metabolic imaging is independent of mechanism of resistance. Fluconazole treatment did not alter *de novo* lipogenesis in the mutants ERG11 (homozygous mutation in ERG11), UPC2 (homozygous activating mutation in UPC2), MRR1 (Mdr1 overexpression), TAC1 (Cdr1 and Cdr2 overexpression). Student's t-test was used for statistical analysis. *** $p < 0.001$. ns (not significant). * Data collected incorporation with Hong, W.

Here, we used single frequency SRS to demonstrate the relationship between lipids and fluconazole resistance, this technique does not give us any information on the composition of the lipids. Lipid composition is a crucial factor in governing membrane fluidity in *C. albicans*. In order to understand how lipid composition influences antifungal susceptibility we can switch to hyperspectral SRS imaging, which would help us to determine the ratio of saturated and unsaturated fatty acids in lipid droplets.[152]

3.4 Concluding Remarks

The key to successful treatment of patients with IFIs is prompt administration of the appropriate antifungal. In *Candida* infections, initiation of appropriate antifungal within the first twelve hours after the first positive blood culture significantly improves the patient's outcome.[118] However, early administration of effective drugs is hampered by the slow turnover of the current

susceptibility testing techniques. Since only a few hours are needed to observe a full metabolic cycle in *C. albicans*, metabolic profiling provides an avenue for rapid antimicrobial susceptibility testing. Here we demonstrated this capability with SRS lipogenesis rate profiling. Unlike the molecular techniques, this method does not require extraction of metabolites or pre knowledge about the strains. With the continuous development of compact and low-cost lasers, we expect clinical translation of this method in the near future.

CHAPTER 4. ISOQUINOLINE ANTIMICROBIAL AGENTS WITH ACTIVITIES AGAINST INTRACELLULAR BACTERIA

4.1 Introduction

Many compounds that inhibit bacterial growth or kill bacteria have been reported since Sir Alexander Fleming discovered penicillin by over 90 years ago, yet the multitude of reported compounds with antibacterial activities have not provided an insurance against an era whereby high mortality due infections by multi-drug resistant will be the norm.[168-170] The CDC approximates currently around 2 million cases of drug-resistant bacterial infections are reported in the US annually, with at least 23,000 fatalities from these infections.[61] The financial burden associated with treatment of bacterial infections is estimated to be around 20 billion dollars in the US alone.[171] The overuse of traditional antibiotics, coupled with the slow introduction of new classes of antibacterial agents have contributed to the rising incidences of multi-drug-resistant bacterial infections.[172] In order to guide research and development of novel antimicrobials, WHO issued a priority list of drug-resistant bacteria for which novel antibacterial agents are vital for human health.[173] Methicillin-resistant *Staphylococcus aureus* (MRSA), vancomycin-resistant *Enterococcus faecium* (VRE) and vancomycin-resistant *S. aureus* (VRSA) were the highest ranked Gram-positive bacteria.[173] Most of the antibacterial agents used today are from the 'golden age' of antibiotics, or are analogs thereof and the indiscriminate use of these agents have led to the emergence of bacterial strains that are resistant to these staple drugs.[174-176] Introduction of new classes of antibiotics such as oxazolidinones and cyclic lipopeptides have significantly improved treatment for resistant Gram-positive bacterial infections such as multidrug-resistant staphylococci, and vancomycin-resistant enterococci.[177] However, the emergence of linezolid-resistance staphylococcus strains[178] highlights the necessity of new antimicrobial classes to keep up with resistance evolution.

In addition to the development of drug-resistance, survival of bacteria inside mammalian cells also contributes to poor clinical outcome. Intracellular bacteria are deemed to be responsible for clinical failures of antibiotics and infections relapse.[179-182] Twaites and Gant referred to leukocytes as the "trojan horses" for metastatic *S. aureus* infections.[179] Consequently, for successful treatment of *S. aureus* infections it is vital that the antibacterial agents are active against both extracellular and intracellular bacteria. Mammalian cells offer a protective niche for bacteria,

and the efficacy of many antibiotics are significantly reduced when tested against intracellular bacteria.[182,183] This is mainly due the poor mammalian cell permeability of many antibiotics. As a result, several strategies have been proposed to improve intracellular accumulation of antibacterial agents. Lehar and co-authors used a protease sensitive antibody-antibiotic conjugate to deliver rifampicin into mammalian cells.[182] On the other hand, Xiong et.al used nanogels to facilitate vancomycin uptake by macrophages.[184] While these approaches significantly increased drug cellular uptake, there is a poor correlation between drug accumulation and activity when it comes to intracellular clearance.[183] This antibiotic mammalian cell permeation issue, coupled with the emergence of drug resistant bacteria[185] calls for new molecular entities that have potent activities against bacteria and are also active against intracellular pathogens.

Our group have been developing novel isoquinoline moiety chemical libraries.[186-188] Several compounds with an Isoquinoline moiety have been reported to have antimicrobial activity (Figure 4.1).[189-191] Compound 25 and 25 are potent against *S. aureus* with a minimal inhibitory concentration of 0.5 µg/mL.[191] These findings present isoquinoline as a prime core of antimicrobial agents. Consequently, we screened our in-house isoquinoline library for antibacterial compounds. In our group we have generated numerous alkynyl isoquinolines via the Sonogashira coupling. [187-189] Herein we present a new class of isoquinolines with activity against a plethora of Gram-positive bacteria, including drug resistant *S. aureus*. Pleasingly, these compounds exhibit low frequency of resistance and also clear intracellular bacteria.

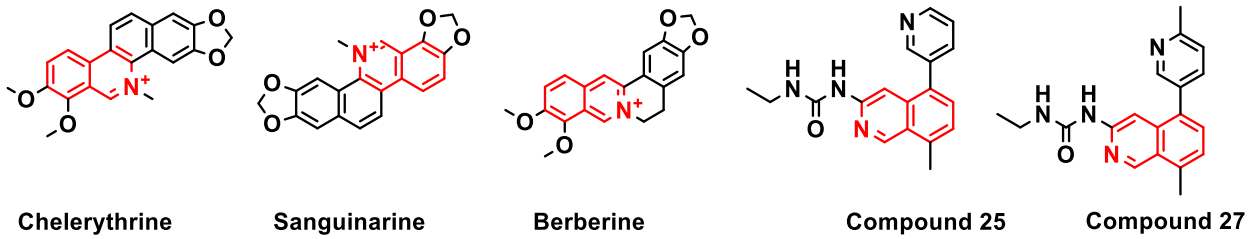

Figure 4.1: Structures of antimicrobial compounds with an isoquinoline moiety.

4.2 Experimental Section

4.2.1 Screening against bacterial isolates

Bacterial strains were incubated at 37°C to early exponential phase in Mueller Hinton Broth. Cells were then treated with 16 µg/mL compounds or DMSO for the control. Cells were incubated overnight at 37^0C. Experiment done in triplicates. 100 µl aliquots were transferred to a 96-well microtiter plate and optical density at 600nm (OD_{600}) determined. Optical density at 600 nm was used to estimate bacterial growth in microbiology. Percent growth inhibition is determined as follows:

$$\%Normalized\ OD_{600} = \left(\frac{X_T - X_o}{X_c - X_o}\right) \times 100$$

Where X_T is the OD_{600} of culture with the compound, X_o is that of media only and X_C is the OD_{600} of the DMSO control. Minimal inhibitory concentration (MIC) for compounds that exhibit potent growth inhibition (>90% inhibition) was then determined. Broth microdilution assay was used to determine the MICs as outlined by Wiegand et al. [192] Plates were incubated at 37^0C for 16-20 hours. The wells are then visually inspected for growth, the lowest concentration without any visible growth is defined as the minimal inhibitory concentration.

4.2.2 *In vitro* cytotoxicity analysis of HSN compounds against J774 cells

HSN compounds were assayed (at concentrations of 16, 32, 64 and 128 µg/mL) against a murine macrophage (J774) cell line. Experiment done as described by Elsebaei and colleagues.[193]

4.2.3 Examination of clearance of intracellular MRSA present in murine macrophage (J774) cells

Experiment conducted as described by Hagras and co-authors.[194]

4.2.4 Florescent Imaging

Murine macrophage (J774) cells were seeded in a glass bottom 15mm petri dish and grown to 80% confluence in DMEM supplemented with 10% FBS. Followed by incubation in medium supplement with 8 µg/mL HSN584 or HSN739 and incubated for 2 hours at 37 °C. After the 2hours

the cells were washed three times with 1xPBS. Cells were then incubated for 1 hour at room temperature in 16% formalin solution. Following the incubation, cells were washed three times with 1xPBS. Then cells were covered with 1xPBS for imaging. Before imaging absorbance spectra for HSN584 and HSN739 were obtained with Biotek Cytation5 image reader. Excitation at the highest absorbance wavelength was then used to generate emission spectra for both compounds (Figure 4.9). Imaging done with Nikon Ti microscope with a plan Apo 20x DIC M N2 objective lens at Purdue Bioscience Imaging Facility.

4.2.5 Resistance selection

A multi-step resistance selection experiment described by Singh *et al*.[195] was used to assess *S. aureus* ability to develop resistance against the alkynyl isoquinolines (HSN 584 and HSN 739), vancomycin and ciprofloxacin. MIC was determined daily over a course of 27 days using the broth microdilution method.

4.2.6 Macromolecule synthesis

To measure macromolecule biosynthesis cells were incubated in TSB supplemented with HSN584 or control compounds (Ciproflaxicin (DNA), Vancomycin (cell wall), rifampicin (RNA) and Linezolid (proteins)) for 10 minutes (DNA, RNA), or 30 minutes for cell wall and protein biosynthesis. 0.5μCi total concentration of radiolabeled macromolecule synthesis precursors ([^{3}H] thymidine (DNA), [^{3}H] leucine (protein), [^{3}H] N-acetylglucosamine (cell wall),[^{3}H] uridine (RNA),) were added to the growth media and cells incubated further at 37^{o}C. For DNA, RNA and cell wall biosynthesis cells were incubated for an additional 10 minutes with the radiolabeled precursors. For cell wall, cells were incubated with [3H] N-acetylglucosamine for 30 minutes. For protein synthesis cells were incubated with [3H] leucine for 1 hour. The reaction was halted using 10% trichloroacetic acid (TCA) in 1:1 ratio (reaction volume to 10% TCA ratio). Following the addition of TCA, cells were incubated on ice for 30 minutes to facilitate macromolecules precipitation. The precipitate was then collected via vacuum filtration and washed times with 5% trichloroacetic acid. Filter papers were dried on a 95^{o}C hotplate. Experiment was done in triplicates. Then filter paper was then transferred to a scintillation vial and after addition of scintillation liquid, activity was determined with a liquid scintillation counter.

4.2.7 *S. aureus* growth on High salt concentration

Exponentially growing cells were transferred to TSB media supplemented with different concentration of NaCl and HSN 584 and growth monitored measuring the optical density as described above.

4.2.8 Global proteomics

Exponentially growing *S. aureus* ATCC cells were treated with 1µg/mL HSN584 or DMSO for 2 hours at 37°C. The samples then washed with 1x PBS three times. Soluble proteins were first extracted by suspending the pellet in 500µl 20Mm Tris-HCl buffer containing 100mM NaCl, 1mM EDTA, 5% glycerol and 0.5mM DTT. The cells were transferred to lysis tubes and lysed with using Precellys® 24 Bead Mill Homogenizer (Bertin Corp., Rockville, MD, USA). The lysates were then centrifuged at 14,000 rpm for 5 min at 4 °C. The supernatant which contained the soluble proteins collected and the debris treated further to extract insoluble proteins. For extraction of insoluble proteins, the pellet was suspended with 8M urea and vortexed for 2hr at room temperature. The sample preparation for insoluble proteins proceeded as outlined in our previous publication.[196] For soluble proteins, we skipped the precipitation step and quantified protein concentration of the supernatants. Reduction, acetylation, digestion and column steps were the same both soluble and insoluble samples. LC-MS/MS acquisition and data analysis were conducted described in our previous publication.[196] With the exception, Inferno software was used to generate the heat map and origin software used to generate the volcano plot.

4.2.9 Checkerboard assay

Double the MIC was used the highest concentration for each drug. 4x Stock solution for each drug will be prepared.50µl aliquots of the 4x stock solution of drug A dispensed to the first column of a 96-well microtiter plate. 25µl of Muller-Hinton broth was aliquoted to the rest of wells and drug A serially diluted along the abscissa. Drug A is not added to column 10 as it used to determine individual MIC of drug B. 4x Stock solution of drug B will be serially diluted in 1.5ml eppendorf tubes. 25µl of the Drug B solutions then added serially along the ordinate. Drug B is not added to row H as it used to determine individual MIC of drug A. Compounds are not added to the last two columns (11 and 12) as they are used as growth control and sterility control.

Bacterial suspension was prepared the same as for microdilution MIC determination as outlined by Wiegand et.al. [192] 50µl of the bacterial suspension is then added to all the columns expect the sterility control column. The plates are then incubated at 37^0C for 16-20 hours. The wells are then visually inspected for growth and the lowest concentration without any noticeable growth is picked as the minimal inhibitory concentration. The Fractional inhibitory concentration (FIC) computed as described below:

$$FIC = \frac{Drug\ MIC\ in\ combination}{MIC\ of\ drug\ alone}$$

$$\varepsilon FIC \leq 0.5\ syngerstic, \varepsilon FIC > 0.5 < 2\ Additive, \varepsilon FIC > 2\ Antagonistic$$

4.3 Results and Discussion

4.3.1 Screening for antibacterial active alkynyl isoquinolines

In efforts to identify a new class of antibacterial agent, we screened our alkynyl isoquinoline library for antibacterial active compounds against *S. aureus*. *S. aureus* cells were incubated at 37°C overnight with 16 µg/mL of compounds and cell viability determined via optical density measurements. We identified several compounds that completely inhibited bacterial growth **(**Fig. 2, Fig. 3a and b). For more precise depiction of the compounds antibacterial activity, minimal inhibitory concentration (MIC) was determined for those compounds with over 80% growth inhibition. HSN490 exhibited the most potent activity against *S. aureus*, and *Enterococcus faecalis* (Figure 4.2, Figure 4.3a and b). Hence, for further studies HSN490 was chosen as the lead compound.

Next, we sought to determine which moieties were important for antibacterial activity. Replacement of the chloro group on the isoquinoline moiety with a fluoro group (HSN584) did not change activity (Figure 4.4, Figure 4.5 and Table 4.1). Loss of the halide group all together did not significantly change the bioactivity, HSN585 shows only a one-fold increase in MIC compared to HSN490 and HSN584 (Fig.4 and Table 1). This result indicates the halide group is not crucial for binding to this biological target in the selected bacterial strains. The replacement of the isoquinoline group with a pyridine (HSN589) resulted in loss of 50% activity (Figure 4.4 and Figure 4.5), indicating the isoquinoline group was vital for potency. Substitution of the phenylethynyl group with a pyridine (HSN736 and HSN740) led to complete loss of activity

(Figure 4.4 and Figure 4.5). From our structure activity relationship studies we concluded the isoquinoline and the phenylethynyl moieties were important for antibacterial activity.

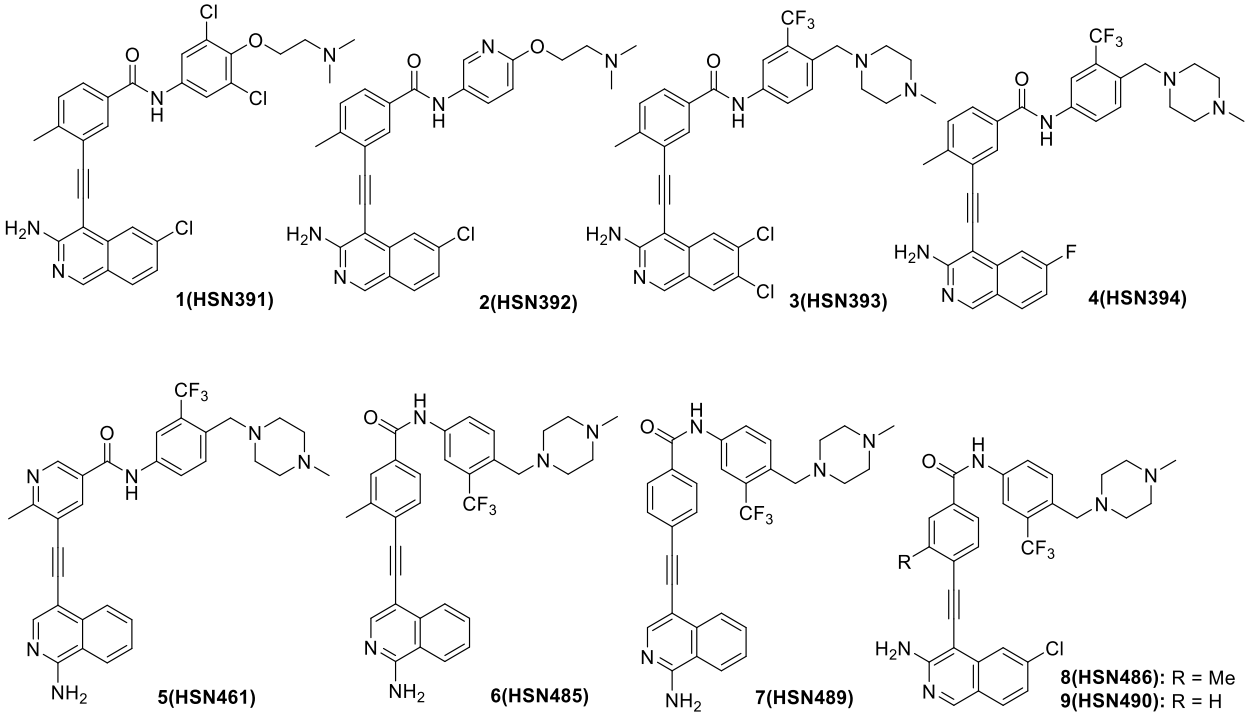

Figure 4.2: Structures of alkynyl isoquinolines with antibacterial activity

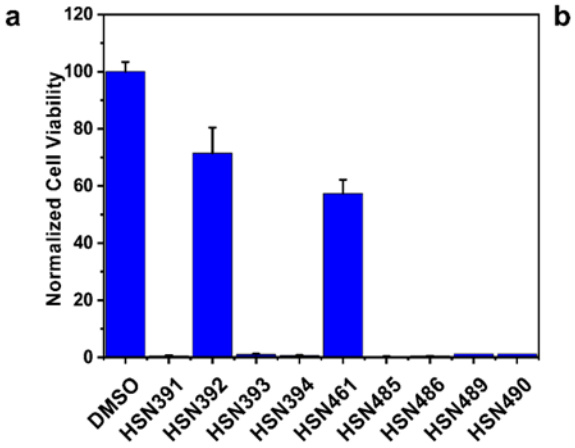

b

	S. aureus ATCC 25923 (µg/mL)	MRSA ATCC 33592 (µg/mL)	MRSA USA 300-0114 (µg/mL)	E. Faecalis (µg/mL)	VRE. Faecalis (µg/mL)
HSN391	32	8	8	8	8
HSN393	64	32	16	16	32
HSN394	8	8	4	4	4
HSN485	4	4	4	2	4
HSN486	8	4	2	4	4
HSN489	4	2	2	4	4
HSN490	2	2	1	2	2
Vancomycin	1	1	2	2	>128

Figure 4.3: Alkynyl isoquinoline inhibition of bacteria growth. a) *S. aureus* cell viability after treatment with 16 µg/mL alkynyl Isoquinolines. b) Minimal inhibitory concentrations for alkynyl isoquinolines compounds against various Gram-positive bacteria. MRSA= Methicillin-resistant *S.aureus* , VRE=Vancomycin-resistant *E. faecalis.*

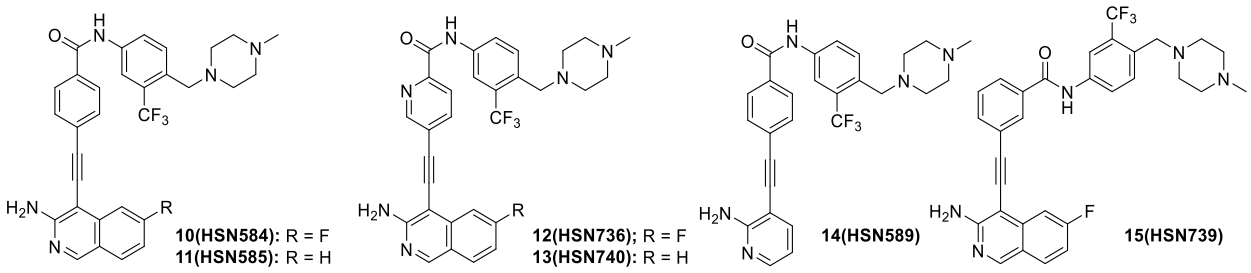

Figure 4.4: HSN490 analogs used for structure activity relationship studies.

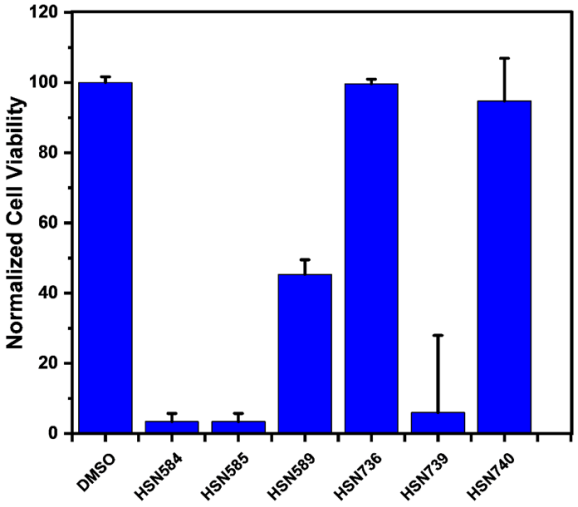

Figure 4.5 : HSN490 analogs effects on inhibition of bacteria growth. *S. aureus* cell viability after treatment with 16 µg/ml NN490 analogs

Table 4.1: HSN490 analogs minimal growth inhibition concentrations (MICs) against S. aureus, MRSA, E. faecalis, and VRE.

	S. aureus ATCC 25923 (µg/mL)	MRSA ATCC 33592 (µg/mL)	MRSA USA 300-0114 (µg/mL)	E. Faecalis (µg/mL)	VRE. Faecalis (µg/mL)
HSN584	2	2	2	2	2
HSN738	8	8	4	2	8
HSN739	2	2	2	1	2
HSN585	4	4	4	4	4

4.3.2 HSN584 and HSN739 exhibit Gram-positive specific bactericidal activity against

Next, we picked three of our most potent compounds (HSN490, HSN584 and HSN739) and screened them against various strains to bacteria to examine the extent of their antibacterial activity (Table 4.2). HSN584 and HSN739 exhibited moderate antibacterial activity (MICs values

within 4 µg/mL to 16 µg/mL range) against a variety of gram-positive bacterial species including *Staphylococcus epidermidis*, *Listeria monocytogenes*, *Streptococcus pneumonia*, *enterococcus faecium*, *clostridium difficile* and *enterococcus faecalis* (Table 4.2). Important to note, both HSN584 and HSN739 also exhibited potent (4 µg/mL or 8 µg/mL) activity against the drug-resistant strains used in the study namely: vancomycin-resistant *E. faecium*, methicillin-resistant *S. pneumonia*, vancomycin-resistant *E. faecalis*, cephalosporin-resistant *S. pneumonia*, *Linezolid-resistant MRSA*, methicillin-resistant *S. epidermidis*, and *MRSA USA400*. HSN490 on the other hand displayed weak antibacterial activity (MIC>16 µg/mL) against most of the strains expect methicillin-resistant *S. pneumonia*, cephalosporin-resistant *S. pneumonia*, methicillin-resistant *S. epidermidis* and *L. monocytogenes* against which it exhibits moderate activity (MICs values within 4 µg/mL to 16 µg/mL range) (Table 4.2). All three HSN compounds showed no activity against wild-type *Escherichia coli (E. coli) or* Tolc mutant (strain lacking the AcrAB-TolC multidrug efflux pump) (Table 4.2). The lack of activity against Tolc mutant is an indication the compounds inactivity against *E. coli* is not a result of efflux by AcrAB-TolC pump, a relevant mechanism of resistance against various clinical antibiotics.[197] The fact the compounds minimum bactericidal concentrations (MBC) is same as the MIC indicates the compounds are bactericidal agents. We also confirmed the alkynyl Isoquinolines bactericidal characteristic by generating time kill profiles (Figure 4.6). Both HSN584 and HSN739 displayed fast bactericidal activity compared to vancomycin, a standard treatment for MRSA infections. Bactericidal activity of some antibiotics have been correlated with disruption of membrane integrity either by degeneration of membrane polarization or via membrane lysing.[198,199] Hence, we investigated the effects of HSN584 on *S. aureus* membrane polarization and permeability. We did not see a concentration dependent enhancement of DISC3 or Sytox green fluorescence after treatment with 2 µg/mL and 20 µg/mL HSN584 (Figure 4.7). These results indicate HSN584 bactericidal activity is not mediated via disruption of membrane potential or lysis of the membrane.

Table 4.2: Evaluation of alkynyl Isoquinolines against variety of bacteria isolates. MIC and minimum bactericidal concentration (MBC) in µg/mL. [a] *E. coli* strain Δ AcrAB-TolC multidrug efflux pump, [b] Wild-type strain of *E. coli* JW55031. NT= not tested. **Data generated by Nader S. Abutaleb

Bacterial Strains	Compounds/Control Drugs									
	HSN 490		HSN 584		HSN 739		Linezolid		Vancomycin	
	MIC	MBC	MIC	MBC	MIC	MBC	MIC	MBC	MIC	MBC
MRSA NRS384 (USA300)	64	64	4	4	4	4	1	16	1	2
MRSA NRS119 (Linezolid-resistant)	32	32	4	4	4	4	64	> 128	2	4
MRSA NRS123 (USA400)	64	64	4	4	4	8	1	16	1	2
Methicillin-resistant Staphylococcus epidermidis NRS101	8	8	4	4	4	4	1	4	1	2
Cephalosporin-resistant Streptococcus pneumoniae ATCC 51916	4	8	4	4	4	8	1	16	1	2
Methicillin-resistant Streptococcus pneumoniae ATCC 700677	8	8	4	4	4	4	0.5	8	1	2
Enterococcus faecalis ATCC 51299 (VRE)	64	> 128	8	8	4	4	1	16	64	> 64
Enterococcus faecium ATCC 700221 (VRE)	16	64	4	4	4	8	1	16	> 64	> 64
Listeria monocytogenes ATCC 19111	8	8	4	4	4	4	1	16	1	1
Escherichia coli JW55031 (TolC mutant)[a]	> 128	> 128	> 128	> 128	> 128	> 128	16	64	NT	NT
Escherichia coli BW25113[b]	> 128	> 128	> 128	> 128	> 128	> 128	> 128	> 128	NT	NT
Clostridium difficile ATCC BAA-1870	64	NT	8	NT	8	NT	NT	NT	1	NT
Clostridium difficile ATCC 43255	32	NT	4	NT	8	NT	NT	NT	0.5	NT
Clostridium difficile strain I9	32	NT	16	NT	8	NT	NT	NT	0.5	NT

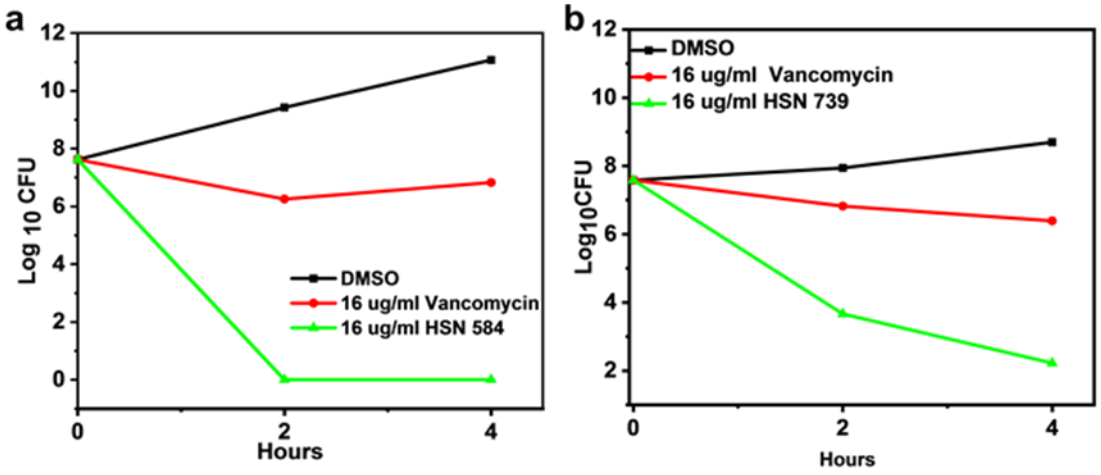

Figure 4.6: Time kill profiles. a) HSN584 time kill profile against MRSA USA 300. b) HSN739 time kill profile against MRSA USA 300. Vancomycin = positive control and DMSO = negative control.

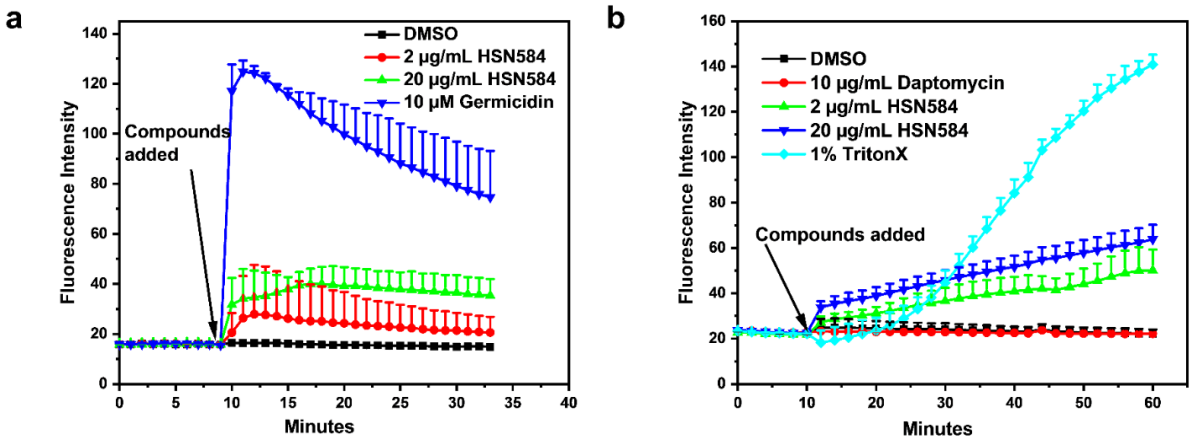

Figure 4.7: HSN584 effects on *S. aureus* membrane integrity**.** a) HSN584 effects on membrane polarization. Germicidin (Positive control), DMSO (negative control) b) HSN584 effects on membrane permeation. 1%TritonX (Positive control), DMSO and Daptomycin (negative control).

4.3.3 Alkynyl Isoquinolines are active against fluoroquinoline-resistant bacteria

Quinolones derivatives such as ciprofloxacin, levofloxacin, norfloxacin etc. are one of the largest class of synthetic antibacterial used in clinic today.[200] Due to the structural similarities between quinolones and isoquinoline moieties, and the fact our structural analysis studies revealed the isoquinoline moiety were crucial for bioactivity (Figure 4.4, Figure 4.5 and Table 4.1) we sought to examine if our compounds were active against fluoroquinolones-resistant *S. aureus.* Resistance to fluoroquinolones has been reported to be significantly high in methicillin-resistant *S. aureus* (MRSA) than in methicillin-sensitive *S. aureus* (MSSA).[201] Hence, we tested our compounds activity against methicillin-resistant *S. aureus* (MRSA), and vancomycin-resistant *S. aureus* (VRSA) strains which are resistant to ciprofloxacin, levofloxacin and norfloxacin. HSN584 and HSN739 exhibited potent activity (4 µg/mL or 8 µg/mL) against fluoroquinolone-resistant *S. aureus* strains (Table 4.3). HSN490 on the other hand displayed moderate to weak activity against the fluoroquinolone-resistant strains (Table 4.3). These results indicate our alkynyl isoquinoline mechanism of action differs from that of fluoroquinolones.

Table 4.3 : MICs and MBCs values in µg/mL of HSN compounds/control drugs against fluoroquinolone-resistant *Staphylococcus aureus* isolates. VRSA=vancomycin resistant *S. aureus*. **Data generated by Nader S. Abutaleb

Bacterial Strains	Compounds/Control Drugs													
	HSN 490		HSN 584		HSN 739		Linezolid		Ciprofloxacin		Levofloxacin		Norfloxacin	
	MIC	MBC	MIC	MBC	MIC	MBC	MIC	MBC	MIC	MBC	MIC	MBC	MIC	MBC
MRSA NRS 385 (USA 500)	8	16	4	4	8	8	2	32	>128	>128	32	32	>128	>128
MRSA NRS 383 (USA200)	16	32	8	8	8	8	2	32	128	128	32	32	>128	>128
MRSA NRS 382 (USA100)	16	32	4	4	8	8	2	64	32	32	16	16	128	128
VRSA 4	16	16	4	4	8	8	1	16	128	128	32	32	>128	>128
VRSA 7	16	16	4	4	4	4	1	16	128	128	32	32	>128	>128
VRSA 8	16	32	4	4	4	4	0.5	16	128	128	32	32	128	128
VRSA 9	16	16	4	8	4	8	1	64	>128	>128	32	32	>128	>128
VRSA 10	16	16	4	8	8	8	1	64	>128	>128	32	64	>128	>128
VRSA 13	16	32	4	4	4	4	1	64	128	128	16	16	>128	>128

4.3.4 HSN584 and HSN789 intracellular effects

One of the main limitations of conventional antimicrobial agents used in clinic today is failure to clear Intracellular bacteria. [182,183] Ability of an antibacterial compound to clear intracellular bacteria is important because intracellular bacteria is responsible for infections relapse and metastasis. [179-182] Consequently, we investigated the ability of our lead compounds (HSN584 and HSN739) to clear intracellular bacteria.

First, we investigated HSN584 and HSN739 compounds toxicity against murine macrophages (J774 cell line). Macrophage cells were incubated with different concentration of the HSN compounds for 24 hours and then viability evaluated. Up to 32µg/mL the HSN compounds were non-toxic to the macrophages (Figure 4.8). Both of our lead molecule are fluorescent, upon excitation at maxima absorbance wavelength (around 400nm) they emit blue light with maxima emission around 450nm (Figure 4.9). Capitalizing on the fluorescent nature of the molecules, we utilized fluorescence microscopy to investigate if the molecule permeates macrophages. Both molecules localize in the cytoplasmic region of the macrophages (Figure 4.10a). Confident the molecules permeate the cells, we went ahead to test the alkynyl Isoquinolines' efficacy in clearance of intracellular MRSA USA 400. We compared our compounds to vancomycin, the preferred drug for management of MRSA infections. With vancomycin we did not see a reduction in bacteria load (Figure 4.10b). On the other hand, HSN584 and HSN739 at the same concentration with

vancomycin showed a significant bacteria load reduction, an approximately 2 log fold reduction (Figure 4.10b).

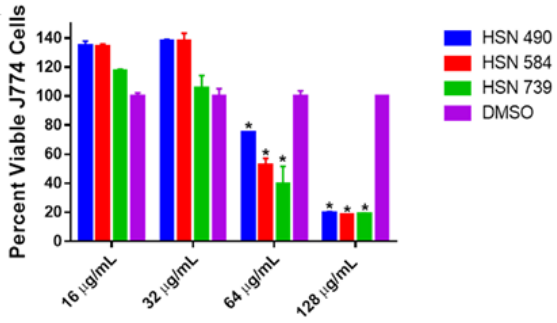

Figure 4.8: HSN490, HSN584 and HSN739 cytotoxicity against murine macrophages (J774 cell line). **Data generated by Nader S. Abutaleb

4.3.5 S. aureus does not develop rapid resistance against HSN584 and HSN789

Bacteria development of resistance against antibacterial agents is a major contributor to poor patients' outcome and the antibiotic crisis we find ourselves in today. Next, we sought to determine how fast the *S. aureus* would develop resistance against the HSN584 and HSN789. We performed a multistep resistance selection study with vancomycin and ciprofloxacin as controls. Vancomycin, HSN584, and HSN739 MIC against *S. aureus* did not change significantly throughout the 27 days (Figure 4.11). A 2-fold change was the highest MIC change observed for these three compounds throughout the entire study. On the other hand, ciprofloxacin MIC by day 6 increased by 8 folds, the MIC continually increased with an observed fold change greater than 200 at the end of the study. Our results are consistent with previous reports that indicate *S. aureus* develop rapid resistance to ciprofloxacin and not vancomycin [202].

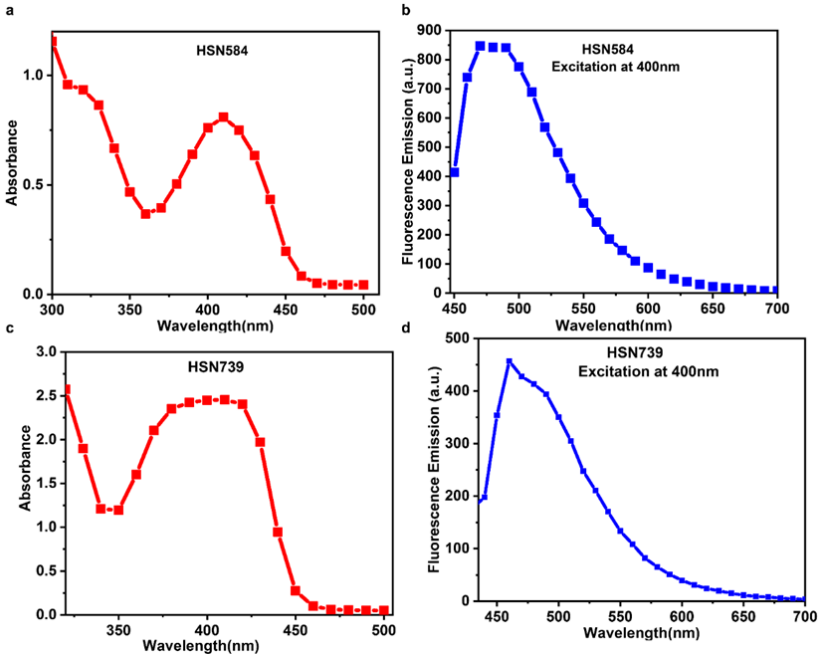

Figure 4.9 : HSN584 and HSN739 absorbance spectrum and emission spectrum upon excitation at 400 nm

4.3.6 Elucidating HSN584 mechanism of action

To gain insight as to how the alkynyl isoquinolines kill bacterium, we investigated the effects HSN584 on *S. aureus* macromolecule synthesis and global protein expression. Effects on macromolecule synthesis were determined via quantification of the uptake of isotope labelled macromolecule biosynthesis precursors by the cells with and without HSN 584 treatment, i.e. [^{3}H] thymidine for DNA synthesis, [^{3}H] leucine for protein synthesis, [^{3}H] uridine for RNA synthesis, and [^{3}H] N-acetylglucosamine for cell wall synthesis. Percent incorporation was calculated with respect to the control group (DMSO). To probe effects of HSN584 on *S. aureus* proteome, cells were treated with 1 µg/mL HSN584 or DMSO for 2 hours at 37°C, lysed and comparative global proteomics analysis conducted.

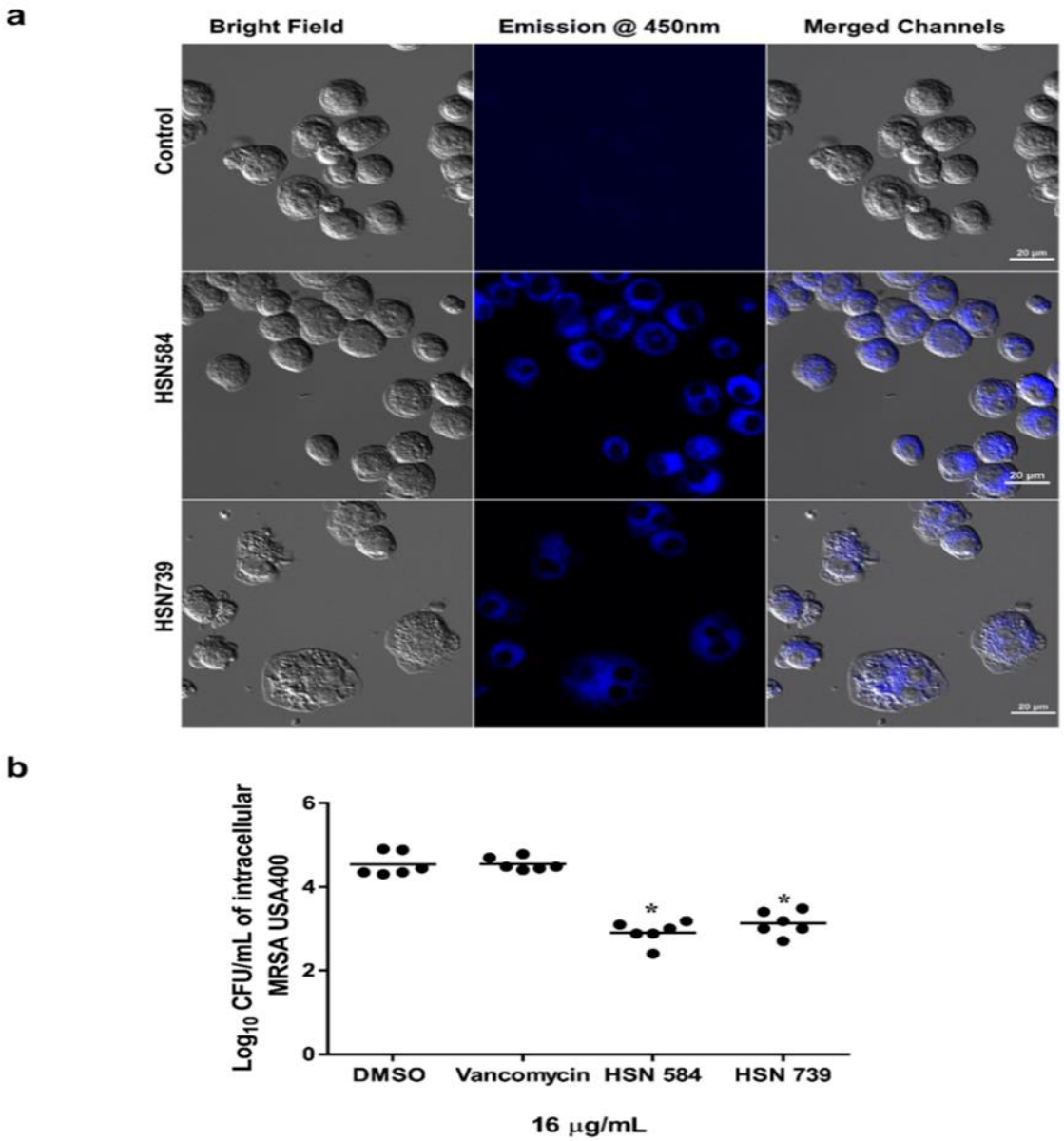

Figure 4.10: Alkynyl isoquinoline intracellular effects. a) HSN584 and HSN739 permeate murine macrophage cells and localize in the cytoplasm. b) **Data generated by Nader S. Abutaleb. HSN584 and HSN739 significantly reduce bacteria (MRSA USA400) load in murine macrophage cells. Significance quantified with the paired t-test ($P < 0.05$). *= significant difference HSN compounds and DMSO group.

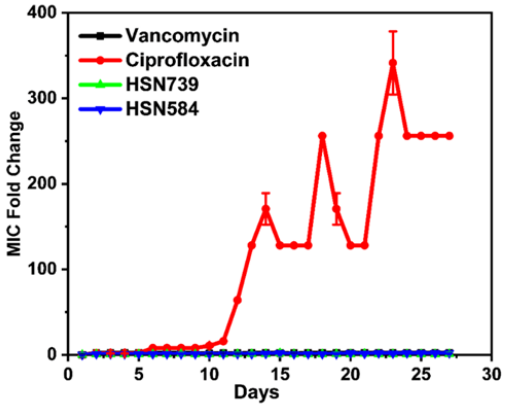

Figure 4.11: Multistep resistance study of vancomycin, ciprofloxacin, HSN584 and HSN739 against *S. aureus*. *S. aureus* was serially passaged over a period of 27 days.

For macromolecule biosynthesis experiment, *S.aurues* cells were treated with three different HSN584 concentrations (0.25xMIC, 0.5xMIC and 1xMIC (MIC = 2 µg/mL)). HSN584 exhibits a concentration dependent inhibition of cell wall, DNA and RNA synthesis (Figure 4.12a, b, and d). However, HSN584 did not exhibit a concentration dependent inhibition of protein synthesis (Figure 4.12 c). For cell wall biosynthesis, HSN584 significantly inhibited incorporation of [^{3}H] N-acetylglucosamine only at 0.5xMIC and 1xMIC concentrations. On the other hand, HSN584 significantly inhibited biosythesis of DNA and RNA at all the three concentrations tested. To confirm the precursors' incorporation was indeed as a result of HSN584 interference of the respective biosynthetic pathway and not because of reduced cell viability, we incubated the cells under the same conditions and measured the cell viability (Figure 4.13). For DNA and RNA biosynthesis, cells were exposed to the antibacterial agents for 20 minutes. This exposure did not significantly affect the cells viability even at high concentration (Figure 4.13a), suggesting the reduction of incorporation of the radiolabeled precursors was indeed due to interference with the biosynthetic pathways. For cell wall biosynthesis, cells were exposed to the antibacterial agents for 1 hour. Cell viability was only significantly affected at high concentrations (8xMIC) (Figure 4.13b). Since HSN584 exhibits a dose dependent reduction in [^{3}H] N-acetylglucosamine incorporation at lower concentration (Figure 4.12a) we can conclude HSN584 interferes with cell wall biosynthesis. For protein synthesis, cells were exposed to the antibacterial agents for 1.5hours. This exposure significantly affected cell viability at all concentration expect 1xMIC HSN584 (Figure 4.13c). Since there was no concentration dependent inhibition of protein synthesis, we concluded our compound does not affected *de novo* protein synthesis.

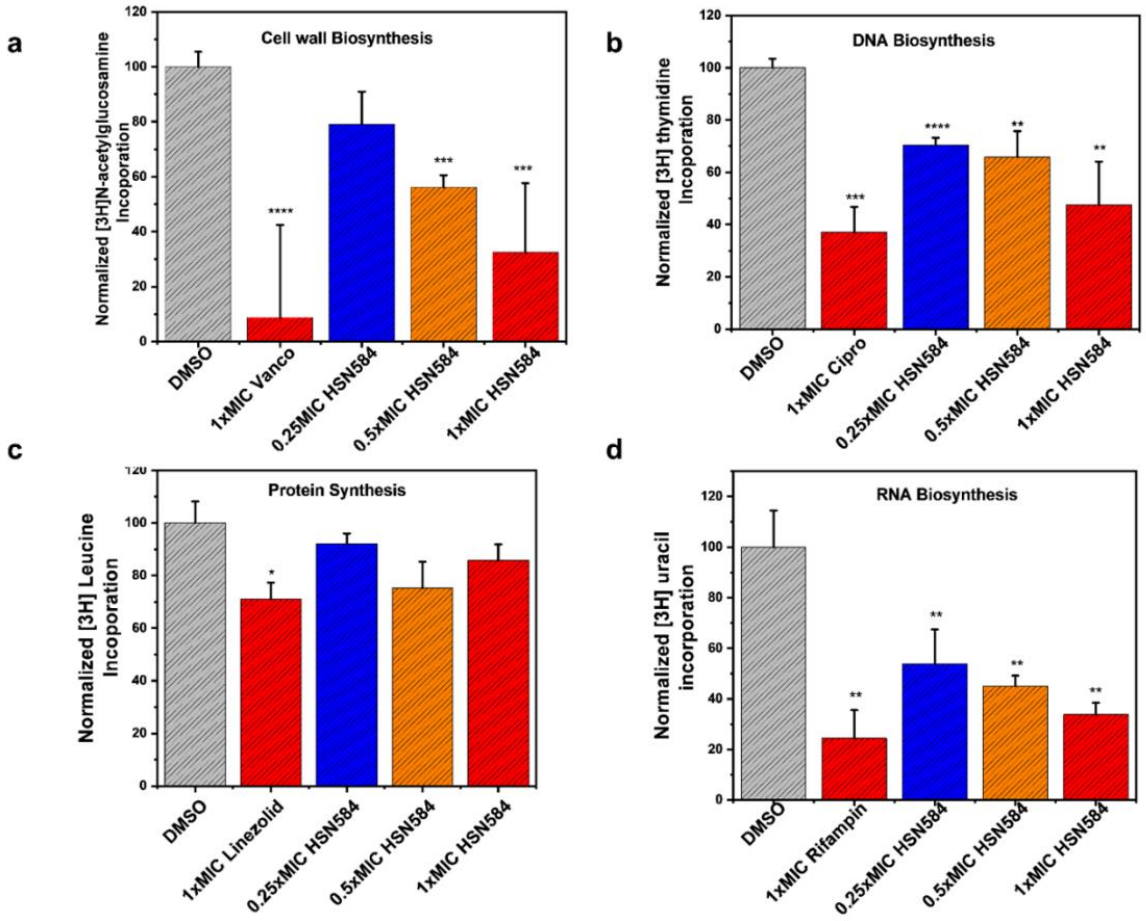

Figure 4.12: HSN584 effects on *S. aureus* macromolecule synthesis. a) HSN584 effects on [^{3}H] N-acetylglucosamine incorporation into *S. aureus* cell wall. b) HSN584 effects on [^{3}H] thymidine incorporation into *S. aureus* DNA. c) HSN584 effects on [^{3}H] leucine incorporation into *S. aureus* proteome. d) HSN584 effects on [^{3}H] uridine incorporation into *S. aureus* RNA.

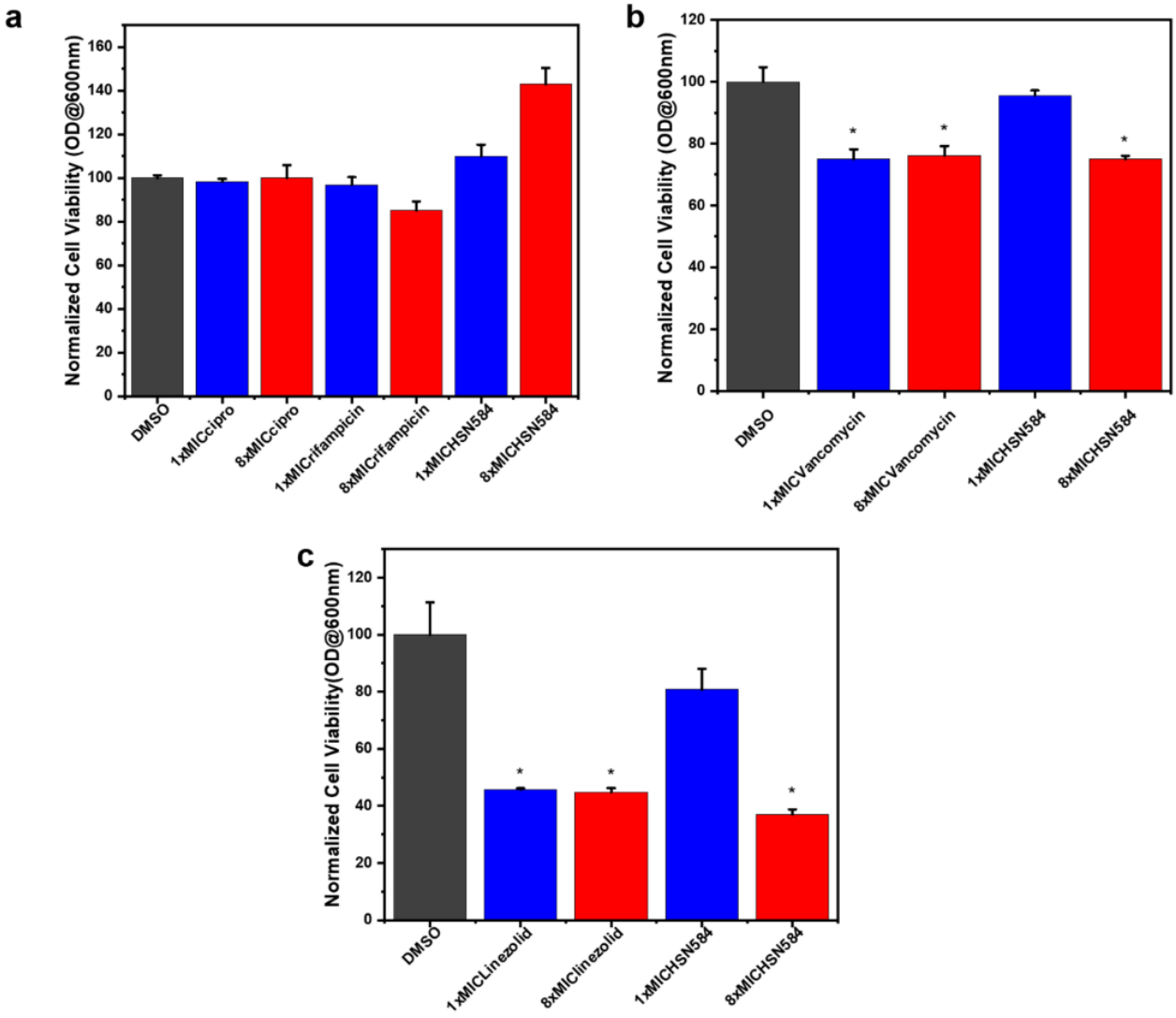

Figure 4.13: Positive controls and HSN584 effects on *S. aureus* cell viability. a) Cells treated for 20 minutes with respective antibacterial agents. (Cipro= Ciproflaxicin) MIC Cipro=0.125 ug/mL, MIC rifampicin=7.8 ng/ml, MIC HSN584=2 ug/mL. b) Cells treated for 1 hour with respective antibacterial agents. MIC Vancomycin=2 ug/mL. c) Cells treated for 1.5 hours with respective antibacterial agents. MIC Linezolid=2 ug/mL. Experiment was done in triplicate Significance evaluated using the student t-test *= P-value<0.05.

HSN584 differentially regulated *S. aureus* protein expression (Figure 4.14a and b). To narrow down the crucially regulated biological processes by HSN584 treatment, we focused on two group of proteins: unique proteins, and significantly regulated protein with $\log_2$ fold greater than 3.5. Unique proteins are those proteins only present in one sample group. Majority of the control group unique proteins are ATP-binding cassette (ABC) transporters (Table 4.4). Additionally, several ABC proteins appear in the list of significant regulated proteins list (Figure

4.15). ABC transporters functions either as importers, bringing nutrients, or exporters that pump toxins or lipids across the membrane. ABC transporters have been implicated in antibiotic resistance (involved in efflux on antibiotics) and bacteria virulence (required for uptake of nutrients crucial for bacteria colonization).[203] Hence, the inhibition of ABC transporters can be detrimental for the cell. One interesting ABC transporter affected by HSN584 is the osmoprotectant ABC transporter (Table 4.4). *S. aureus* has ability to survive high-salt conditions, a characteristic that enable the bacteria to colonize human skin.[204] To validate our proteomics data, we investigate the ability of *S. aureus* to grow in different concentrations of NaCl with and without HSN584 treatment. HSN584 inhibited growth of *S. aureus* in 0.8 M and 2M NaCl (Figure 4.16).

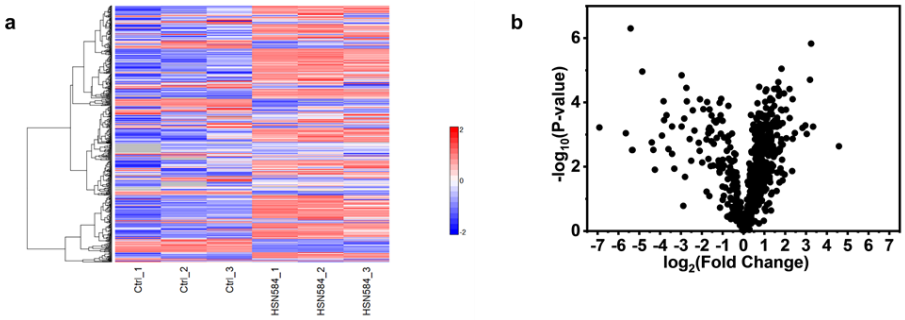

Figure 4.14 : HSN584 effects on *S. aureus* protein expression. a) Heat map depicting expression of *S. aureus* proteins in the absence and present of HSN584. b) Visualization of *S. aureus* proteins regulation by HSN584 via Volcano plot.

Table 4.4: Control group unique proteins.

Protein name	Average MS/MS COUNT
DUF5067 domain-containing protein	73
Multidrug transporter	38
Nickel ABC transporter	35
Peptide ABC transporter substrate-binding protein	30
Phosphonate ABC transporter substrate-binding protein	23
Osmoprotectant ABC transporter substrate-binding protein	21
Tandem-type lipoprotein	19
Staphopain B	17
Protein EssB	14
Gamma-hemolysin component C	13
Glycerophosphodiester phosphodiesterase	11
Peptidase M23B	10
Iron ABC transporter substrate-binding protein	10
Teichoic acid ABC transporter ATP-binding protein	7
Polysaccharide deacetylase	7
Sodium ABC transporter permease	6
Cell division protein FtsQ	6
Peptide ABC transporter permease	5
Nitrate ABC transporter substrate-binding protein	5

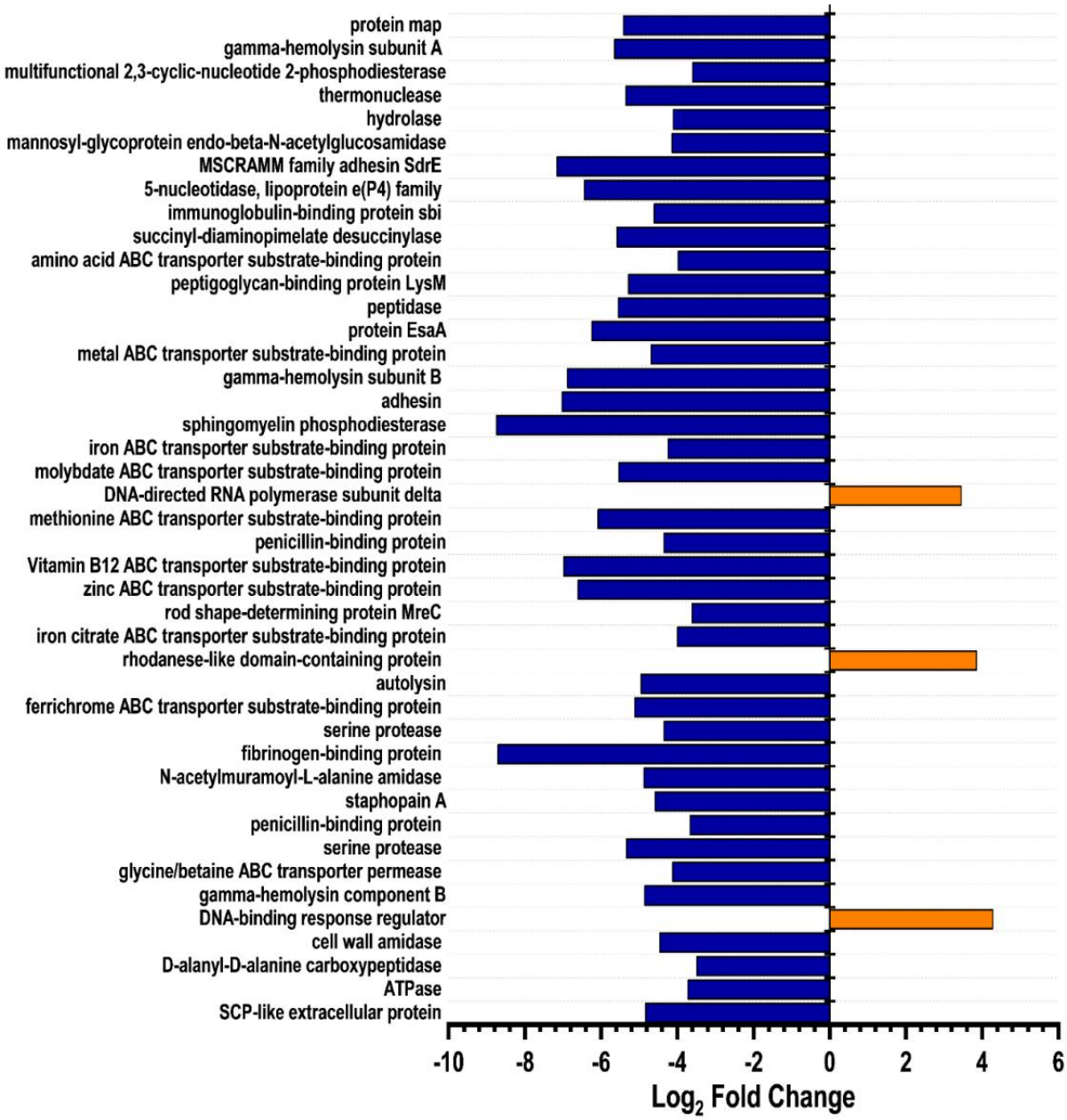

Figure 4.15: *S. aureus* proteins regulated by a $\log_2$ fold greater than 3 by HSN584 treatment.

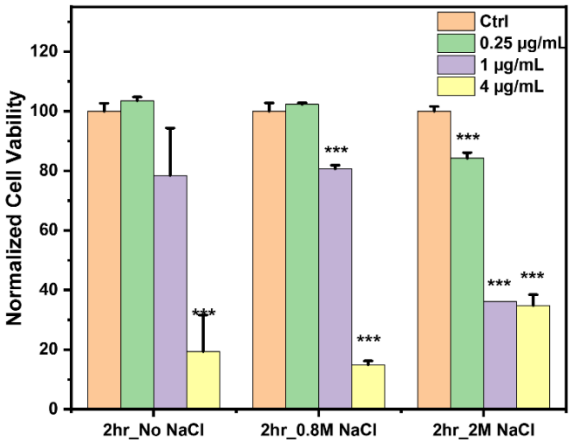

Figure 4.16: HSN584 effects on *S. aureus* growth in different concentration of NaCl.

Another interesting group of proteins downregulated by HSN584 treatment are the cell wall (CW) hydrolases namely: N-acetylmuramoyl-L-alanine amidase, peptidase M23B, and mannosyl-glycoprotein endo-beta-N-acetylglucosamidase (Figure 4.15). During growth and cell division the peptidoglycan (PG) is actively remodeled to allow expansion of the PG and accommodation of cell shape changes, a process facilitated by the CW hydrolases.[205] Consequently, CW hydrolases are important for cell wall maturation. CW amidases hydrolyze the amide bond connecting the glycan chain and the stem peptide while, CW peptidase cleave amide bond between amino acids in the stem peptide.[205] We also see down regulation of a penicillin binding proteins (PBPs) D-alanyl-D-alanine carboxypeptidase and two other PBPs (Figure 4.15), PBPs are transpeptidase enzymes which are involved in the final step of PG synthesis i.e cross linking of peptides. The down regulation of CW hydrolases and a PBPs affirms our macromolecular results which showed HSN584 affects incorporation of isotope labelled [^{3}H] N-acetylglucosamine into the PG. However, going by the proteomics data this effect is likey from inhibition of PG maturation rather than the inhibition of UDP-[^{3}H] *N*-acetylglucosamine (UDP-GlcNAc) which happens in the first step of PG biosynthesis.

Next, we looked at the expression of proteins involved in nucleic acid metabolism to see if our proteomics data could explain the inhibition of DNA and RNA biosynthesis exhibited by HSN584. Several proteins involved in DNA metabolism were overexpressed in the treated group namely: Nuclease SbcCD subunit C, DNA mismatch repair protein MutT, Holliday junction resolvase RuvX, DNA mismatch repair protein MutL, Holliday junction branch migration protein RuvA,DNA repair protein RadA and transcription-repair coupling factor (Table 4.5). Nuclease

SbcCD subunit C cleaves DNA hairpin structures which are known to halt DNA replication.[206] Overexpression of nuclease SbcCD subunit C upon treatment with HSN584 could be a mechanism the cell adapts to counter interact the DNA replication inhibitory effects of HSN584. MutT repairs mismatch during replication, while MutL is part of methyl-directed mismatch repair system which repairs post replicative errors.[207] DNA repair protein RadA, Holliday junction resolvase RuvX, and Holliday junction branch migration protein RuvA are all involved in the homologous recombination. Homologous recombination is a vital pathway for DNA damage repair. Transcription-repair coupling factor terminates transcription at site of stalled RNA polymerase and recruits nucleotide excision repair (NER) to the site of the damage.[208,209] Upregulation of Transcription-repair coupling factor could explain the down regulation of RNA biosynthesis as cells are known to shut down transcription as a response mechanism to the presence of transcription-blocking DNA lesions.[210]

Several virulence factors are downregulated by HSN584 treatment including staphopain B, protein map, MSCRAMM (microbial surface components recognizing adhesive matrix molecules) family adhesin SdrE, gamma-hemolysin, and sphingomyelinase (Figure 4.15 and Table 4.4). Virulence factors allows bacterial cell to adhere to surfaces, invade host, circumvent host immune system and induce cytotoxicity to host cells. Staphopain B, and protein map proteins have been shown to regulate immune response.[211-213] Gamma-hemolysin, and sphingomyelinase are membrane-damaging exotoxins that facilitate *S. aureus* pathogenesis.[214]

4.3.7 HSN584 synergizes with trimethoprim against trimethoprim-resistant MRSA

Combination of two or more drugs for treatment of bacterial infections has been adapted as an alternative treatment of bacterial infections. Combinational therapy advantages include: prevention of resistance emergence, lower toxicity and more rapid antibacterial activity.[215] Next, we sought to find if HSN584 synergizes with any known antibacterial agent against MRSA. Using a checker board assay, we examined HSN584 interactions with 19 commercial antibacterial agents. Synergy was determined by calculating sum fractional inhibitory concentration (εFIC).[216] HSN584 did not exhibit any antagonistic interactions with any of the antibacterial agents (εFIC<2), importantly it exhibited a synergistic effect with trimethoprim (εFIC<0.5) (Table 4.6). Trimethoprim alone exhibited an MIC> 128 ug/mL against MRSA ATCC strain. In the presence of 1 ug/mL HSN584, trimethoprim (TMP) MIC drops to 4 ug/mL. In clinic, trimethoprim is

administered as a combination with sulfamethoxazole (SMX). Next, we compared the efficacies of TMP/ SMX and TMP/HSN584 combinations against MRSA ATTC. There was no synergy between TMP and SMX, bacterial growth was evident even with high concentrations of both drugs (Figure 4.17). On the other hand, TMP/HSN584 combination was highly synergistic (Figure 4.17).

Table 4.5: Treated group unique proteins.

Protein Name	Average MS/MS COUNT
Ribosome silencing factor RsfS	28
DNA mismatch repair protein MutT	13
XRE family transcriptional regulator	13
Mevalonate kinase	12
Ribosome maturation factor	12
DNA repair protein RadA	12
Shikimate dehydrogenase	12
Betaine-aldehyde dehydrogenase	12
Dihydroxyacetone kinase subunit L	11
Glycine cleavage system protein H	11
Endoribonuclease YbeY	11
Molybdopterin synthase sulfur carrier subunit	11
Phosphomevalonate kinase	10
Cell division protein FtsK	10
Transcription-repair coupling factor	10
tRNA pseudouridine(55) synthase TruB	10
Ketol-acid reductoisomerase	10
Two-component sensor histidine kinase	10
HAD family hydrolase	10
FAD-dependent oxidoreductase	9
Signal peptidase II	9
Type II secretion protein	9
3-dehydroquinate synthase	9
DNA polymerase/3-5 exonuclease PolX	9
Polyisoprenoid-binding protein	9
Cytidine deaminase	9
Acylphosphatase	9
Initiation-control protein YabA	9
Exodeoxyribonuclease 7 large subunit	8
Isochorismate synthase	8
LytTR family transcriptional regulator	8
Cell division protein ZapA	8
Nuclease SbcCD subunit C	7
Holliday junction resolvase RuvX	7
3-phosphoshikimate 1-carboxyvinyltransferase	7
Holliday junction branch migration protein RuvA	7
DNA methyltransferase	7
DNA mismatch repair protein MutL	6

Table 4.6 : Individual and combination MICs of several commercial antibacterial agents and HSN584 against MRSA ATTC.

Compound	individual MIC (µg/mL)	Combination MIC (µg/mL)	HSN584 individual MIC (µg/mL)	Combination MIC (µg/mL)	εFIC
Methicilllin	128	64	4	2	1
Fosfomycin	128	0.5	4	4	1.003
cetriaxone	128	32	4	2	0.75
Carbecillin	>128	64	4	4	1.5
Doxycline	8	4	4	2	1
Gentamycin	<0.5	0.5	4	4	>2
Bacitracin	128	64	4	2	1
Ampicillin	128	0.5	4	4	1.003
Chloramphenicol	128	32	4	2	0.75
Linezolid	<0.5	0.5	4	0.5	>1.125
Trimethoprim	>128	4	4	1	<0.28
Amikacin	1	0.5	4	2	1
Erythromycin	128	0.5	4	4	1.003
D-cycloserine	32	32	4	2	1.5
Norfloxacin	<0.5	0.5	4	0.5	>1.125
Cloxacin	8	8	4	1	1.25
Clindamycin	<0.5	0.5	4	0.5	>1.125
Kanamycin	>128	128	4	2	<1.5
Danofloxacin	<0.5	0.5	4	0.5	>1.125

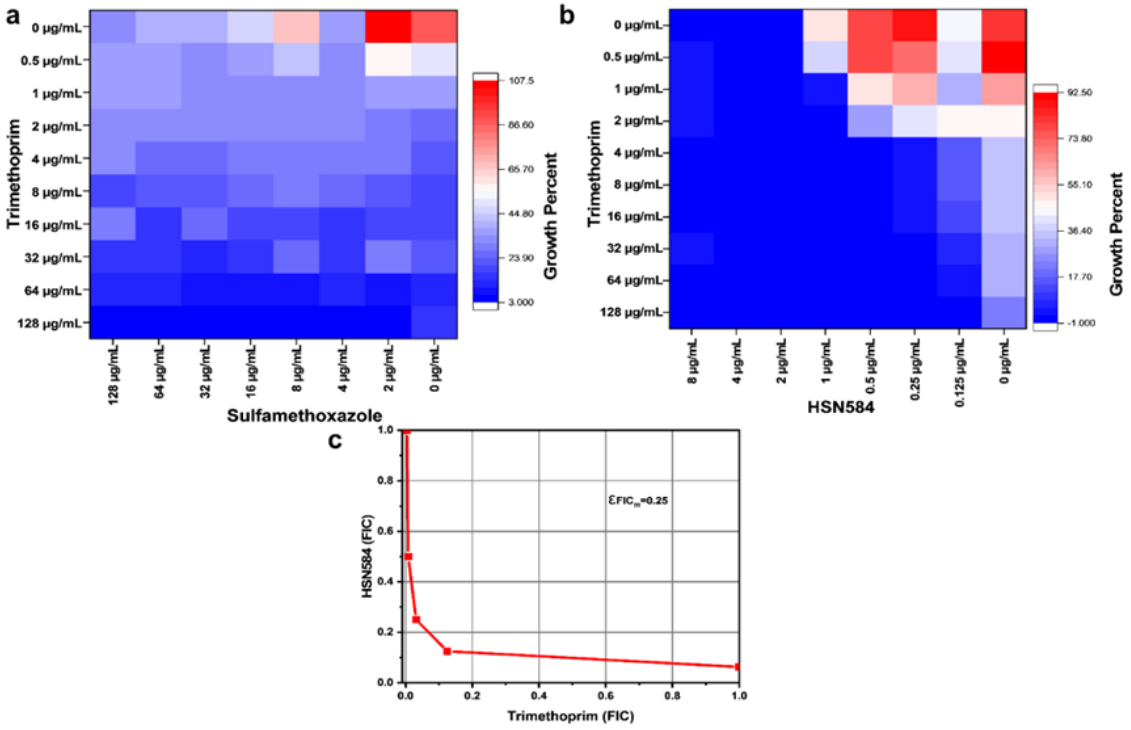

Figure 4.17: HSN584 synergizes with Trimethoprim against methicillin-resistant *S. aureus***.** a) Trimethoprim verses Sulfamethoxazole Checkboard assay. a) Trimethoprim verses HSN584 Checkboard assay. c) Trimethoprim verses HSN584 isobologram plot.

4.4 Concluding Remarks

The continuous emergence of drug-resistance microbes highlights the need for development of new antimicrobial agents to evade the probable post antibiotic era. Discovery of novel scaffolds with antibacterial activity is vital for successfully manage multidrug-resistant bacterial infections. To this end, we screened our alkynyl isoquinoline chemical library for active antibacterial agents and tested the ability of our potent compounds to clear intracellular bacteria. We identified alkynyl isoquinoline with gram-positive specific antibacterial activity, we showed the lead compound can clear intracellular MRSA and against which a *S. aureus* exhibit a low frequency of resistance development. Our preliminary studies show the alkynyl isoquinoline molecule exhibit its antibacterial activity by inhibiting three major bacterial processes, DNA synthesis, RNA synthesis and cell wall synthesis. In our future studies we will seek to evaluate the exact mechanisms by which the alkynyl isoquinoline inhibit these processes. Our Findings potentiates alkynyl isoquinoline scaffolds as ideal lead molecules for discovery of potent antibacterial agents

CHAPTER 5. IDENTIFICATION OF A SELECTIVE MYCOBACTERIUM TUBERCULOSIS CYCLIC DINUCLEOTIDE PHOSPHODIESTERASE INHIBITOR

5.1 Introduction

Cyclic dinucleotides (CDNs) have emerged as vital second messengers that regulate a dizzying array of processes in all kingdoms. In bacteria, c-di-GMP, 3'3'-cGAMP and c-di-AMP have been shown to regulate different aspects of bacterial physiology, ranging from biofilm formation, antibiotic resistance to adaptation to different environmental conditions.[66,78,217] CDNs cellular levels are maintained by CDN synthesizing enzymes and degrading enzymes phosphodiesterase (PDEs). Metazoans also make cyclic dinucleotides, such as 2'3'-cGAMP (which contains one non-canonical 2'5'-phosphodiester linkage).[67,218] 2'3'-cGAMP (cGAMP), synthesized by cyclic GMP-AMP synthase (cGAS), regulates immune response via the STING-TBK1 pathway.[219] Bacterial cyclic dinucleotides also activate the STING pathway and hence immune cells are able to sense the presence of intracellular bacteria by either making their own cGAMP upon sensing bacterial DNA in the cytosol or via the binding of bacterial cyclic dinucleotides to STING.[220] Due to the vital role that CDNs play in bacterial physiology and the innate immune system, bacterial CDN synthesizing and degrading enzymes have been targeted for the development of therapeutic agents. Diguanylate cyclase inhibitors with antibiofilm properties have been reported.[85-87] Several diadenylate cyclase inhibitors, which have antibacterial properties and also potentiate existing traditional antibiotics, have been identified as well.[89,90,221] Our group was the first to report a diadenylate cyclase inhibitor with antibacterial and antibiofilm activity.[92] In contrast to the many reported CDN synthase inhibitors, which have been reported, there is a paucity of identified bacterial CDN phosphodiesterase (PDE) inhibitors.

C-di-AMP is vital for many human pathogens (mainly Gram positive bacteria and mycobacteria) as it regulates key processes, such as osmoregulation.[78,222] For intracellular bacteria, especially those that infect phagocytic cells (such as MTB), the release of bacterial CDN into the host's cytosol can also elicit host's immune response via the STING-TBK1 pathway to facilitate pathogen clearance. Successful pathogens, such as MTB and group B streptococcus (which can also exist intracellularly) have developed sophisticated systems to evade regulation whiles inside phagocytic cells.[69,76,223] MTB harbors a c-di-AMP phosphodiesterase (CdnP) that not only

hydrolyzes bacterial derived c-di-AMP to attenuate activation of STING but also modulates host-derived cGAMP, the mechanism via which MTB Cdnp is attain access to host cGAMP is known [76] (Figure 5.1a). An analogous pathogen attenuation of host signaling has also been described in group B streptococcus whereby bacterial cyclic dinucleotide phosphodiesterase (membrane anchored and extracellular) degrades any c-di-AMP that is secreted out of the bacteria, thereby reducing the pathogen associated molecular pattern (PAMP) level that could be sensed by the host.[69] Recently, it was disclosed that certain viruses also harbor cyclic dinucleotide phosphodiesterases (such as poxins), which degrade host cGAMP[224]. Thus, it is appearing that one of the major ways that pathogens circumvent immune response is to disable the host's STING signaling response. Consequently, selective cyclic dinucleotide phosphodiesterase inhibitors are needed as tool compounds to decipher the roles of various cyclic dinucleotide phosphodiesterases in bacterial and immune cell physiology. Additionally, these compounds could be developed into antivirulence and/or immune adjuvants or boosters. It is crucial that selective CdnP inhibitors are developed to avoid perturbing the dynamics of commensal or resident bacteria.

Many compounds that inhibit mammalian cGMP or cAMP PDEs have been developed and some are used in the clinic for diverse diseased states, such as cardiac failure (example is PDE3 inhibitor enoximone, half maximal inhibitory concentration (IC50) = 10 μM[225]), psoriatic arthritics (example is PDE4 inhibitor apremilast , IC50 = 74 nM[226]), erectile dysfunction (example is PDE5 inhibitor sildenafil, IC50 = 5.22 nM[227]) and vasospasm (example is PDE10 inhibitor papaverine, IC50 = 92.3nM[228]), see Figure 5.1b for structures of PDE inhibitors. As stated earlier, only a handful of compounds that inhibit cyclic dinucleotide phosphodiesterases (for few reported examples, see Figure 5.1c) have been reported, although it is emerging that these enzymes could also play important roles in various disease progressions[88,229,230]. The Sintim group reported a benzoisothiazolinone derivative (Compound 1) as a selective inhibitor of c-di-GMP PDE RocR.[88] This compound could inhibit swarming motility in *Pseudomonas aeruginosa*. In another report, the Sintim group also reported that linear dinucleotides with hydrolysis resistant phosphodiester linkages could inhibit MTB CdnP, a virulence factor.[76] A major limitation of these linear dinucleotide analogs is poor cell permeation. Herein, we disclose the identification of a selective non nucleotide-based MTB CdnP inhibitor, which does not inhibit cyclic dinucleotide PDEs from other bacteria. Consequently, this compound or analogs thereof could be used as tool compounds

to provide insights into how MTB CdnP regulates various aspects of infection and may even be developed into antivirulence MTB therapeutics.

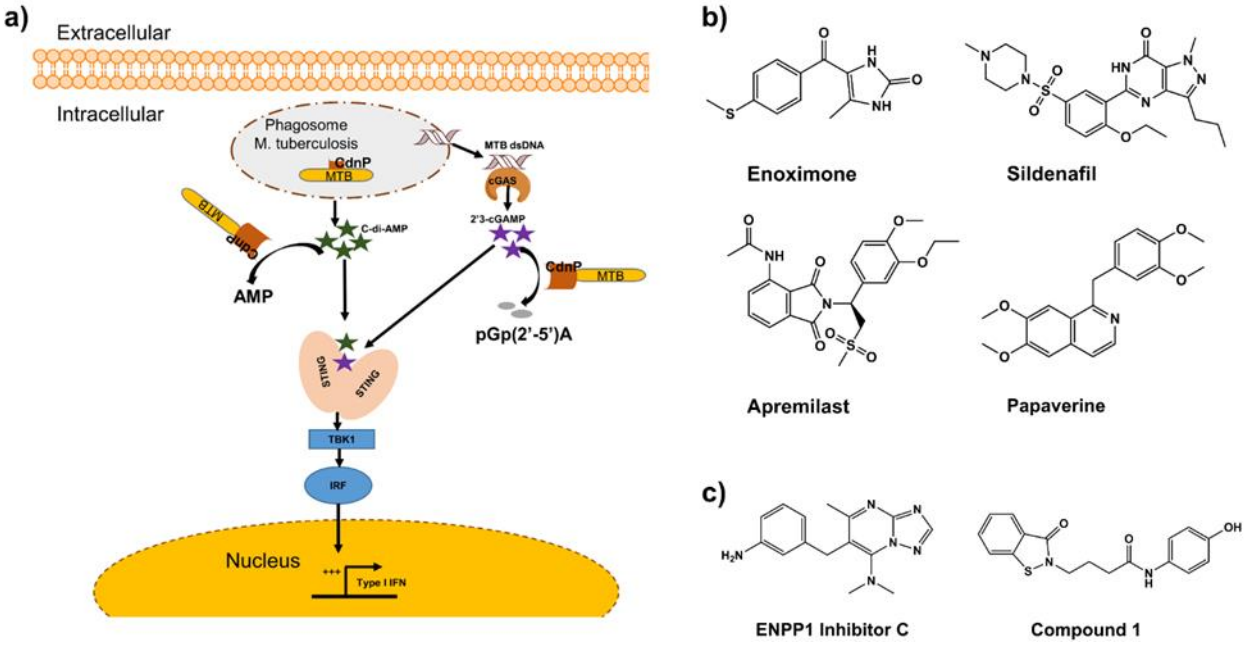

Figure 5.1: MTB CdnP phosphodiesterase activity inside a macrophage and structures of PDEs inhibitors. a) Schematic illustration of c-di-AMP and cGAMP induction of interferon response via the STING pathway and attenuation of this response by MTB CdnP phosphodiesterase (CdnP) inside a macrophage. b) Inhibitors of cyclic mononucleotide PDEs. c) Inhibitors of cyclic dinucleotide PDEs. ENPP1 IC50 =260 nM [229]. IC50s of the commercial PDEs inhibitors indicated in the text.

5.2 Experimental Section

5.2.1 Protein expression and purification

Overnight cultures of *E. coli* BL21(DE3) containing plasmid of interest were inoculated in 1 L terrific broth media supplemented with selection antibiotics and grown to exponential phase (OD = 0.6) at 37 °C. MTB Cdnp plasmid was a gift from William R Bishai.[76] Yybt plasmid was a gift from Zhao-xun Liang.[231] GBS plasmid was a gift from Pierre-Alexandre Kaminski.[77] Poxin plasmid was a gift from Philip J. Kranzusch[224]. RocR plasmid was a gift from Zhao-Xun Liang.[232] Cells was then supplemented with 0.5 mM IPTG to induce expression. After addition of IPTG, cells were incubated at 16 °C for 18 h. The cells were then centrifuged at 4 °C for 25 min and the pellet resuspended in lysis buffer (25 mM Tris-HCl, 20 mM imidazole and 500 mM NaCl pH =

8.2 for Mtb CdnP, DisA and YybT, 20 mM Hepes-KOH, 30 mM imidazole, 400 mM NaCl, 10% glycerol and 1 mM DTT, 1 mM PMSF pH = 7.5 for poxin). The cells were lysed by sonication followed by centrifugation at 22,000 rpm (25 min). The supernatants were passed through HisTrap HP 5 mL columns (GE). Wash buffer (lysis buffer + 50 mM imidazole, for Mtb CdnP, GBS Cdnp and YybT, lysis buffer+ 30 mM imidazole for poxin) was then passed through the column. The wash step was repeated once. Proteins were eluted with lysis buffer supplemented with 200 mM imidazole for Mtb CdnP, DisA and YybT, and 300 mM imidazole for poxin. Eluted proteins were then dialyzed, and concentration determined via UV absorbance (280 nm).

5.2.2 Cyclic dinucleotide synthesis

C-di-AMP used in this study was enzymatically synthesized using DisA. 20 mL reaction volume containing 1 mM ATP, and 2 µM DisA was set up. The reaction was incubated at 37 °C overnight. The reaction was halted by denaturing (95 °C, 5 min). The reaction was then filtered and c-di-AMP purified using HPLC [COSMOSIL C18-MS-II Packed column (running buffers= 0.1 M TEAA and 100% acetonitrile)]. Gradient is as follows: 0 – 16 minutes: 99 % - 87 % 0.1 M TEAA, 1% -13% acetonitrile, 16 – 23 minutes: 87 % - 10 % 0.1 M TEAA, 13 % -90 % acetonitrile, 23 – 25 minutes: 10 % - 99 % 0.1 M TEAA, 90 % -1 % acetonitrile. The purified c-di-AMP was dried with a speed vacuum and the residue was then re-suspended in water. C-di-AMP concentration was quantified via UV absorbance (260 nm).

5.2.3 IC50 Determination

Reactions of 20 µl in volume containing 50 nM MTB Cdnp, 10 mM KI, 10 µM coralyne 100 µM c-di-AMP, in 1x reaction buffer (50 mM Tris-HCl, 5 mM $MnCl_2$, pH 9.0,) supplemented with 0.0025% Triton X-100 and varying concentrations of identified hits were set up in Greiner FLUOTRAC 384well plate. Experimental parameters optimized to keep hydrolysis in the linear range. Real time c-di-AMP hydrolysis kinetics was monitored by measuring fluorescence intensity at λ_{em} = 475 nm (λ_{ex} = 420 nm) at 2 min intervals for 10 min. Reader (Biotek Cytation 5 multi-mode reader) chamber temperature set to 30 °C. Slope of the curve used to estimate initial velocity. Experiment done in triplicates.

5.2.4 Calibration curves generation

10 µM coralyne in 1x MTB Cdnp reaction buffer (see above (section 5.2.3)) was mixed with varying concentrations of c-di-AMP or AMP and fluorescence emission measured (λ_{em} = 475 nm, λ_{ex} = 420 nm).

5.2.5 Mtb CdnP coralyne based Michealis-Menten curve

Reactions of 100 µl in volume containing 50 nM Mtb CdnP, 10 µM coralyne, 3 mM KI, and varying concentrations of c-di-AMP in 1x reaction buffer ((see above (section 5.2.3)) and various **C82** concentrations were set up in Greiner FLUOTRAC 96 well plate. Real time c-di-AMP hydrolysis was monitored by quantifying fluorescence intensity at λ_{em} = 475 nm (λ_{ex} = 420 nm) at 1 min intervals for 10 min (reaction still in linear range). Reader (Biotek Cytation 5 multi-mode reader) chamber temperature set to 30 °C. Slope of the curve used to estimate initial velocity. Experiment done in triplicates. C-di-AMP calibration curve was used to estimate change in c-di-AMP concentration at the end of reaction.

5.2.6 High-throughput screening

Mtb CndP reaction parameters were optimized to yield a Z-factor in 0.5-1 range (Figure 5.4). 0.5 µM Mtb CdnP and 10 µM coralyne were used. Z-factor was computed with the following equation:

$$Z = 1 - \frac{3(\sigma_p + \sigma_n)}{|\mu_p - \mu_n|} \qquad \text{Equation 5.1}$$

Where σ is the standard deviation, µ is the mean, p = positive control and n = negative control. HTS was conducted at the chemical genomics facility at the Purdue Institute for Drug Discovery. Reactions of 20 µl in volume containing 70 µM c-di-AMP, 10 µM coralyne, 10 mM KI, 5 mM $MnCl_2$, 10 µM compound from the library and 0.5 µM Mtb CdnP in the Tris buffer (50 mM Tris-HCl, pH = 9.0,) were set up. 10 µl of a reaction mix (1x reaction buffer, 2x c-di-AMP, 2x coralyne, 2x $MnCl_2$, and 2x KI) was dispensed into Greiner FLUOTRAC 384 plates. Compounds were then dispensed with a robot, and finally 10 µl of enzyme mix (2x MTB cdnp in 1x reaction buffer (without $MnCl_2$)) was added to the plates. Fluorescence readings were taken immediately following the addition of the enzyme for kinetic-based screens. C-di-AMP hydrolysis was

monitored by measuring fluorescence intensity at λ_{em} = 475 nm (λ_{ex} = 420 nm) at 1 min intervals for 15 min. On the other hand, plates were incubated for 30 minutes at 37°C. The reactions were then quenched with 30 mM EDTA and then fluorescence emission at 475 nm determined.

5.2.7 HPLC analysis

Mtb CdnP reactions (70 µM C-di-AMP, 100 nM Mtb CdnP, 1x reaction buffer) were set up with and without 50 µM compound, incubated at 37°C for 3 hours or 12 hours. The enzyme was then denatured (95 °C ,5 minutes) to stop the reactions. The reaction was then and analyzed using HPLC as described above.

For GBS CdnP, reactions containing 50 µM c-di-AMP, 1x reaction buffer (50 mM Tris-HCl, 5 mM $MnCl_2$, pH = 7.5) and 100 nM GBS CdnP were set up in the presence and absence of **C82**. Reactions were incubated for 15 minutes at room temperature. The enzyme was then denatured (95 °C ,5 minutes) to stop the reactions. The reaction was then and analyzed using HPLC as described above.

For poxin, reactions containing 20 µM 2'3 cGAMP (Chemietek), 1x reaction buffer (20 mM Hepes-KOH, pH = 7.5) and 5 nM poxin were set up in the presence and absence of **C82**. Reactions were incubated for 20 minutes at room temperature. The enzyme was then denatured (95 °C ,5 minutes) to stop the reactions. The reaction was then and analyzed using HPLC as described above.

For Yybt, reactions containing 70 µM c-di-AMP, 1x reaction buffer (0.1M Tri-HCl, 20 mM KCl, 0.5 mM $MnCl_2$ pH = 8.0,) and 1 µM Yybt were set up in the presence and absence of **C82**. Reactions were incubated for 60 minutes at 37 °C. The enzyme was then denatured (95 °C ,5 minutes) to stop the reactions. The reaction was then and analyzed using HPLC as described above.

For RocR, reactions containing 25 µM C-di-GMP, 1x reaction buffer (100 mM Tris-HCl, pH = 8.0, 20 mM KCl and 25 mM $MgCl_2$) and 10 nM RocR were set up in the presence and absence of **C82**. Reactions were incubated for 60 minutes at 37 °C. The enzyme was then denatured (95 °C ,5 minutes) to stop the reactions. The reaction was then and analyzed using HPLC as described above.

For ENNP1, reactions containing 25 µM cGAMP, 1x reaction buffer (50 mM Tris, 250 mM NaCl, pH 9.5) and 4.58 nM ENNP1 were set up in the presence and absence of **C82**. Reactions

were incubated for 60 minutes at 37 °C. The enzyme was then denatured (95 °C ,5 minutes) to stop the reactions. The reaction was then and analyzed using HPLC as described above.

5.2.8 Radiolabeling experiments

^{32}P-c-di-AMP synthesized by incubating 0.033 µM [α^{32}P]-ATP (Perkin Elmer), 3 mM ATP and 10 µM DisA in a buffer of pH 7.5 containing 40 mM Tris-HCl, 10 mM $MgCl_2$ and 100 mM NaCl at 37 °C overnight. DisA reaction was stopped by heat denaturing. For the inhibition test, reaction contained 0.5 µM Mtb CdnP ,25 µM c-di-AMP, 3.3 nM ^{32}P-c-di-AMP, and varying concentrations of compounds. The reactions were incubated for 60 minutes at 37 °C. 1 µL of reaction mixture was blotted on a cellulose TLC plate (EMD Millipore). The blot was dried at room temperature. Development of the TLC plate was done with saturated $(NH_4)_2SO_4$: 1.5 M KH_2PO_4 buffer. The plates dried by using a hot plate (95 °C) before they were exposed to GE Storage Phosphor screen (overnight). The screen was visualized with Typhoon^{TM} FLA 9500 biomolecular imager.

5.2.9 Intrinsic Fluorescence

Solutions containing 2 µM Mtb CndP, and varying concentrations of **C82** in 1x PBS were incubated at room temperature for 30 minutes. Fluorescence spectra then obtained by measuring fluorescence intensities in the 310 nm-400 nm range following an excitation at 290 nm wavelength.

5.2.10 DRaCALA assay

Reaction mixtures containing 20 µM MTB Cdnp, 1x reaction buffer (see above without $MnCl_2$), 5 mM calcium chloride, 200 pM ^{32}P c-di-AMP, and varying c-di-AMP or **C82** concentrations (total volume =20 µl) were set up and incubated for ten minutes at room temperature. 5 µl of the reaction was blotted onto dry untreated nitrocellulose membrane (GE Healthcare) and allowed to dry at room temperature. Membrane then exposed to the GE Storage Phosphor screen for 8 hours and then visualized with TyphoonTM FLA 9500 biomolecular imager.

5.2.11 Fluorescence polarization competition assay

Reaction mixtures containing 150 µM MTB Cdnp, 1x reaction buffer (see above without $MnCl_2$) 5 mM calcium chloride, 50 nM 2'-Fluo-AHC-c-diGMP (Biolog) and varying concentrations of c-di-AMP or **C82** (total volume =20 µl) were set up and incubated at room temperature for ten minutes. Fluorescence polarization was determined Biotek Cytation 5 multi-mode reader (excitation 485 nm / 20 and emission 528 nm / 20). Anisotropy was calculated using the Gen 5 ^{TM} microplate reader and imaging software.

5.2.12 Cell viability

4000 cells/ well (200 µl) were plated into a 96 well plate and incubated for 18 hours at 37 °C with 5% CO_2. Followed by treatment with compounds or dimethyl sulfoxide for the control group. The cells were incubated with the compounds for 24 hours. Viability was then determined with the CellTiter-Blue® Cell Viability Assay as per the manufacturer specifications Cell viability determined by measuring fluorescence (excitation 560 nm and emission 590 nm) with Biotek Cytation 5 multi-mode reader. Cells were grown with Dulbecco's Modified Eagle Medium supplemented with 10% Fetal Bovine Serum. Cell lines = MDA-MB-231, and MRC-5.

5.3 Results and Discussion

5.3.1 HTS for MTB CdnP inhibitor.

The coralyne assay, developed by our group,[233] was used to conduct high throughput screens for Mtb CdnP inhibitors. The assay capitalizes on the fact that c-di-AMP protects coralyne from iodide quenching via the formation of an inclusion complex (Figure 5.2). Following the formation of the complex, coralyne fluorescence emission is greatly enhanced. Since c-di-AMP enhance coralyne fluorescence emission in a concentration dependent manner (Figure 5.3a) while AMP does not (Figure 5.3b) coralyne assay is deal for tracking c-di-AMP degradation by MTB CdnP and therefore could be used to identify MTB CdnP inhibitors. Prior to conducting the HTS, the assay was optimized for both kinetics and endpoint analysis. Experimental parameters were adjusted to obtain an optimal screening window, and at the same time ensuring that MTB CdnP kinetics stayed in the linear range. The screening window was quantified using the Z-factor, a

screening window coefficient (Equation 5.1).[234] An ideal assay for HTS ought to have a Z-factor between 1 and 0.5. Hence, we optimized the experimental conditions to obtain ideal assay conditions for the HTS assay. The Z-factors for different c-di-AMP concentrations, chosen to be close to the apparent Km (obtained via the coralyne assay) were computed (Supplementary Information, Figure 5.4a and b). The concentration of potassium iodide, KI, which is used as an anion quencher to reduce the fluorescence of the unbound coralyne[233], was also varied and Z-factor computed. Optimal assay conditions for both kinetic (Z-factor =0.61) and endpoint (Z-factor =0.71) approaches were found to be 70 µM c-di-AMP and 10 mM KI (Supplementary Information, Figure 5.3b). Thus, the HTS was conducted with these conditions. 90,000 compounds (Purdue Chemical Genomics Facility compound library), which included kinase inhibitor library, natural products, and diversity library, were screened for CdnP inhibition. Compounds that exhibited over 40% inhibition were selected as potential Mtb CdnP inhibitors (Figure 5.5 and Figure 5.6).

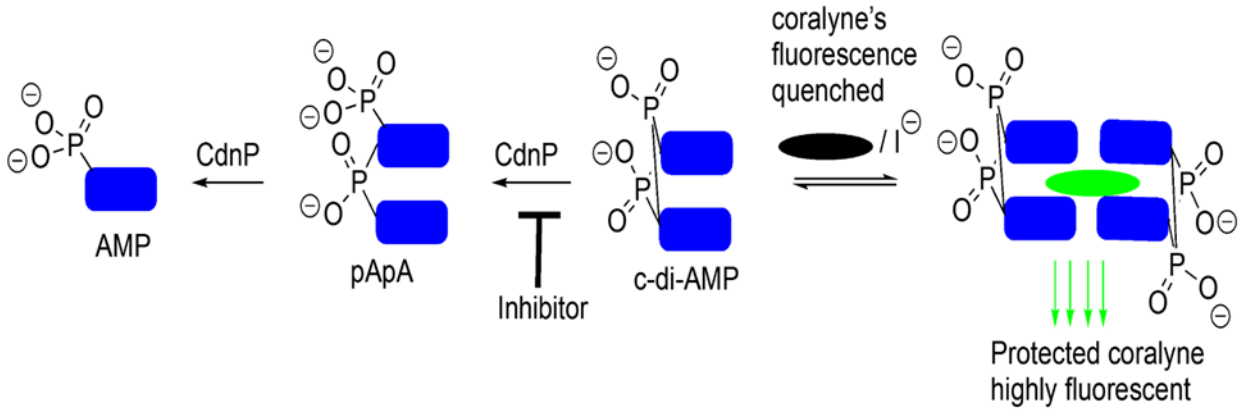

Figure 5.2: Monitoring of c-di-AMP hydrolysis by MTB CdnP with the coralyne assay. C-di-AMP-coralyne complex enhance coralyne fluorescence. MTB Cdnp degrade c-di-AMP to AMP which does not enhance coralyne fluorescence.

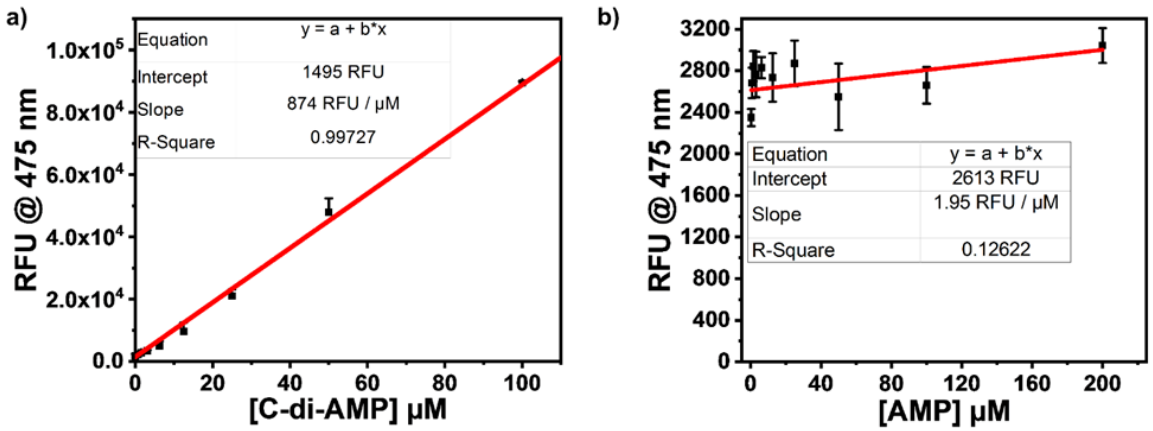

Figure 5.3: C-di-AMP and AMP effects on coralyne fluorescence emission. a) Calibration for coralyne fluorescence as function of c-di-AMP concentration. b) Calibration for coralyne fluorescence as function of AMP concentration.

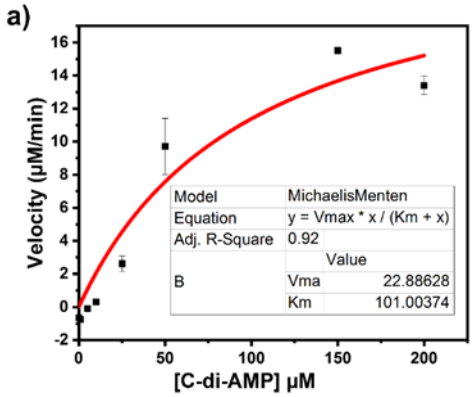

b)

[C-di-AMP]	[KI]	Z-Factor
50 µM(Kinetics)	3 mM	0.33
50 µM (Kinetics)	10 mM	0.41
70 µM (Kinetics)	10 mM	0.61
70 µM (Endpoint)	10 mM	0.71

Figure 5.4: Optimization of coralyne assay for HTS of MTBCdnP inhibitors. a) Michealis menten curve for MTB CdnP determined using coralyne assay. b) Z-factor for different experimental parameters determined with 0.5 µM MTB Cdnp.

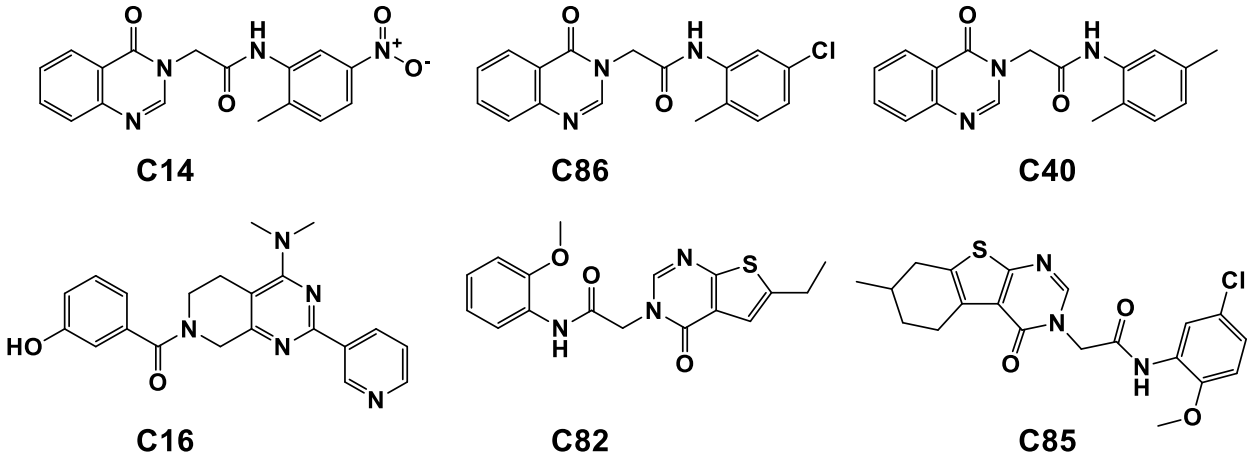

Figure 5.5: Structures of inhibitors of Mtb CdnP, which were identified from the HTS.

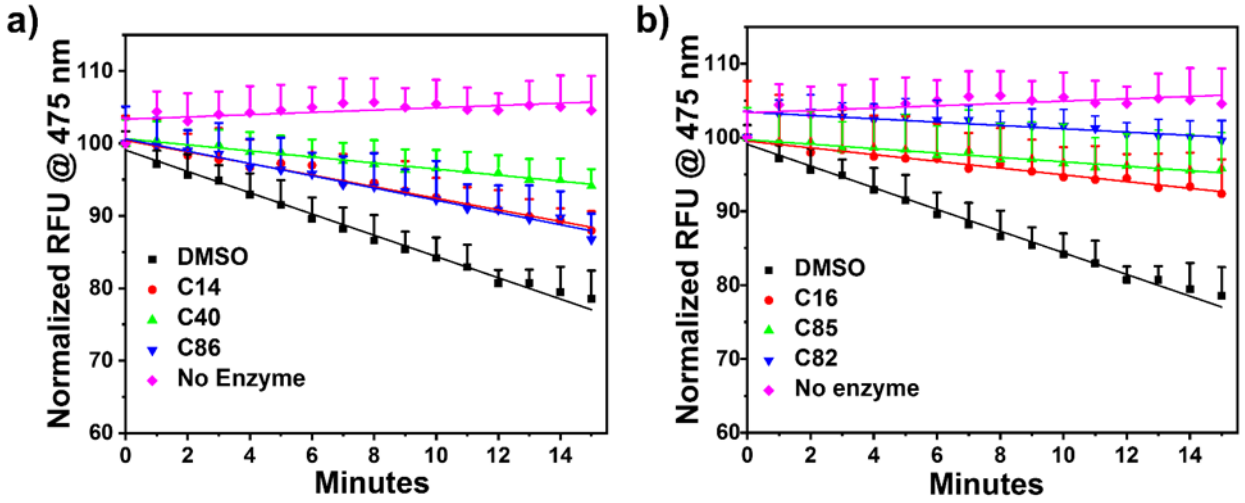

Figure 5.6: Mtb CdnP c-di-AMP hydrolysis in the presence of identified HTS hits visualized with the coralyne. a) Coralyne assay profiles of Mtb Cdnp hydrolysis kinetics in the presence of C14, C40, and C86 molecules. b) Coralyne assay profiles of Mtb Cdnp c-di-AMP hydrolysis kinetics in the presence of C16, C85, and C82 molecules. * Assay parameters: 10 µM compounds, 0.5 µM MTB Cdnp, 10 µM, 10 mM KI, 1x reaction buffer. Experiment conducted in triplicates at Conducted at 30 °C.

5.3.2 Confirmation of HTS hits.

Next, we ran HPLC based enzymatic reactions to confirm the putative CdnP inhibitors identified from the HTS. MTB CdnP was incubated with and without the hit compounds, reactions were quenched and then analyzed via liquid chromatography. The reactions were analyzed at two different time points (after 3 h and 12 h incubations). All of the compounds, save C16 and C40, showed substantial inhibition after 3 h incubation; C86, C82, and C14 showed the most potent

inhibitory effects (Figure 5.7a). Only C82 retained any inhibitory effect after an overnight incubation (Figure 5.7b) and thus we designated it as our most potent MTB CdnP inhibitor. The fact that C16, the only molecule lacking the N-phenyl-6-oxo-pyrimidine-1-carboxamide moiety did not show any activity after 3 h incubation indicates that this moiety is important for inhibitory activity. The lower enzymatic inhibition by C40, compared to C14 and C86, indicates that substituents of the phenyl ring impacts activity and hence provides a strategy to improve inhibitor potency in future optimization campaigns.

We further confirmed the inhibitory effects our hit compounds using comparative radioisotope thin layer chromatography (TLC). ^{32}P-c-di-AMP was made by incubating MTB DisA, a c-di-AMP synthase enzyme, with hot ATP (^{32}P-ATP) and cold ATP as previously reported.[235] MTB CdnP reactions were set up with varying inhibitor concentrations (20 to 150 μM), and c-di-AMP hydrolysis visualized via TLC. Ethylenediaminetetraacetic acid (ETDA) was used as a surrogate for a potent inhibitor. MTB CdnP enzymatic activity requires Mn^{2+} cofactor, hence divalent metal chelators such as ETDA can quench the reaction. Therefore, upon treatment with ETDA we expected c-di-AMP cleavage to be diminished. All compounds showed a concentration dependent inhibitory activity with C82 exhibiting the most potent inhibition (Figure 5.8 and Supplementary Information, Figure 5.9). C40 and C16 were the least potent compounds. C40 was the only compound that did not show any inhibitory effect at 20μM concentration (Figure 5.8). C16 exhibited very little inhibitory effect at 20μM (Figure 5.8). From the three complementary assays (coralyne, HPLC and TLC) we concluded that C82 was the most potent inhibitor. To confirm this, we also determined the IC50 of enzyme inhibition by compounds using the safer and more convenient coralyne assay. Consistent with the earlier data C82 was the most potent compound. C82, C85, C14, C40, C16 and C86 inhibited MTB Cdnp enzymatic activity (50 nM MTB Cdnp and 80 μM c-di-AMP) with IC50 values of 17.37 μM, 21.4 μM, 24.5 μM, 34.6 μM, 48.86 μM, and > 60 μM respectively (Figure 5.10).

5.3.3 Determining C82 mode of inhibition.

Next, we sought to determine C82 mode of inhibition. Firstly, we confirmed that C82 does indeed bind to MTB CdnP, using intrinsic fluorescence assay.[236] MTB CdnP intrinsic fluorescence decayed in C82 concentration dependent manner, confirming C82 does bind to MTB CdnP (Figure 5.11). We sought to determine if C82 could displace bound c-di-AMP from MTB Cdnp. To do

this, we incubated MTB Cdnp with radiolabeled c-di-AMP and tried to displace the bound cyclic dinucleotide with different concentrations of C82 using the DRaCALA assay .Whiles, unlabeled c-di-AMP could displace radiolabeled c-di-AMP from MTB Cdnp (Figure 5.12a), C82 even at 300 μM, did not displace radiolabeled c-di-AMP from the enzyme (Figure 5.12b). We also used a secondary fluorescent polarization displacement assay to confirm this finding. Briefly, fluorescent labeled c-di-GMP was incubated with MTB Cdnp and treated with different concentrations of C82, or c-di-AMP in the presence of calcium to inhibit the cleavage of the bound CDN.[76] Consistent with the DRACALA results, C82 did not displace the fluorescent labeled c-di-GMP, whiles the unlabeled c-di-AMP was able to displace fluorescent labelled c-di-GMP from MTB Cdnp in a concentration dependent manner (Figure 5.12c, d). We therefore concluded that C82 inhibits MTB Cdnp by binding to a non-cyclic dinucleotide binding site. Our kinetics studies reveal C82 is a mixed inhibitor (Figure 5.13) with an apparent inhibition constant of approximately 8 μM (Figure 5.14).

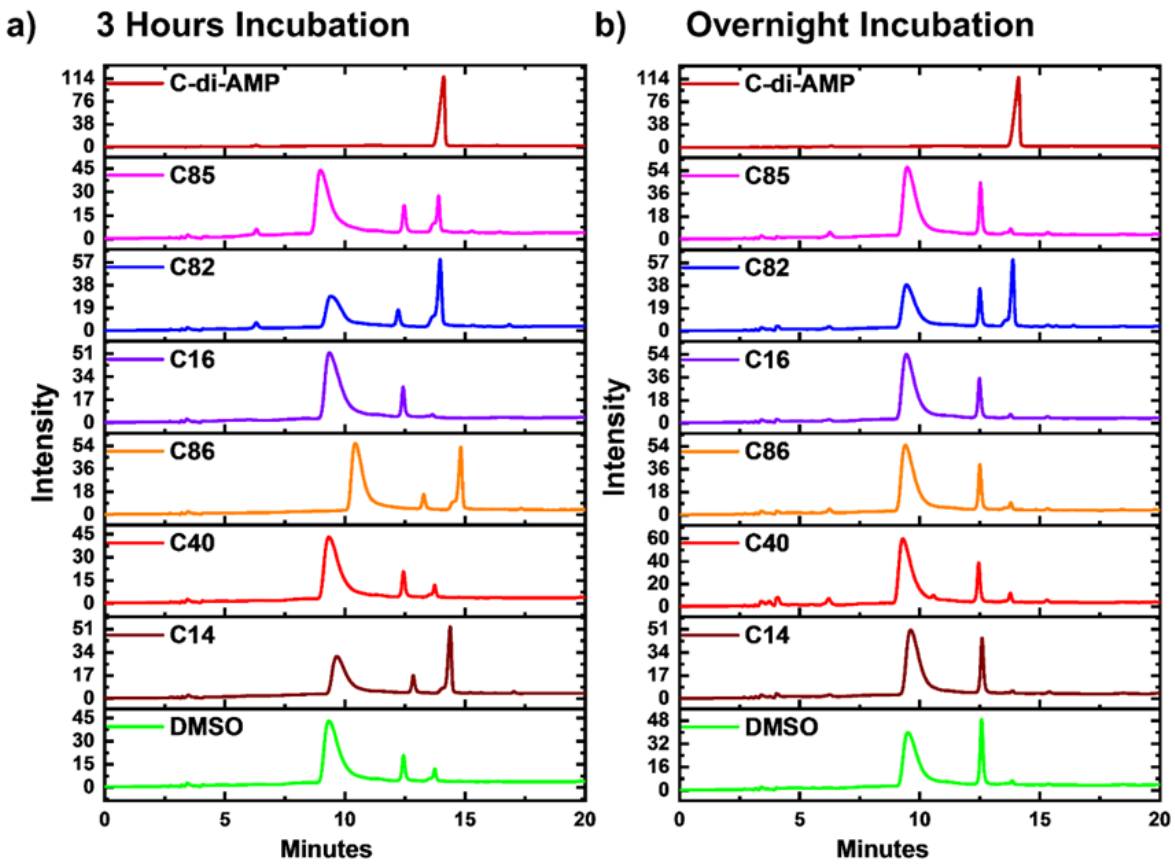

Figure 5.7: Inhibition of MTB CdnP enzymatic activity by compounds, analyzed via HPLC. a) HPLC profiles of C-di-AMP cleavage by Mtb CndP in the absence and presence of inhibitors after 3-hour incubation. b) HPLC profiles of C-di-AMP cleavage by Mtb CndP in the absence and presence of inhibitors after 12-hour incubation.

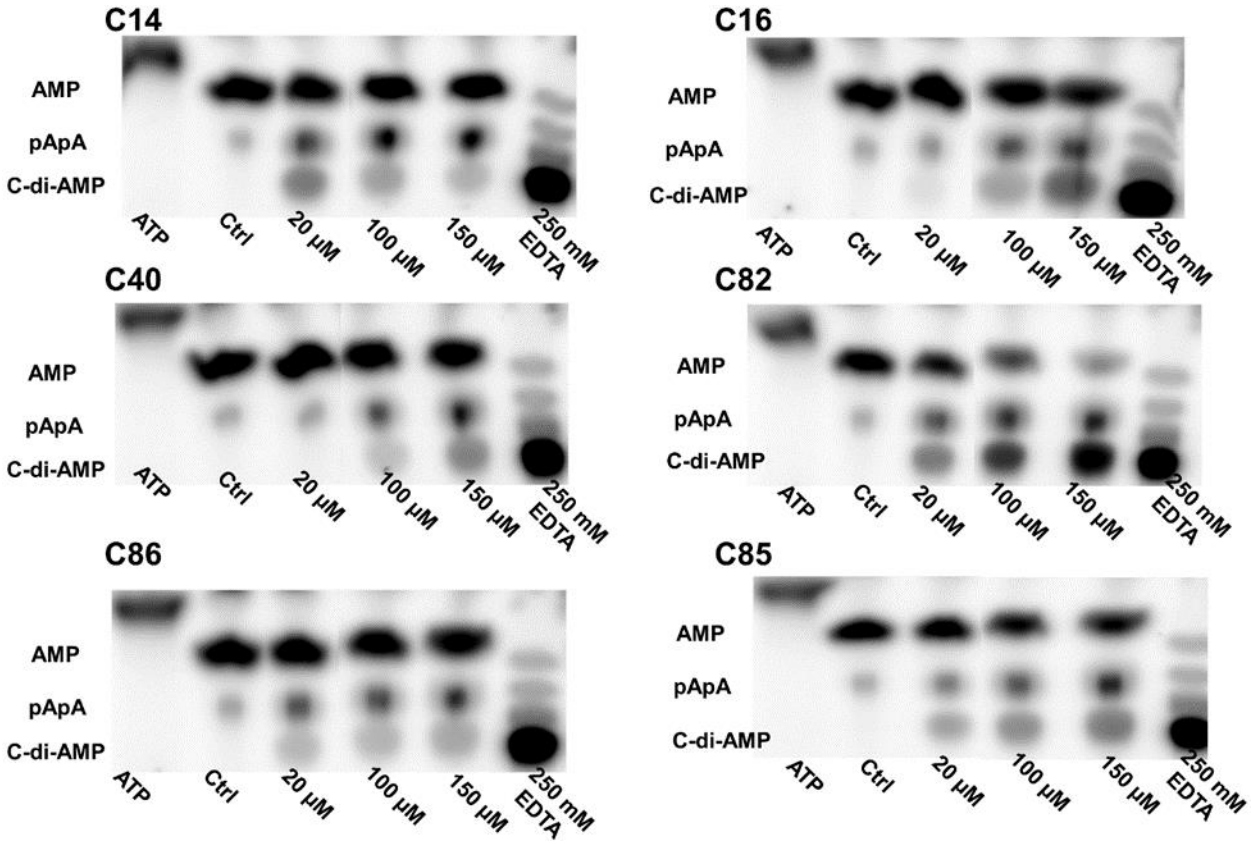

Figure 5.8: Inhibition of MTB CdnP enzymatic activity by compounds, analyzed via TLC. Visualization of c-di-AMP cleavage by 0.5 µM MTB CdnP in the presence and absence of varying hit compounds concentration. 'Ctrl'= control group treated with dimethyl sulfoxide (DMSO).

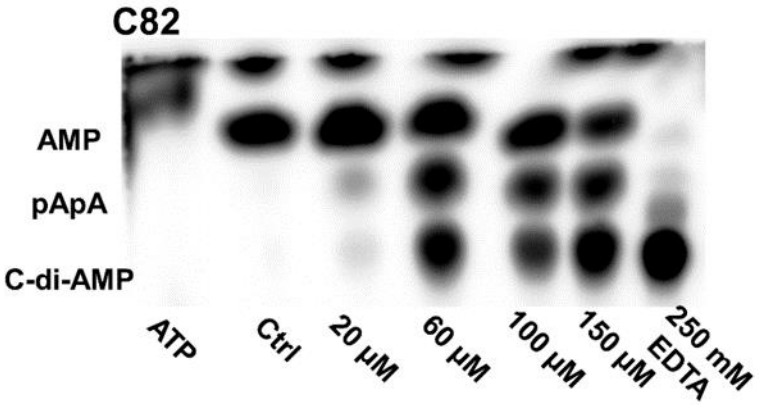

Figure 5.9: Visualization of C-di-AMP cleavage by 0.75 µM Mtb CndP in the presence of varying concentration of **C82.**

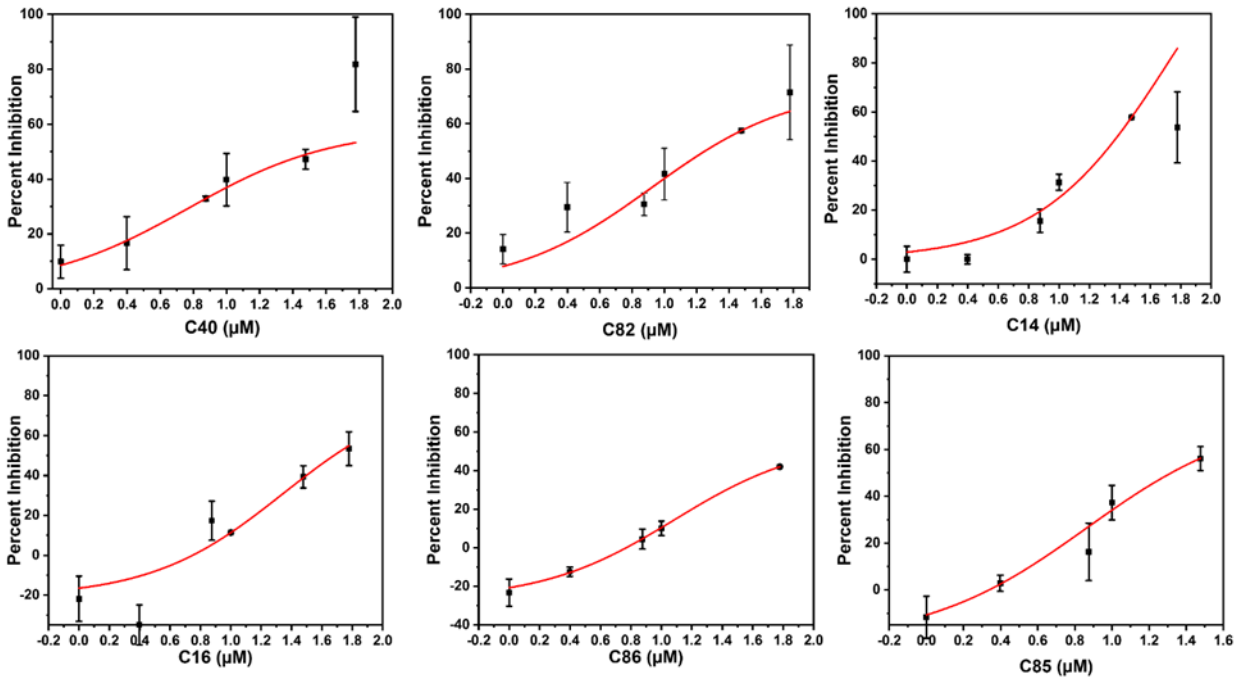

Figure 5.10: Concentration dependent Mtb CdnP inhibition by HTS hits quantified with the coralyne assay. Curves were generated with origin in-built dose response function with the slope factor constrained to 1. Experiment done in triplicates.

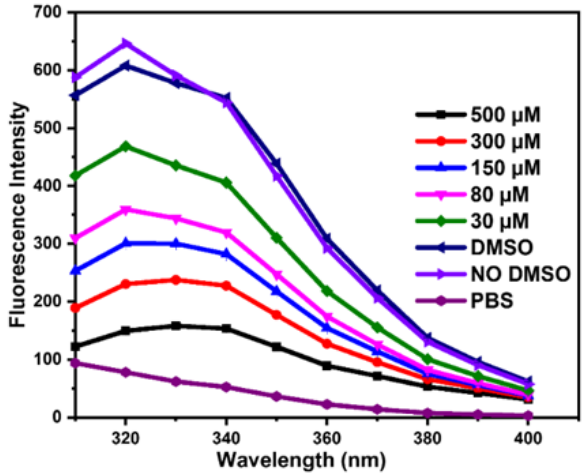

Figure 5.11: C82 effects on MTB CdnP intrinsic Fluorescence. Experiment conducted with 2 μM MTB CdnP in 1x PBS with varying C82 concentrations. Enzyme-compound mix was incubated at room temperature for 30 minutes before reading fluorescence emission in 310 nm-400 nm range following an excitation at 290 nm.

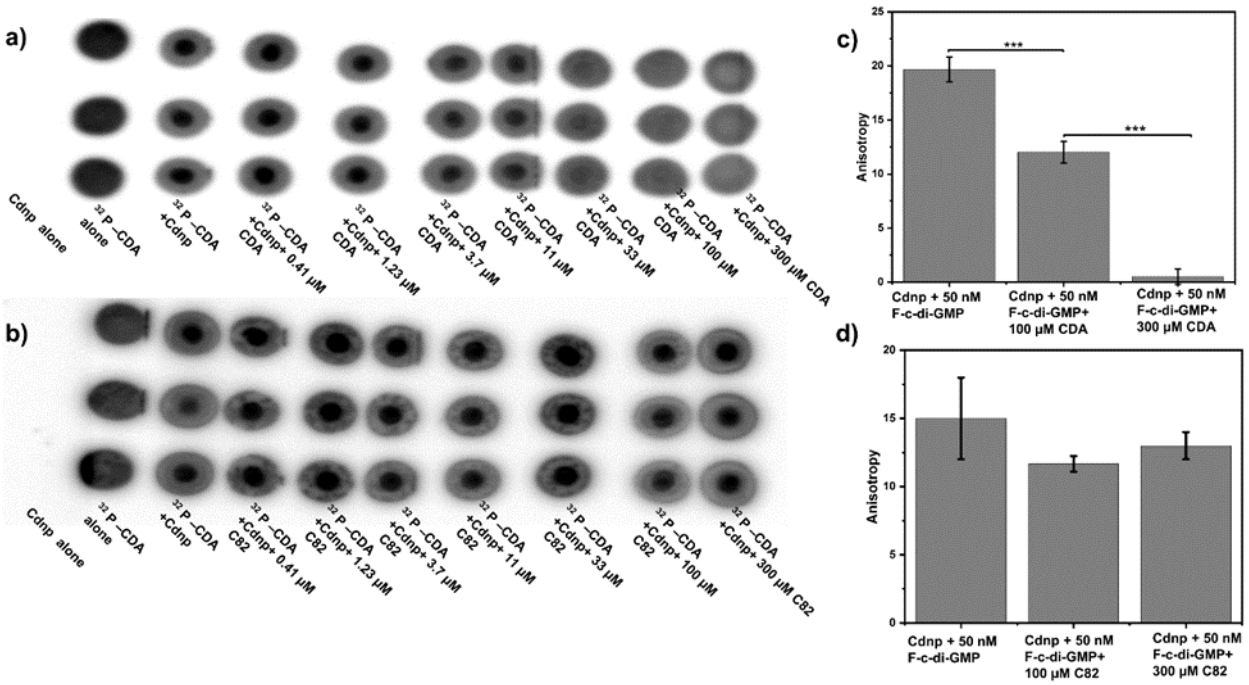

Figure 5.12: C82 does not displace c-di-AMP from MTB Cdnp. a) unlabeled c-di-AMP inhibits ^{32} P-c-di-AMP sequestering by MTB Cdnp in a concentration dependent manner. b) C82 effects on ^{32} P-c-di-AMP sequestering by MTB Cdnp. c) C-di-AMP significantly attenuates fluorescent c-di-GMP anisotropy in a concentration dependent manner. d) C82 does not attenuate fluorescent c-di-GMP anisotropy. CDA = c-di-AMP. *** = p- value < 0.001. Statistical analysis conducted using the student's t-test.

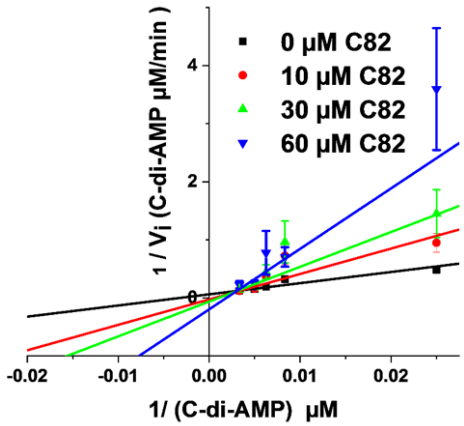

Figure 5.13: C82 lineweaver-Burk plot. Initial velocity was determined using slope of c-di-AMP hydrolysis kinetics.

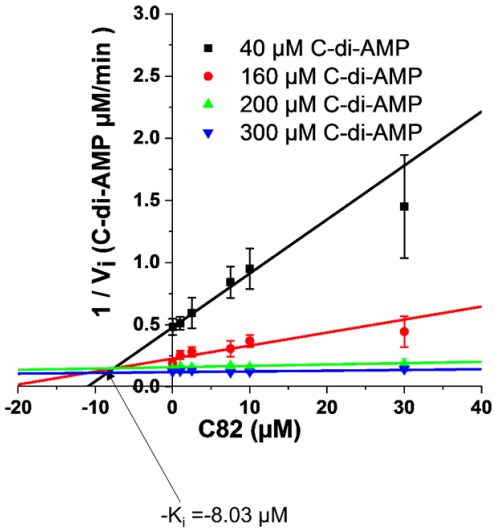

Figure 5.14: C82 Dixon plot. Initial velocity was determined using slope of c-di-AMP hydrolysis kinetics.

5.3.4 C82 selectivity.

We proceeded to investigate if C82 was promiscuous CDN phosphodiesterase (PDE) inhibitor. We screened C82 against three bacterial CDN PDEs (Ybt, RocR and GBS-CdnP), one mammalian CDN PDE, ENPP1 and poxin, a viral CDN PDE. Ybt is a *Bacillus subtilis* CDN PDE that degrades both c-di-AMP and c-di-GMP.[237] RocR is a *P. aeruginosa* c-di-GMP PDE and GBS-CdnP is Group B Streptococcus (GBS) c-di-AMP PDE.[77,238] GBS-CdnP, just like MTB CdnP, has been shown to dampen STING-dependent type I interferon induction.[77] Mammalian ENPP1, is capable of degrading both cGAMP and bacterial CDNs.[76] Consequently, ENPP1 is an excellent target for development of immunotherapy agents for both cancer and infections management. Poxins (poxvirus immune nuclease) are 2′ 3′-cGAMP-degrading enzymes, whose activities result in dampened STING-dependent signaling.[224] For selectivity studies, the assays conditions were optimized to ensure most of the substrate was not hydrolyzed. C82 did not inhibit any of these enzymes (Figure 5.15); thus C82 can be considered as MTB CdnP specific inhibitor (at least when compared to five other cyclic dinucleotide PDEs).

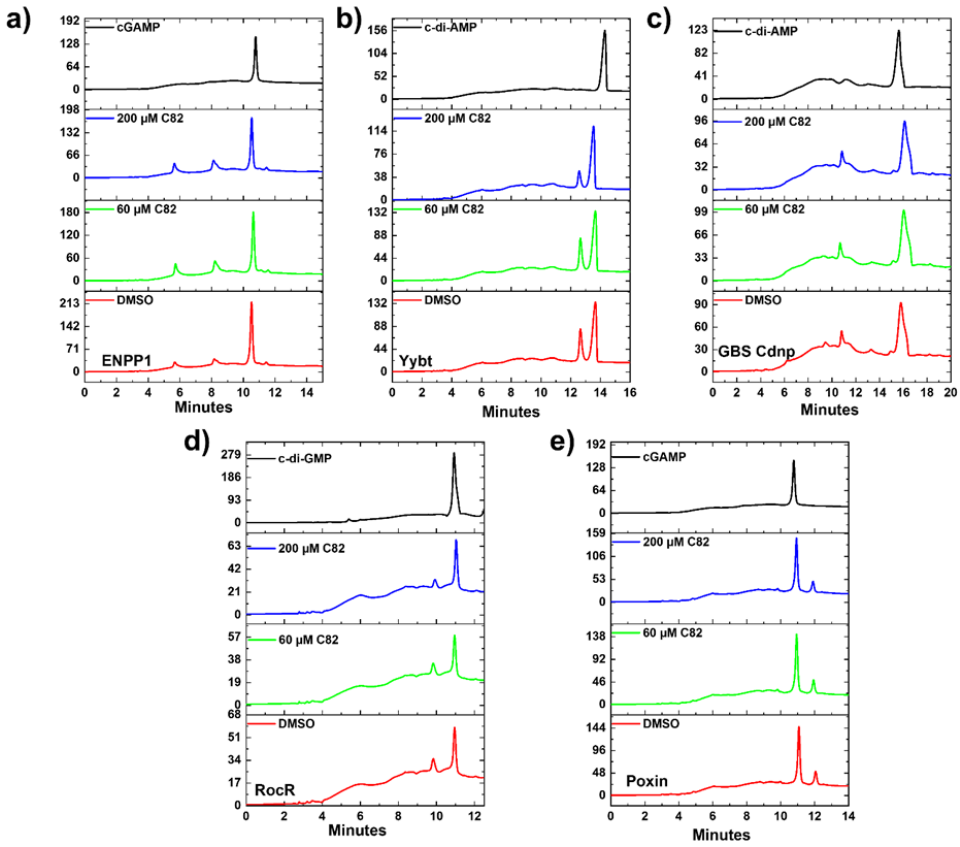

Figure 5.15: C82 activity against other CDN PDEs. a) ENPP1 cGAMP cleavage in the presence and absence of C82. b) Yybt c-di-AMP cleavage in the presence and absence of C82 c) GBS_CdnP c-di-AMP cleavage in the presence and absence of C82. d) RocR c-di-GMP cleavage in the presence and absence of C82. e) Poxin 2'3-cGAMP cleavage in the presence and absence of C82.

5.3.5 C82 cytotoxicity

Lastly, we evaluated C82 cytotoxicity against mammalian cells. Up to 100 μM, C82 did not significantly attenuate cell viability (Figure 5.16). This finding potentiates C82 as an ideal scaffold for development of MTB anti-virulence therapy.

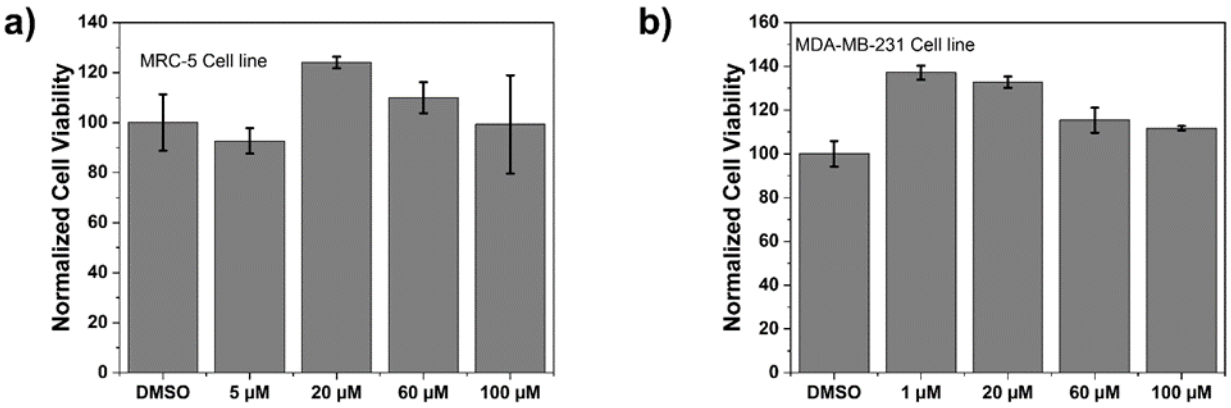

Figure 5.16: C82 cytotoxicity against mammalian cell lines. a) C82 cytotoxicity against MRC-5 cell line after 24 hours incubation with compound. b) C82 cytotoxicity against MDA-MB-231 cell line after 24 hours incubation with compound.

5.4 Concluding remarks

Due to the vital roles of CDNs in bacteria cell physiology and the modulation of the innate immune system, CDNs metabolizing enzymes are attractive therapeutic targets. Several inhibitors of bacterial CDN synthase enzymes have been reported. In contrast, only one non-nucleotide bacterial CDNs PDE inhibitor has been described. To fill in the gap, we embarked on the search of a MTB CdnP PDE inhibitor, which could be used as a tool compound or potential therapeutic. To our knowledge, this is the first report of non-nucleotide MTB CdnP PDE selective inhibitor. C82 and analogs thereof, which contain the 2-(4-oxothieno [2,3-*d*]pyrimidin-3(4*H*)-yl)acetamide or 2-(4-oxoquinazolin-3(4*H*)-yl)acetamide moieties, are excellent starting compounds to develop novel cyclic dinucleotide phosphodiesterase inhibitors

CHAPTER 6. A STING-BASED FLUORESCENT POLARIZATION ASSAY FOR MONITORING ACTIVITIES OF CYCLIC DINUCLEOTIDE METABOLIZING ENZYMES

6.1 Introduction

Cyclic dinucleotides are important signaling molecules in both prokaryotes and eukaryotes and the last decade has witnessed an upsurge in research activities related to these fascinating molecules and the enzymes that make or degrade dinucleotides as well as receptors that bind them.[239,240] Cyclic GMP-AMP synthase (cGAS) and stimulator of interferon genes (STING) are key players in the cGAS-STING pathway, and have emerged as potential drug targets for various disease states, such as viral and bacterial infections, ulcerative colitis, Crohn's disease and cancer.[241-243] The cGAS-STING pathway in higher organisms, which likely originated in bacteria,[244] is activated when cytosolic double stranded DNA (pathogen-derived or host-derived) promotes cGAS liquid phase separation and enzyme activity enhancement to produce 2'3- cGAMP (referred to as cGAMP hereafter), which is a noncanonical cyclic dinucleotide containing one 3'-5- and one 2'-5'-phosphodiester linkages.[67,245-247] cGAMP binds to dimeric STING, causing profound conformational change and inducing STING aggregation/polymerization, and subsequent TBK1 phosphorylation and activation of IRF3.[248-252] Interestingly, cGAMP also inhibits STING activation via a negative feed-back by triggering ULK1 phsphorylation of STING.[253] cGAS-STING signaling has been demonstrated to be pivotal for mediation of the innate immune recognition of infected cells and cancer cells.[254-257] Degradation of cGAMP has emerged as an immune evasion strategy employed by both viral and bacterial pathogens as well as cancer cells.[76,224,258] The central roles played by host's cGAMP synthase, cGAS, and cGAMP degrading enzymes (host's ENPP1 (Mammalian ectonucleotide pyrophosphate phosphodiesterase 1) or viral poxins) in diseased states have increased interests in finding inhibitors of these enzymes as potential therapeutics. For example patients who harbor TREX1 mutations that lead to loss of DNase activity, and hence are unable to degrade cytosolic DNA (cGAS activator), suffer various inflammatory pathologies.[259,260] Thus it is expected that inhibitors of cGAS could lessen cGAS-STING pathway activation/inflammation in such patients.[261,262] Inhibitors of ENPP1 or viral poxins are expected to boost the effects of native cGAMP[263] and could have applications in cancer immunotherapy[9] and anti-viral therapy.[8] bacterial C-di-GMP and c-di-AMP are also vital second

messengers regulating key various processes including virulence factor production, biofilm formation, resistance to antibiotics and metals, amongst many other processes.[239,264]Thus inhibitors of c-di-GMP and c-di-AMP synthases and phosphodiesterases are also highly sought after as potential new-generation anti-infectives.[265]

Cheap and reliable assays that could be used to monitor cGAS and cGAMP phosphodiesterases or c-di-GMP/c-di-AMP synthases or phosphodiesterases will undoubtedly facilitate the development of therapeutics that target cGAS-STING pathway or c-di-GMP/c-di-AMP mediated processes in bacteria. Thus far many strategies have been reported for the detection of cyclic dinucleotides or monitoring dinucleotide metabolism enzymes. For example, radioactive thin-layer chromatography (TLC) has been used to monitor cGAS or ENPP1 activities respectively, but this assay is not convenient due to cost, safety and environmental concerns.[67,266] Liquid chromatography-mass spectrometry (LC-MS)-based methods can also be used to monitor these enzymes but this method is low throughput. ELISA kits that utilize antibodies to detect cGAMP are commercially available but are expensive. Other methods such as RNA fluorescent c-di-GMP or c-di-AMP or cGAMP sensors,[267-269] pyrophosphatase-coupled assay,[270] cGAMP-luciferase assay[271] and BioSTING assay,[272] which utilizes FRET, have been described for monitoring cyclic dinucleotides, highlighting the high interests in identifying convenient methods to monitor the aforementioned critical enzymes in the cGAS-STING pathway. Whiles these prior developed assays/biosensors have facilitated cGAMP research, especially the fluorescent RNA and BioSTING biosensors, which are ideal for *in cellulo* assays, we found that these methods are not ideal for our interest in screening medium-to-high throughput libraries for cGAMP metabolizing enzymes inhibitors. In the past, we had revealed simple aggregation-based assays for detecting c-di-GMP[273] or c-di-AMP,[233] which we have used to identify inhibitors of c-di-AMP synthase via medium throughput screening.[89,92] Unfortunately, our aggregation-based assay is not ideal for monitoring enzymes that degrade cGAMP (our current interest). Thus we sought a more convenient, inexpensive and universal method to monitor the synthesis or degradation of all of the natural cyclic dinucleotides. Herein we disclose a simple method (Figure 6.1), which can be used to monitor the degradation or synthesis of any cyclic dinucleotide, which can bind to STING, using readily available fluorescently labeled cyclic dinucleotide probe. We anticipate that others will find this assay useful for their screening campaigns.

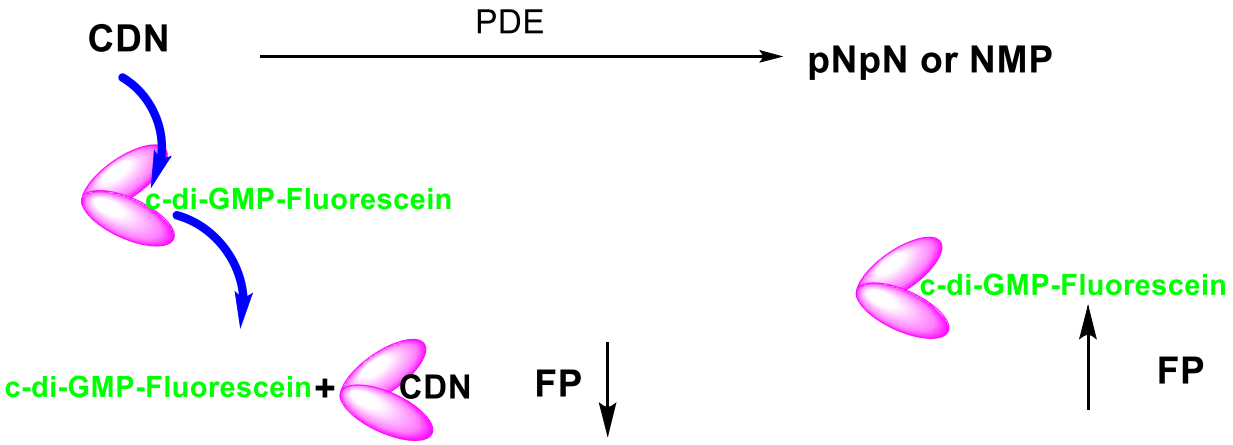

Figure 6.1: Schematic illustration of the working principle of hSTING competitive fluorescence polarization assay. PDE= phosphodiesterase, FP = fluorescence polarization, CDN = Cyclic dinucleotide. pNpN = linear dinucleotide. NMP = nucleoside monophosphate. N= nucleoside

6.2 Experimental Section

6.2.1 hSTING expression and purification.

hSTING plasmid was a gift from Pingwei Li.[274] hSTING plasmid (PET28a, SUMO) transformed into Novagen's E.coli Rosetta™2(pLysS) cells using chloramphenicol (50 µg/mL) and kanamycin (50 µg/mL) as selection agents. A single colony was then inoculated in 10 mL LB broth supplemented with selection agents. followed by incubation at 37 °C for 12 hours. The next day, the 10 mL culture was inoculated into 1L terrific broth supplemented with selection agents and grown to exponential phase (OD 600 = 0.6) by incubation at 37 °C. 1 mM was added to the culture and temperature lowered to 25 °C to induce protein expression (incubated at 25 °C for 18 hours). The cells were then pelleted by centrifugation at 5000 rpm for 20 min. The pellet was resuspended in 25 mL lysis buffer containing 50 mM Na_3PO_4 (pH=7.4), 1x Roche's inhibitor cocktail, 300 mM NaCl, 1 mM phenylmethylsulfonyl fluoride, 20 mM imidazole, 10 % glycerol, and 5 mM mercaptoethanol, followed by lysis via sonication. The lysates were then centrifuged at 22,000 rpm for 25 min. The supernatant was ran through a His trap Nickel column and hSTING protein eluted with lysis buffer supplemented with 300 mM imidazole. hSTING was dialyzed overnight to using a buffer containing 300 mM NaCl, 50 mM Na_3PO_4, 5 mM mercaptoethanol, and 10% glycerol (pH=7.4). Protein was quantified using UV absorbance at 280 nM.

6.2.2 Poxin expression and purification

Poxin plasmid was a gift from Philip J. Kranzusch.[224] The plasmid was transformed into Novagen's E.coli Rosetta™2(pLysS) cells using kanamycin (50 µg/mL) and chloramphenicol (50 µg/mL) as selection agents. The enzyme was expressed and purified as described above. Using 30 mM imidazole, 20 mM Hepes-KOH, 10% glycerol, 1M NaCl, and 1 mM DTT (pH=7.5) as wash buffer. Wash buffer supplemented with 400 mM NaCl, and 300 mM imidazole as elution buffer and wash buffer supplemented with 30 mM imidazole as dialysis buffer.

6.2.3 DisA expression and purification

DisA plasmid was a gift from Karl-Peter Hopfner.[275] DisA plasmid (PET28a) was transformed into Novagen's E.coli BL21 (DE3) cells using kanamycin (50 µg/mL). The enzyme was expressed and purified as described above. Using 25 mM Tris-HCl, 10% glycerol, 500 mM NaCl, and 50 mM imidazole pH=8.2 as wash buffer. Wash buffer supplemented with 200 mM imidazole as elution buffer and wash buffer containing no imidazole as dialysis buffer.

6.2.4 WspR expression and purification

WspR plasmid was a gift from WspR plasmid (pVL1394) was a gift from Md A Motaleb.[276] The plasmid transformed into Novagen's E. coli BL21 (DE3) cells using carbenicillin (100 µg/mL). Wash buffer, elution buffer and dialysis buffer same as the buffers used for DisA purification.

6.2.5 hSTING titration

All four probes were purchased from Biolog. F-cGAMP-A = Cyclic (guanosine- (2' −> 5')-monophosphate- 2'- O- (6- [fluoresceinyl]aminohexylcarbamoyl)adenosine- (3' −> 5')-monophosphate) sodium salt. F-cGAMP-B = Cyclic (8- (2- [fluoresceinyl]aminoethylthio)-guanosine- (2' −> 5')- monophosphate- adenosine- (3' −> 5')- monophosphate) (c[8-Fluo-AET-G(2',5')pA(3',5')p]), sodium salt. F-c-di-GMP = 2'- O- (6- [Fluoresceinyl]aminohexylcarbamoyl)- cyclic diguanosine monophosphate (2'-Fluo-AHC-c-diGMP), sodium salt. F-c-di-AMP = 2'- O- (6- [Fluoresceinyl]aminohexylcarbamoyl)- cyclic diadenosine monophosphate (2'-Fluo-AHC-c-diAMP), sodium salt.

50 nM probe was incubated with various concentrations of hSTING in 1x Phosphate Buffered Saline for 5 min at room temperature and fluorescence polarization (excitation 485 nm / 20 and emission 528 nm / 20) detected with Biotek Cytation 5 multi-mode reader. Anisotropy was calculated using the Gen 5 ^{TM} microplate reader and imaging software. Anisotropy was normalized by equating measurements of the 0 µM hSTING group to zero. Experiment was done in triplicates using a 384 fluorometric plate.

6.2.6 Probes displacement assays

50 nM F-c-di-GMP was incubated with 20 µM hSTING and different concentrations of cGAMP for 5 min at room temperature and Anisotropy determined as described above. Anisotropy was normalized by equating measurements of 0 µM cGAMP group to 100. Experiment was done in triplicates using a 384 fluorometric plate.

6.2.7 ENPP1 cGAMP hydrolysis tracking

A reaction was set up containing 50 µM cGAMP, and 9.16 nM hENPP1(purchased from R&D Systems (Minneapolis, Minnesota)) using the reaction buffer recommended by the manufacturer (50 mM Tris and 250 mM NaCl, pH 9.5). At specific time points, 90 µL was drawn from the reaction, reaction stopped by heat denaturation and cGAMP concentration detected via the FP assay and HPLC analysis. For FP detection, 35 µL of the reaction was mixed with 10 µM hSTING, 50 nM F-c-di-GMP and topped to 70 µL with 1x Phosphate Buffered Saline. The Mix was incubated for 5 min at room temperature. 20 µL of the mix was aliquoted into each well of the 384 fluorometric plate and anisotropy determined as described above. Anisotropy was normalized by equating measurements at time zero group to zero. Experiment was done in triplicates using a 384 fluorometric plate. 50 µL of the reaction was subjected to HPLC analysis using a COSMOSIL C18-MS-II Packed column (mobile phase = 0.1 M TEAA, 100% acetonitrile). Gradient is as follows: 0 – 16 minutes: 99 % - 87 % 0.1 M TEAA, 1% -13% acetonitrile, 16 – 23 minutes: 87 % - 10 % 0.1 M TEAA, 13 % -90 % acetonitrile, 23 – 25 minutes: 10 % - 99 % 0.1 M TEAA, 90 % -1 % acetonitrile, 25 -30 minutes: 10 % - 99 % 0.1 M TEAA, 90 % -1 % acetonitrile. Nucleotides were detected by measuring absorbance at 260nm.

6.2.8 Poxin cGAMP hydrolysis tracking

A reaction was set up containing 50 µM cGAMP, and 5 nM poxin using the reaction buffer (50 mM HEPES-KOH, 1 mM DTT and 35 mM KCl pH 7.5). At specific time points, 90 µL was drawn from the reaction, reaction stopped by heat denaturation and cGAMP concentration detected via the FP assay and HPLC analysis. FP detection and HPLC analysis were conducted as described above.

6.2.9 WsPR c-di-GMP synthesis detection with FP assay

A reaction was set up containing 100 µM GTP, and 11 µM WsPR in WsPR buffer (10 mM Tris-HCl, 5mM $MgCl_2$, and 100 mM Nacl pH 7.5) and incubate at 37^{o}C for 16 h. The reaction was stopped by incubating at 95^{o}C for 5 min. C-di-GMP synthesis was detected using 10 µM hSTING and 50 nM F-c-di-GMP in a 96 well fluorometric plate.

6.2.10 WsPR c-di-GMP synthesis detection with HPLC

A reaction was set up containing 100 µM GTP, and 11 µM WsPR in WsPR buffer (10 mM Tris-HCl pH 7.5, 100 mM Nacl, and 5mM $MgCl_2$). Incubated overnight at 37^{o}C. The reaction was stopped by incubating at 95^{o}C for 5 minutes. 100 µL of reaction was filtered in an ultrafree centrifuge filter and subjected to the HPLC analysis. Conditions for HPLC detection was the same as described in the hydrolysis tracking of ENPP1.

6.2.11 DisA c-di-AMP synthesis detection with FP assay

A reaction was set up containing 100 µM ATP, 1 µM DisA in DisA buffer (40 mM Tris-HCl, 10mM $MgCl_2$ and100 mM NaCl pH 7.5). and incubate at 37^{o}C for 16 h. FP detection is as described for WsPR.

6.2.12 DisA c-di-AMP synthesis detection with HPLC

A reaction was set up containing 100 µM ATP, and 1 µM DisA in DisA buffer (40 mM Tris-HCl pH 7.5, 100 mM Nacl, and 10mM $MgCl_2$) and incubate at 37^{o}C for 16 h. HPLC detection conditions for DisA was the same as WsPR.

6.2.13 Emission spectrum of fluorescent probes

F-cGAMP-A, F-cGAMP-B, F-c-di-GMP and F-c-di-AMP at a concentration of 12.5 nM in 200 µL 1x phosphate-buffered saline (PBS) was used for the emission spectra. The excitation was done at 480 nm and fluorescence detected in 510 nm - 600 nm range.

6.2.14 Data analysis

Curves were generated with origin software using in-built nonlinear functions or stimulated with equation 6.3.

6.3 Results and Discussion

6.3.1 F-c-di-GMP is an ideal probe for hSTING FP assay

STING has a high affinity for cyclic dinucleotides and secondly fluorescence polarization has been demonstrated to be a robust technique to probe protein-ligand interactions.[277-279] Thus we rationalized that an appropriately fluorescent-labeled cyclic dinucleotide could be used to monitor the presence of unlabeled cGAMP via competition for STING binding (as shown in Figure 6.1). STING can be readily expressed in E. coli,[249] so a fluorogenic displacement assay using STING could be cheaper to perform than previously described assays for detecting cyclic dinucleotides (such as cGAMP), which use monoclonal antibodies.[280] Additionally, since STING can also bind to other CDNs (c-di-GMP and c-di-AMP), we reasoned that a STING-based fluorescent polarization assay could be readily adapted to monitor CDN metabolizing enzymes whereas the monoclonal antibody approach would generally require specific antibodies for each dinucleotide. The working principle of the assay is illustrated in Figure 6.1. In the presence of STING binding CDNs the fluorescence polarization of the probe is low owing to the fact unlabeled cyclic dinucleotide displaces the probe from hSTING. However, following the addition of a cyclic dinucleotide degrading enzyme such as ENPP1 or viral poxin, there would be an increase in the fluorescence polarization as time progresses. As time progresses, the unlabeled cyclic dinucleotide is degraded and concentration decreases allowing the labeled probe to bind STING leading to increase in fluorescence polarization. The converse will be true for a cyclic dinucleotide synthase, which would increase the amount of cGAMP or c-di-GMP or c-di-AMP, which would compete

with the fluorescent probe to decrease signal. Thus, the assay is a universal one for monitoring enzymatic dynamins of either CDN synthase or phosphodiesterase.

At the onset of the project, it was not clear how modification with a fluorophore would affect STING binding. The binding constants for the natural cyclic dinucleotides for hSTING are: K_d for cGAMP is 3.79 nM; K_d for c-di-GMP is 1210 nM and K_d for c-di-AMP is 1382 nM.[9] Because cGAMP has an ultra-potent affinity for STING, we rationalized that even if modification reduced binding affinity, there could still be some affinity for STING left for practical detection. Thus, we selected two labeled cGAMP probes, where the fluorescein modifications were at the 2'-position of adenosine (F-cGAMP-A) and at the C8-position of guanosine (F-cGAMP-B) (Figure 6.2).We were however aware that the crystal structure of cGAMP bound to STING indicates cGAMP makes intimate contacts with the protein residues and also the ligand is bound in the closed conformation whereby cGAMP is engulfed by the protein.[248,281] Therefore there was a high probability that any modification of cGAMP would drastically reduce STING binding. C-di-AMP or c-di-GMP on the other hand bind to STING in the open conformation and we hypothesized that c-di-GMP would better tolerate fluorescein modification at the 2'-OH (see F-c-di-GMP and F-di-AMP, Figure 6.2) than any modifications to cGAMP.[282,283] This hypothesis was supported by literature precedence, whereby Wu et al. showed that c-di-GMP that was modified at the 2'-OH position with a bulky glycopeptide could still activate STING.[284]

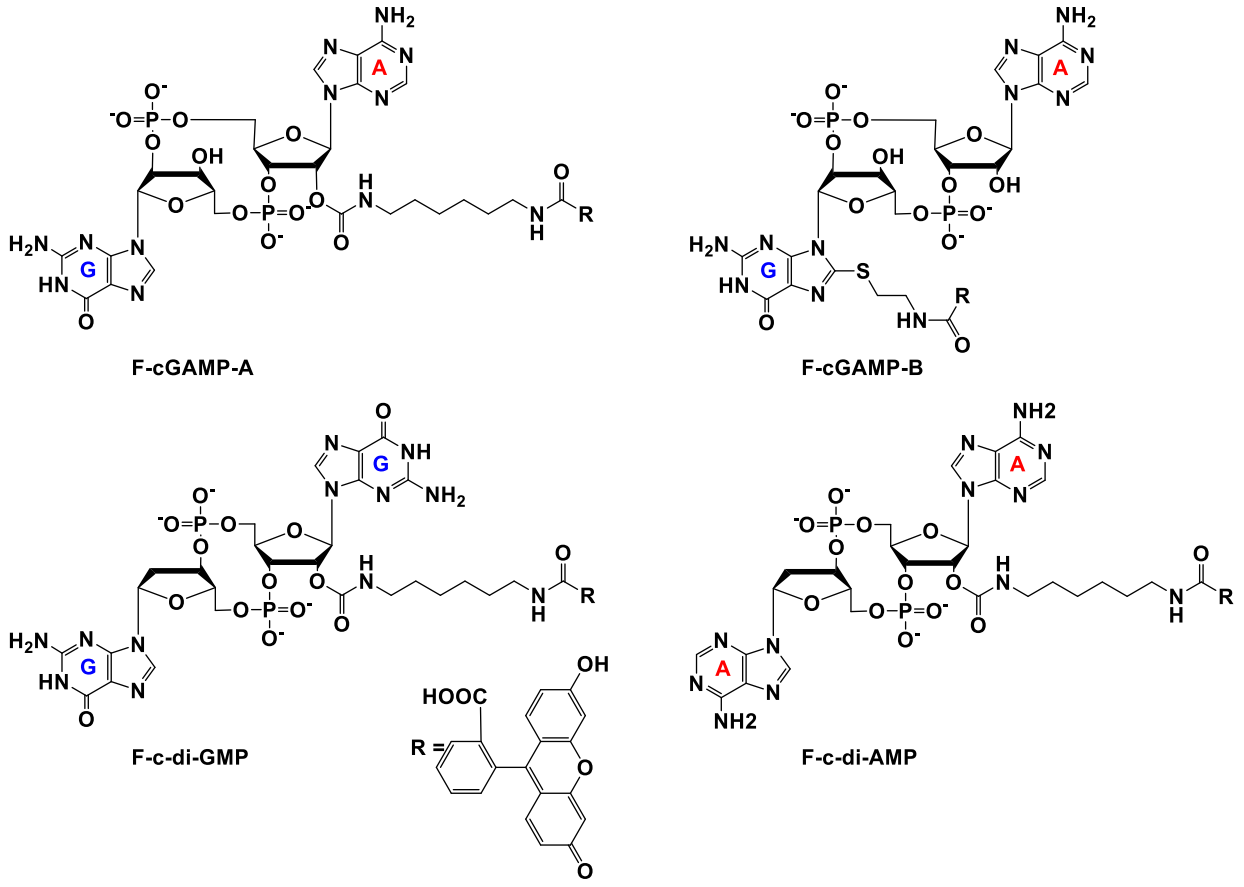

Figure 6.2: Structures of fluorescein labeled cyclic dinucleotide used in this work

To identify the ideal probe for the assay, we investigated which of the four fluorescein labeled cyclic dinucleotide probes bound hSTING best by titrating each probe (50 nM) with different concentrations of hSTING and measuring fluorescence polarization (FP). Fluorescence polarization measurements were then converted into fluorescence anisotropy using Equation 6.1.[285]

$$r = \frac{I\parallel - I\perp}{I_T} \qquad \text{Equation 6.1}$$

Where $I \parallel$ and $I \perp$ represents intensity of the parallel emission and perpendicular emission respectiviely and I_T is total intensity. To rank the binding affinities of the probes, anisotropy was converted to fraction bound (equation 6.2)[286] and the dissociation constant (K_d) of each probe evaluated.

$$F_{bound} = \frac{r - r_{free}}{(r_{bound} - r)Q + (r - r_{free})} \qquad \text{Equation 6.2}$$

Where r is anisotropy at a specific hSTING concentration, r_{free} is anisotropy of free ligand, r_{bound} is the anisotropy of hSTING-probe at saturation and Q is the ratio of fluorescence intensities of bound versus free ligand. Fraction bound versus hSTING concentration curves were generated using equation 3 (Figure 6.3a-d).[287,288]

$$FB = \frac{1}{1+(Kd/(R-0.5(L+R+Kd)-((L+R+Kd)^2-4*R*L)^{0.5}))} \quad \text{Equation 6.3}$$

Where FB is fraction bound, Kd is the dissociation constant, R and L represents protein and probe concentration.

Despite possessing the lowest emission intensity, F-c-di-GMP is the best hSTING binder with a K_d of 3.45 ± 0.48 µM, whiles F-c-di-AMP is the weakest hSTING binder with a K_d of 29.8 ± 6.3 µM (Figure 6.3**,** Figure 6.4 and Figure 6.5). In spite of the fact that F-cGAMP-B binds hSTING slightly better than F-cGAMP-A, F-cGAMP-A exhibits a higher signal range than F-cGAMP-B. High anisotropy is observed in the F-cGAMP-A group compared to F-cGAMP-B (Figure 6.4a-b). This phenomenon is likely due to guanine quenching the fluorophore in F-cGAMP-B, which is attached to guanine via a short linker; guanine is a known fluorescence quencher.[289] Expectedly, F-cGAMP-B emission intensity is lower than that of F-cGAMP-A (Figure 6.5).

We picked F-c-di-GMP as our ideal probe since it has the highest binding affinity to STING, compared to the other fluorescein-labeled probes. Next, we sought to determine if unlabeled cyclic dinucleotides could displace F-c-di-GMP from hSTING. Displacement of the probes from STING would lead to a decline in anisotropy, brought about by the increase in the concentration of free fluorescent ligands. As expected unlabeled cyclic dinucleotides displaced F-c-di-GMP in a concentration dependent manner with apparent IC_{50} of 8.95±0.54 µM (cGAMP), 7.41±0.49 µM (c-di-GMP), and 7.35±0.86 µM (c-di-AMP) (Figure 6.6 a-c). These findings illustrate our assay could be used to track enzymatic dynamics of cyclic dinucleotide metabolizing enzymes. Consequently, we proceeded to investigate if our assay could track the progresses of cGAMP degradation by two enzymes: ENPP1 and poxin.

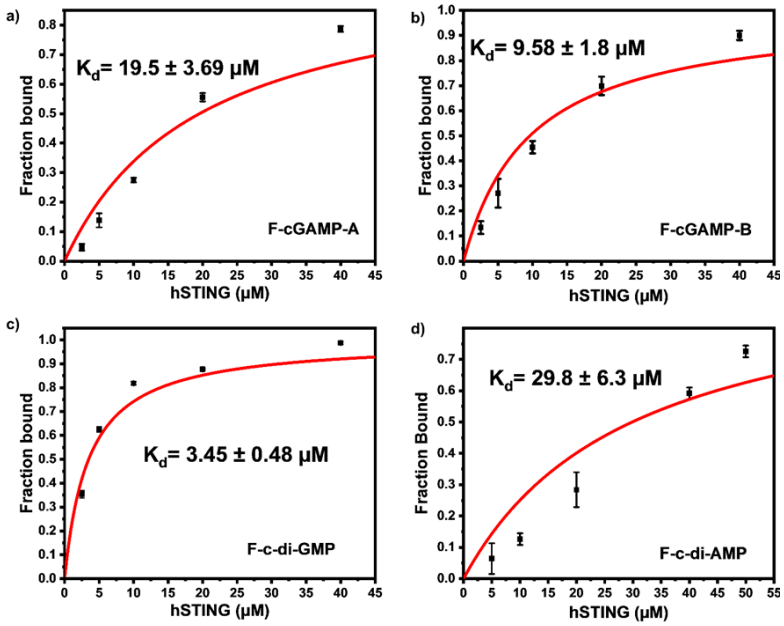

Figure 6.3: F-c-di-GMP is an ideal probe for hSTING fluorescence polarization competitive assay. Fraction bound versus concentration of STING of a) F-cGAMP-A; b) F-cGAMP-B; c) F-c-di-GMP; d) F-c-di-AMP. Error bars represents the standard deviation. Experiment done in triplicates.

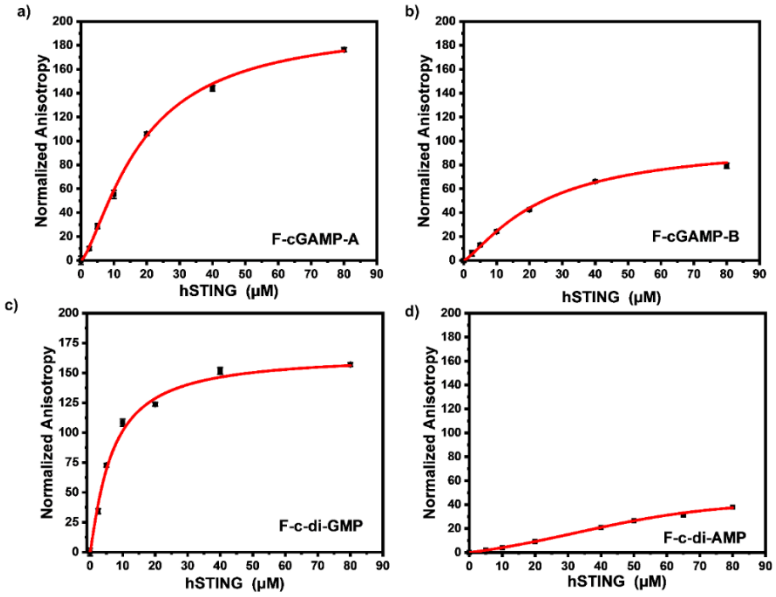

Figure 6.4: hSTING titration curves in the presence of different probes. a) hSTING titration in the presence of F-cGAMP-A. b) hSTING titration in the presence of F-cGAMP-B. c) hSTING titration in the presence of F-c-di-GMP. d) hSTING titration in the presence of F-c-di-AMP. Curves generated with origin in-built dose response function. * Wilson W.S. Ong helped produce figure 6.3 d

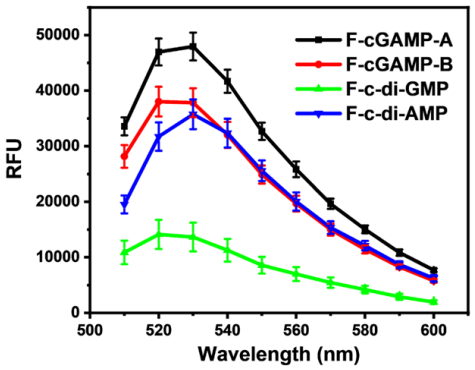

Figure 6.5: F-cGAMP-A and F-cGAMP-B emission spectra. Emission spectra generated using 12.5 nM probe in 1x PBS. Excitation: 480/20 nm. Error bars = standard deviation. Experiment done in triplicates.

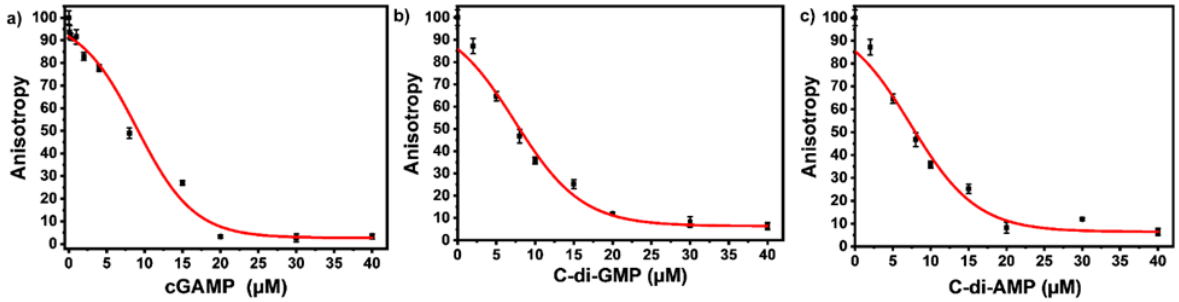

Figure 6.6: Displacement of F-c-di-GMP with unlabeled cyclic dinucleotides. a) Displacement using cGAMP. b) Displacement using c-di-GMP. c) Displacement using c-di-GMP. 50 nM F-c-di-GMP and 10 μM hSTING used for all three displacement experiments. Curves generated with origin in-built dose response function. * Wilson W.S. Ong helped produce figure 6.6 c

6.3.2 Monitoring ENPP1 hydrolysis of cGAMP with hSTING competitive assay

ENPP1 hydrolyzes cGAMP into GMP and AMP, which both do not bind hSTING. Hence, we hypothesized that our assay could be used to monitor ENPP1 hydrolysis of cGAMP. We conducted a time trace experiment whereby ENPP1 reactions were stopped by heat denaturation after a specific time and cGAMP concentration detected with the FP assay and via liquid chromatography analysis (HPLC). Since ENPP1 cGAMP hydrolysis end products, AMP and GMP, do not bind to hSTING fluorescence anisotropy is expected to increase as a function of time. As expected, anisotropy increased with time (Figure 6.7a). More importantly, the assay correlated with the HPLC analysis (Figure 6.7b and c). At time zero, anisotropy is almost zero indicating probe is not binding to hSTING due to the high concentration of unlabeled cGAMP as evident in the HPLC trace for time zero (Figure 6.7a and b). As time progress, cGAMP is hydrolyzed by

ENPP1, which leads to an increase in FP and decrease of the cGAMP peak in the HPLC traces. After 30 minutes, there is no significant change in anisotropy, an indication that most of the cGAMP is hydrolyzed (Figure 6.7a). This observation roughly correlates with the HPLC traces, which also indicate that over 70% of the reaction cGAMP is hydrolyzed within 30 min (Figure 6.7b).

6.3.3 Monitoring poxin hydrolysis of cGAMP with hSTING competitive assay

Poxin is a metal-independent nuclease conserved in most *Orthopoxvirus* viruses that cleaves cGAMP to inhibit hSTING signaling.[224] Poxin degrades cGAMP into linear Gp[2′–5′]Ap[3′], which does not bind hSTING.[224] Thus poxin cleavage of cGAMP could also be monitored with hSTING competitive fluorescence polarization assay. To test this, poxin reactions were set up and after a specific time the reaction was stopped by heat denaturation and cGAMP concentration detected with our assay and via HPLC analysis. Just as in the case of ENPP1, the assay trend agreed with the HPLC analysis. Both the hSTING assay and the HPLC show poxin degraded most of the cGAMP within 50 min (Figure 6.8). After 50 min, there is no significant change in the anisotropy measurements (Figure 6.8a and c**)**. Similarly, there is no significant change in both cGAMP and poxin product peaks after 50 min as visualized in the HPLC traces (Figure 6.8b).

6.3.4 Monitoring the synthesis of c-di-GMP and c-di-AMP with hSTING competitive assay

Our group is also interested in identifying compounds that inhibit c-di-GMP or c-di-AMP synthesis in bacteria. Thus, we sought to determine if the FP assay could also track the synthesis of c-di-AMP or c-di-GMP. We set up reactions with WspR (c-di-GMP synthase)[290] and DisA (c-di-AMP synthase)[275] and probed them with the FP hSTING competitive assay and with HPLC. After incubation, reactions were stopped by heat denaturing and half analyzed with the hSTING assay and the other half subjected to HPLC analysis. As expected, due to presence of CDNs, anisotropy was significantly lower for reactions containing both WspR and DisA compared to reactions that did not contain the synthases (Figure 6.9). To confirm the low anisotropy was indeed a result of displacement by unlabeled c-di-AMP or c-di-GMP, we obtained HPLC traces of both

the DisA and WspR reactions. Both enzymes synthesized each respective cyclic dinucleotide (Figure 6.10a-b and Figure 6.11a-b).

a)

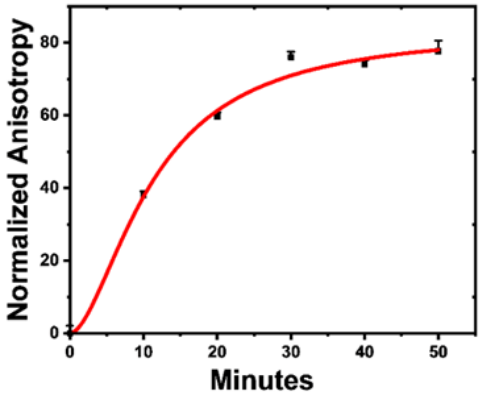

b)

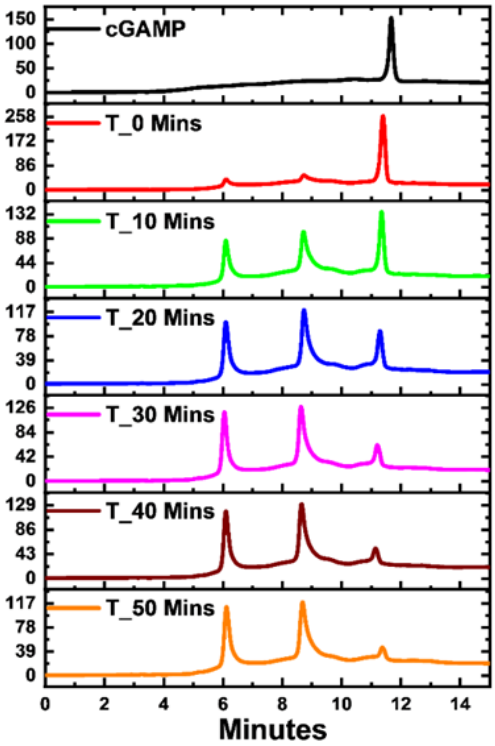

c)

Minutes	cGAMP percent cleavage	
	FP Assay	HPLC
0	0	0
10	49	44
20	77	56
30	98	72
40	95	76
50	100	85

Figure 6.7: hSTING fluorescence polarization competitive assay can track ENPP1 cGAMP hydrolysis. a) Time trace anisotropy of ENPP1 reactions. Curve generated with origin in-built hill function. b) HPLC Time trace of ENPP1 reactions. c) cGAMP percent cleavage at specific time points quantified with either FP assay or HPLC analysis. cGAMP percent cleavage was calculated by assuming anisotropy after 50 min represented 100% cleavage for the FP assay. For HPLC analysis, peak area of cGAMP at time zero was used to normalize cGAMP signal in all the time points then percent cleavage was computed by subtracting the normalized peak area from 100. * Kofi S. Yeboah helped in data collection.

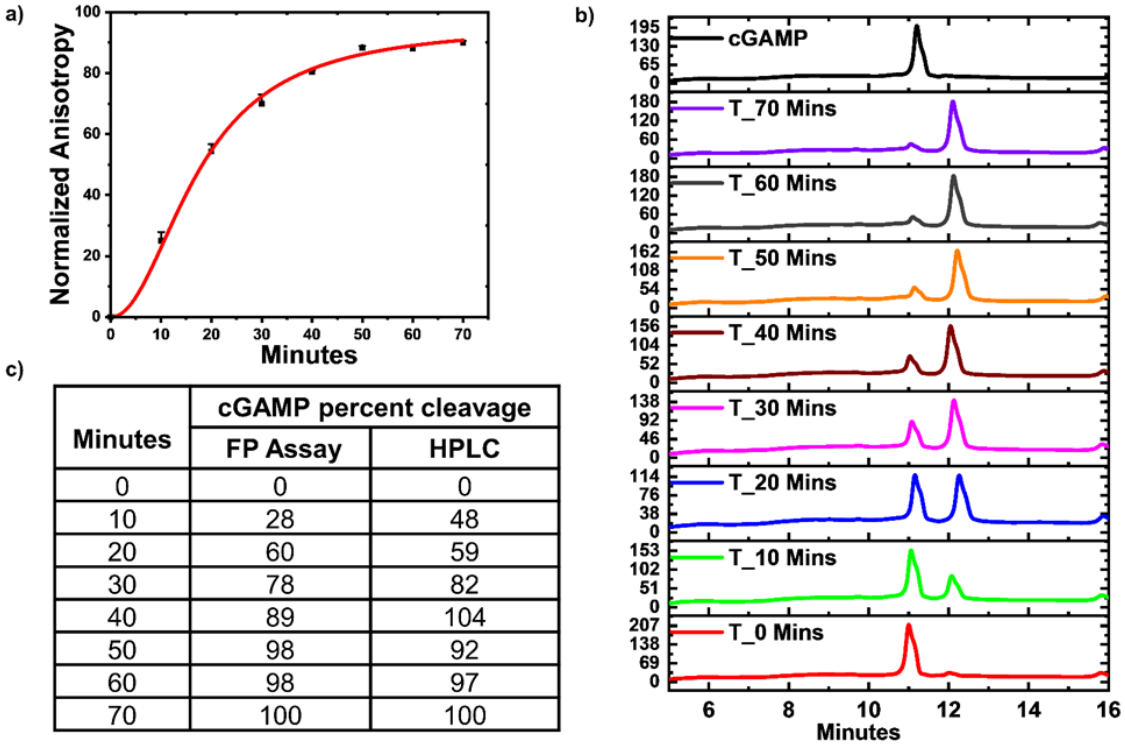

c)

Minutes	cGAMP percent cleavage	
	FP Assay	HPLC
0	0	0
10	28	48
20	60	59
30	78	82
40	89	104
50	98	92
60	98	97
70	100	100

Figure 6.8: hSTING fluorescence polarization competitive assay can track poxin cGAMP hydrolysis. a) Time trace anisotropy of poxin reactions. Curve generated with origin in-built hill function. b) HPLC Time traces of poxin reactions. c) cGAMP percent cleavage at specific time points quantified with either FP assay or HPLC analysis. cGAMP percent cleavage was calculated by assuming anisotropy after 70 min represented 100% cleavage for the FP assay. For HPLC analysis, peak area of poxin product at 70 min was assumed to represent 100% cleavage. * Kofi S. Yeboah helped in data collection.

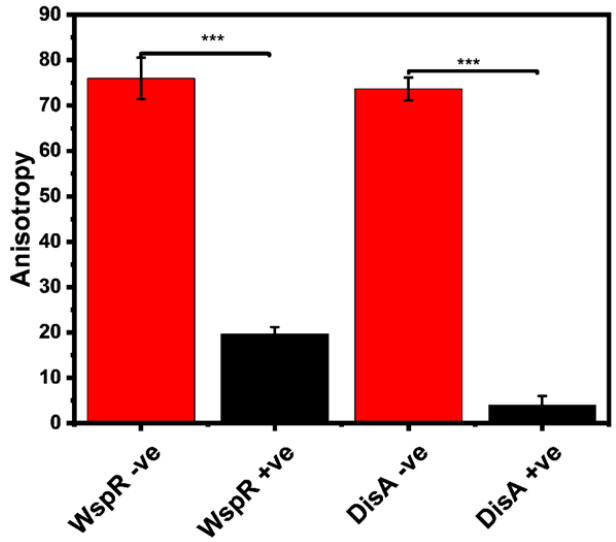

Figure 6.9: hSTING fluorescence polarization competitive assay can track WSPR and DisA synthesis dynamics. DisA –ve = Reactions containing no DisA. DisA +ve = Reactions containing DisA. Error bars = standard deviation. Experiments done in triplicates. * Wilson W.S. Ong and Kofi S. Yeboah helped in data collection.

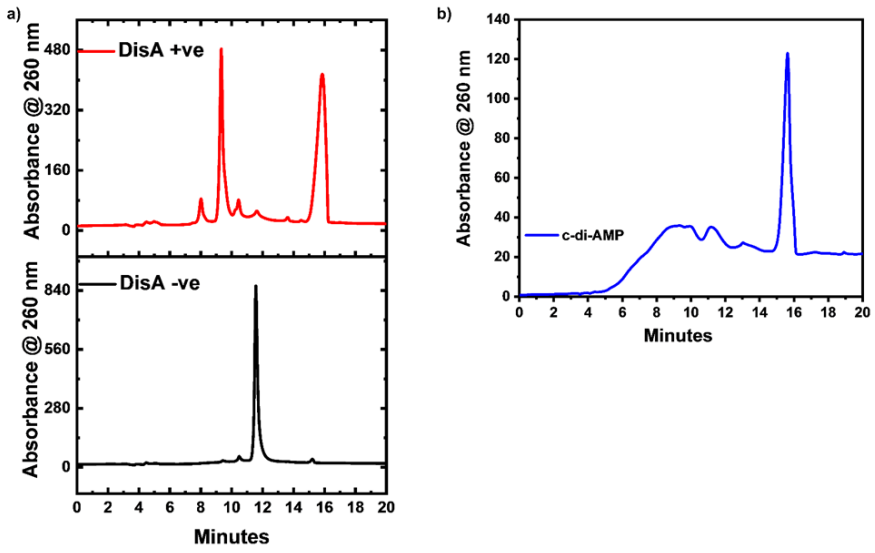

Figure 6.10: HPLC traces of DisA reactions. a) HPLC traces of DisA +ve and DisA -ve reactions. DisA –ve = Reactions containing no DisA. DisA +ve = Reactions containing DisA. b) HPLC trace of c-di-AMP standard. * Wilson W.S. Ong and Kofi S. Yeboah helped in data collection.

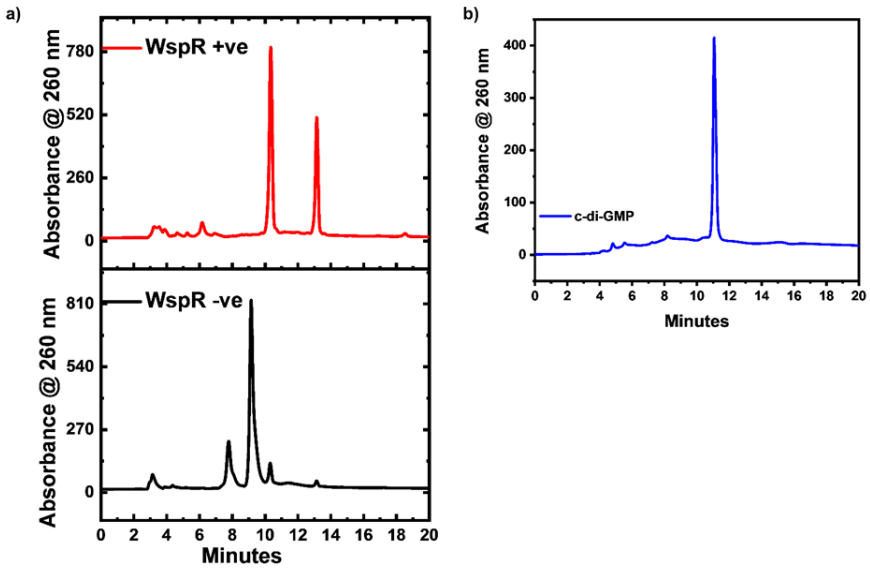

Figure 6.11: HPLC traces of DisA reactions. a) HPLC traces of WspR +ve and WspR -ve reactions. WspR –ve = Reactions containing no WspR. WspR +ve = Reactions containing WspR. b) HPLC trace of c-di-GMP standard. * Wilson W.S. Ong and Kofi S. Yeboah helped in data collection.

6.4 Concluding Remarks

There is an immense interest in CDNs biological research due to the central roles they play in various physiological processes in both bacteria and metazoans.[291] Enzymes and adaptor proteins that sense and/or regulate these second messengers are now bona fide drug targets and there is a need for simpler and cheaper assays to detect these molecules for various applications.[65] In 2011 we provided one of the earliest detections of cyclic dinucleotides using homogeneous aggregation strategy.[273] In 2012, we reported the first RNA-based detection of cyclic dinucleotides.[269] Since then various strategies have been described to detect cyclic dinucleotides.[268,292-296] We have since been looking for a universal and simple assay that could be used to detect all of the dinucleotides. Here, we present a simple assay that can facilitate cyclic dinucleotide research as well as provide a platform to discover compounds, which will translate the beautiful biology of cyclic dinucleotides into real life therapeutics. Although we have used a few enzymes, ENPP1, poxin, WspR and DisA, to demonstrate this concept in the manuscript, there is no conceptual impediment preventing the adaptation of this assay to detect any cyclic dinucleotide metabolism enzymes. This newly developed assay has streamlined our work

evaluating cyclic dinucleotide metabolism enzymes and we hope that others will also find the described assay useful.

REFERENCES

1 Karamanou, M., Panayiotakopoulos, G., Tsoucalas, G., Kousoulis, A. & Androutsos, G. From miasmas to germs: A historical approach to theories of infectious disease transmission. *Le infezioni in medicina : rivista periodica di eziologia, epidemiologia, diagnostica, clinica e terapia delle patologie infettive* **20**, 58-62 (2012).

2 Tulchinsky, T. H. & Varavikova, E. A. in *The New Public Health (Third Edition)* (eds Theodore H. Tulchinsky & Elena A. Varavikova) 1-42 (Academic Press, 2014).

3 Smith, K. A. Louis pasteur, the father of immunology? *Front Immunol* **3**, 68-68, doi:10.3389/fimmu.2012.00068 (2012).

4 Berche, P. Louis Pasteur, from crystals of life to vaccination. *Clinical Microbiology and Infection* **18**, 1-6, doi:10.1111/j.1469-0691.2012.03945.x (2012).

5 Blevins, S. M. & Bronze, M. S. Robert Koch and the 'golden age' of bacteriology. *International Journal of Infectious Diseases* **14**, e744-e751, doi:https://doi.org/10.1016/j.ijid.2009.12.003 (2010).

6 National Research Council (US) Committee to Update Science, M., and Animals. Science, Medicine, and Animals. Washington (DC). A Theory of Germs. *National Academies Press (US)* (2004).

7 Balloux, F. & van Dorp, L. Q&A: What are pathogens, and what have they done to and for us? *BMC Biology* **15**, 91, doi:10.1186/s12915-017-0433-z (2017).

8 Perry, R. D. & Fetherston, J. D. Yersinia pestis--etiologic agent of plague. *Clinical Microbiology Reviews* **10**, 35-66, doi:10.1128/cmr.10.1.35 (1997).

9 Acuna-Soto, R., Stahle, D. W., Cleaveland, M. K. & Therrell, M. D. Megadrought and megadeath in 16th century Mexico. *Emerg Infect Dis* **8**, 360-362, doi:10.3201/eid0804.010175 (2002).

10 Martini, M., Gazzaniga, V., Bragazzi, N. L. & Barberis, I. The Spanish Influenza Pandemic: a lesson from history 100 years after 1918. *J Prev Med Hyg* **60**, E64-E67, doi:10.15167/2421-4248/jpmh2019.60.1.1205 (2019).

11 Littman, R. J. The Plague of Athens: Epidemiology and Paleopathology. *Mount Sinai Journal of Medicine: A Journal of Translational and Personalized Medicine* **76**, 456-467, doi:10.1002/msj.20137 (2009).

12 Bloom, D. E. & Cadarette, D. Infectious Disease Threats in the Twenty-First Century: Strengthening the Global Response. *Front Immunol* **10**, 549-549, doi:10.3389/fimmu.2019.00549 (2019).

13 *The top 10 causes of death*, <https://www.who.int/news-room/fact-sheets/detail/the-top-10-causes-of-death> (2018).

14 Hay, S. I. *et al.* Global, regional, and national disability-adjusted life-years (DALYs) for 333 diseases and injuries and healthy life expectancy (HALE) for 195 countries and territories, 1990–2016: a systematic analysis for the Global Burden of Disease Study 2016. *The Lancet* **390**, 1260-1344, doi:https://doi.org/10.1016/S0140-6736(17)32130-X (2017).

15 Organization, W. H. Global health risks. (2009).

16 Bhutta, Z. A., Salam, R. A., Das, J. K. & Lassi, Z. S. Tackling the existing burden of infectious diseases in the developing world: existing gaps and the way forward. *Infectious Diseases of Poverty* **3**, 28, doi:10.1186/2049-9957-3-28 (2014).

17 Levitt, A. M., Khan, A. S. & Hughes, J. M. in *Infectious Diseases (Third Edition)* (eds Jonathan Cohen, Steven M. Opal, & William G. Powderly) 56-69 (Content Repository Only!, 2010).

18 Sponseller, J. K., Griffiths, J. K. & Tzipori, S. The evolution of respiratory Cryptosporidiosis: evidence for transmission by inhalation. *Clinical microbiology reviews* **27**, 575-586, doi:10.1128/CMR.00115-13 (2014).

19 Aguilar, P. V. *et al.* Endemic Venezuelan equine encephalitis in the Americas: hidden under the dengue umbrella. *Future Virol* **6**, 721-740, doi:10.2217/FVL.11.5 (2011).

20 Sejvar, J. J. West nile virus: an historical overview. *Ochsner J* **5**, 6-10 (2003).

21 Sklenovská, N. & Van Ranst, M. Emergence of Monkeypox as the Most Important Orthopoxvirus Infection in Humans. *Front Public Health* **6**, 241-241, doi:10.3389/fpubh.2018.00241 (2018).

22 Bishop, R. Discovery of rotavirus: Implications for Child health. *Journal of Gastroenterology and Hepatology* **24**, S81-S85, doi:10.1111/j.1440-1746.2009.06076.x (2009).

23 Choo, Q. *et al.* Isolation of a cDNA clone derived from a blood-borne non-A, non-B viral hepatitis genome. *Science* **244**, 359-362, doi:10.1126/science.2523562 (1989).

24 Breman, J. G. *et al.* Discovery and Description of Ebola Zaire Virus in 1976 and Relevance to the West African Epidemic During 2013-2016. *The Journal of infectious diseases* **214**, S93-S101, doi:10.1093/infdis/jiw207 (2016).

25 Gonçalves, D. U. *et al.* Epidemiology, treatment, and prevention of human T-cell leukemia virus type 1-associated diseases. *Clinical microbiology reviews* **23**, 577-589, doi:10.1128/CMR.00063-09 (2010).

26 Vaccaro, L. *et al.* First Case of Legionnaire's Disease Caused by Legionella anisa in Spain and the Limitations on the Diagnosis of Legionella non-pneumophila Infections. *PLoS One* **11**, e0159726-e0159726, doi:10.1371/journal.pone.0159726 (2016).

27 Prevention, C. f. D. C. a. *Zoonotic Diseases*, <https://www.cdc.gov/onehealth/basics/zoonotic-diseases.html> (2017).

28 Series, N. C. S. in *NIH Curriculum Supplement Series* (2007).

29 O'Neill, J. Review on Antimicrobial Resistance Antimicrobial Resistance: Tackling a crisis for the health and wealth of nations. (2014).

30 O'NEILL, J. TACKLING DRUG-RESISTANT INFECTIONS GLOBALLY:FINAL REPORT AND RECOMMENDATIONS. (2016).

31 *High-Level Meeting on Antimicrobial Resistance*, <https://www.un.org/pga/71/2016/09/21/press-release-hl-meeting-on-antimicrobial-resistance/> (2016).

32 Bassett, E., Keith, M., Armelagos, G., Martin, D. & Villanueva, A. Tetracycline-labeled human bone from ancient Sudanese Nubia (A.D. 350). *Science* **209**, 1532-1534, doi:10.1126/science.7001623 (1980).

33 Nelson, M. L., Dinardo, A., Hochberg, J. & Armelagos, G. J. Brief communication: Mass spectroscopic characterization of tetracycline in the skeletal remains of an ancient population from Sudanese Nubia 350–550 CE. *American Journal of Physical Anthropology* **143**, 151-154, doi:10.1002/ajpa.21340 (2010).

34 Aminov, R. I. A brief history of the antibiotic era: lessons learned and challenges for the future. *Frontiers in microbiology* **1**, 134-134, doi:10.3389/fmicb.2010.00134 (2010).

35 Piddock, L. J. V. The crisis of no new antibiotics—what is the way forward? *The Lancet Infectious Diseases* **12**, 249-253, doi:https://doi.org/10.1016/S1473-3099(11)70316-4 (2012).

36 Lederberg, J. Infectious History. *Science* **288**, 287-293, doi:10.1126/science.288.5464.287 (2000).

37 Adedeji, W. A. THE TREASURE CALLED ANTIBIOTICS. *Annals of Ibadan postgraduate medicine* **14**, 56-57 (2016).

38 Brachman, P. S. Infectious diseases—past, present, and future. *International Journal of Epidemiology* **32**, 684-686, doi:10.1093/ije/dyg282 (2003).

39 Rossolini, G. M., Arena, F., Pecile, P. & Pollini, S. Update on the antibiotic resistance crisis. *Current Opinion in Pharmacology* **18**, 56-60, doi:https://doi.org/10.1016/j.coph.2014.09.006 (2014).

40 CDC. Achievements in Public Health, 1900-1999: Control of Infectious Diseases. *MMWR Morb Mortal Wkly Rep* **48**, 621-629 (1999).

41 Gould, K. Antibiotics: from prehistory to the present day. *Journal of Antimicrobial Chemotherapy* **71**, 572-575, doi:10.1093/jac/dkv484 (2016).

42 Buchwalow, I., Boecker, W. & Tiemann, M. The contribution of Paul Ehrlich to histochemistry: a tribute on the occasion of the centenary of his death. *Virchows Archiv* **466**, 111-116, doi:10.1007/s00428-014-1677-4 (2015).

43 Schwartz, R. S. Paul Ehrlich's Magic Bullets. *New England Journal of Medicine* **350**, 1079-1080, doi:10.1056/NEJMp048021 (2004).

44 Williams, K. J. The introduction of 'chemotherapy' using arsphenamine - the first magic bullet. *J R Soc Med* **102**, 343-348, doi:10.1258/jrsm.2009.09k036 (2009).

45 Greenwood, D. *Antimicrobial Drugs: Chronicle of a Twentieth Century Medical Triumph*. 57-58 (Oxford University Press, 2008).

46 Tan, S. Y. & Tatsumura, Y. Alexander Fleming (1881-1955): Discoverer of penicillin. *Singapore Med J* **56**, 366-367, doi:10.11622/smedj.2015105 (2015).

47 Gaynes, R. The Discovery of Penicillin—New Insights After More Than 75 Years of Clinical Use. *Emerg Infect Dis* **23**, 849-853 (2017).

48 *American Chemical Society International Historic Chemical Landmarks. Discovery and Development of Penicillin*, <http://www.acs.org/content/acs/en/education/whatischemistry/landmarks/flemingpenicillin.html>

49 Chain, E. *et al*. THE CLASSIC: Penicillin as a Chemotherapeutic Agent. *A Publication of The Association of Bone and Joint Surgeons® | CORR®* **439**, 23-26, doi:10.1097/01.blo.0000183429.83168.07 (2005).

50 Ribeiro da Cunha, B., Fonseca, L. P. & Calado, C. R. C. Antibiotic Discovery: Where Have We Come from, Where Do We Go? *Antibiotics (Basel)* **8**, 45, doi:10.3390/antibiotics8020045 (2019).

51 Shampo, M. A. & Kyle, R. A. Daniel Bovet-Nobel Laureate in Medicine. *Mayo Clinic Proceedings* **74**, 1016, doi:10.4065/74.10.1016 (1999).

52 Powers, J. H. Antimicrobial drug development – the past, the present, and the future. *Clinical Microbiology and Infection* **10**, 23-31, doi:https://doi.org/10.1111/j.1465-0691.2004.1007.x (2004).

53 Chopra, I., Hesse, L. & O'Neill, A. in *Pharmacochemistry Library* Vol. 32 (ed Henk van der Goot) 213-225 (Elsevier, 2002).

54 Coates, A., Hu, Y., Bax, R. & Page, C. The future challenges facing the development of new antimicrobial drugs. *Nature Reviews Drug Discovery* **1**, 895, doi:10.1038/nrd940 (2002).

55 Munita, J. M. & Arias, C. A. Mechanisms of Antibiotic Resistance. *Microbiol Spectr* **4**, 10.1128/microbiolspec.VMBF-0016-2015, doi:10.1128/microbiolspec.VMBF-0016-2015 (2016).

56 Lowy, F. D. Antimicrobial resistance: the example of Staphylococcus aureus. *The Journal of clinical investigation* **111**, 1265-1273, doi:10.1172/jci18535 (2003).

57 Pier, G. B. On the Greatly Exaggerated Reports of the Death of Infectious Diseases. *Clinical Infectious Diseases* **47**, 1113-1114, doi:10.1086/592123 (2008).

58 Spellberg, B. & Gilbert, D. N. The future of antibiotics and resistance: a tribute to a career of leadership by John Bartlett. *Clinical infectious diseases : an official publication of the Infectious Diseases Society of America* **59 Suppl 2**, S71-S75, doi:10.1093/cid/ciu392 (2014).

59 Finland, M. *et al.* Round table: are new antibiotics needed? *Antimicrob Agents Chemother (Bethesda)* **5**, 1107-1114 (1965).

60 Petersdorf, R. G. The Doctors' Dilemma. *New England Journal of Medicine* **299**, 628-634, doi:10.1056/nejm197809212991204 (1978).

61 Centers for disease control and prevention (CDC). Antibiotic resistance threats in the United State. (2013).

62 Chen L, T. R., Kiehlbauch J, Walters M, Kallen A. Notes from the Field: Pan-Resistant New Delhi Metallo-Beta-Lactamase-Producing Klebsiella pneumoniae — Washoe County, Nevada,2016. *MMWR Morb Mortal Wkly Rep* **66**, doi:http://dx.doi.org/10.15585/mmwr.mm6601a7 (2017).

63 Laxminarayan, R. *et al.* Antibiotic resistance—the need for global solutions. *The Lancet Infectious Diseases* **13**, 1057-1098, doi:https://doi.org/10.1016/S1473-3099(13)70318-9 (2013).

64 Cegelski, L., Marshall, G. R., Eldridge, G. R. & Hultgren, S. J. The biology and future prospects of antivirulence therapies. *Nat Rev Microbiol* **6**, 17-27, doi:10.1038/nrmicro1818 (2008).

65 Opoku-Temeng, C., Zhou, J., Zheng, Y., Su, J. & Sintim, H. O. Cyclic dinucleotide (c-di-GMP, c-di-AMP, and cGAMP) signalings have come of age to be inhibited by small molecules. *Chemical Communications* **52**, 9327-9342, doi:10.1039/c6cc03439j (2016).

66 Kalia, D. *et al.* Nucleotide, c-di-GMP, c-di-AMP, cGMP, cAMP, (p)ppGpp signaling in bacteria and implications in pathogenesis. *Chemical Society Reviews* **42**, 305-341, doi:10.1039/C2CS35206K (2013).

67 Diner, Elie J. *et al.* The Innate Immune DNA Sensor cGAS Produces a Noncanonical Cyclic Dinucleotide that Activates Human STING. *Cell Reports* **3**, 1355-1361, doi:https://doi.org/10.1016/j.celrep.2013.05.009 (2013).

68 Woodward, J. J., Iavarone, A. T. & Portnoy, D. A. c-di-AMP Secreted by Intracellular *Listeria monocytogenes* Activates a Host Type I Interferon Response. *Science* **328**, 1703-1705, doi:10.1126/science.1189801 (2010).

69 Andrade, Warrison A. *et al.* Group B *Streptococcus* Degrades Cyclic-di-AMP to Modulate STING-Dependent Type I Interferon Production. *Cell Host & Microbe* **20**, 49-59, doi:10.1016/j.chom.2016.06.003 (2016).

70 Barker, J. R. *et al.* STING-Dependent Recognition of Cyclic di-AMP Mediates Type I Interferon Responses during *Chlamydia trachomatis* Infection. *mBio* **4**, e00018-00013, doi:10.1128/mBio.00018-13 (2013).

71 Dey, B. *et al.* A bacterial cyclic dinucleotide activates the cytosolic surveillance pathway and mediates innate resistance to tuberculosis. *Nature Medicine* **21**, 401, doi:10.1038/nm.3813
https://www.nature.com/articles/nm.3813#supplementary-information (2015).

72 Xia, P. *et al.* The ER membrane adaptor ERAdP senses the bacterial second messenger c-di-AMP and initiates anti-bacterial immunity. *Nature Immunology* **19**, 141-150, doi:10.1038/s41590-017-0014-x (2018).

73 McFarland, A. P. *et al.* Sensing of Bacterial Cyclic Dinucleotides by the Oxidoreductase RECON Promotes NF-κB Activation and Shapes a Proinflammatory Antibacterial State. *Immunity* **46**, 433-445, doi:https://doi.org/10.1016/j.immuni.2017.02.014 (2017).

74 Foley, J. F. Sensing bacterial infection. *Science Signaling* **11**, eaat1224, doi:10.1126/scisignal.aat1224 (2018).

75 Jakobsen, M. R. ERAdP standing in the shadow of STING innate immune signaling. *Nature Immunology* **19**, 105-107, doi:10.1038/s41590-017-0026-6 (2018).

76 Dey, R. J. *et al.* Inhibition of innate immune cytosolic surveillance by an M. tuberculosis phosphodiesterase. *Nature Chemical Biology* **13**, 210-217, doi:10.1038/nchembio.2254 (2017).

77 Andrade, Warrison A. *et al.* Group B *Streptococcus* Degrades Cyclic-di-AMP to Modulate STING-Dependent Type I Interferon Production. *Cell Host & Microbe* **20**, 49-59, doi:10.1016/j.chom.2016.06.003 (2016).

78 Fahmi, T., Port, G. C. & Cho, K. H. c-di-AMP: An Essential Molecule in the Signaling Pathways that Regulate the Viability and Virulence of Gram-Positive Bacteria. *Genes* **8**, 197 (2017).

79 Simm, R., Morr, M., Kader, A., Nimtz, M. & Römling, U. GGDEF and EAL domains inversely regulate cyclic di-GMP levels and transition from sessility to motility. *Molecular Microbiology* **53**, 1123-1134, doi:10.1111/j.1365-2958.2004.04206.x (2004).

80 Corrigan, R. M. & Gründling, A. Cyclic di-AMP: another second messenger enters the fray. *Nature Reviews Microbiology* **11**, 513-524, doi:10.1038/nrmicro3069 (2013).

81 Commichau, F. M., Heidemann, J. L., Ficner, R. & Stülke, J. Making and Breaking of an Essential Poison: the Cyclases and Phosphodiesterases That Produce and Degrade the Essential Second Messenger Cyclic di-AMP in Bacteria. *Journal of Bacteriology* **201**, e00462-00418, doi:10.1128/jb.00462-18 (2019).

82 Witte, C. E. *et al.* Cyclic di-AMP Is Critical for *Listeria monocytogenes* Growth, Cell Wall Homeostasis, and Establishment of Infection. *mBio* **4**, e00282-00213, doi:10.1128/mBio.00282-13 (2013).

83 Mehne, F. M. P. *et al.* Cyclic Di-AMP Homeostasis in Bacillus subtilis: BOTH LACK AND HIGH LEVEL ACCUMULATION OF THE NUCLEOTIDE ARE DETRIMENTAL FOR CELL GROWTH. *Journal of Biological Chemistry* **288**, 2004-2017, doi:10.1074/jbc.M112.395491 (2013).

84 Bowman, L., Zeden, M. S., Schuster, C. F., Kaever, V. & Gründling, A. New Insights into the Cyclic Di-adenosine Monophosphate (c-di-AMP) Degradation Pathway and the Requirement of the Cyclic Dinucleotide for Acid Stress Resistance in Staphylococcus aureus. *Journal of Biological Chemistry* **291**, 26970-26986, doi:10.1074/jbc.M116.747709 (2016).

85 Lieberman, O. J., Orr, M. W., Wang, Y. & Lee, V. T. High-Throughput Screening Using the Differential Radial Capillary Action of Ligand Assay Identifies Ebselen As an Inhibitor of Diguanylate Cyclases. *ACS Chemical Biology* **9**, 183-192, doi:10.1021/cb400485k (2014).

86 Sambanthamoorthy, K. *et al.* Identification of Small Molecules That Antagonize Diguanylate Cyclase Enzymes To Inhibit Biofilm Formation. *Antimicrobial Agents and Chemotherapy* **56**, 5202-5211, doi:10.1128/aac.01396-12 (2012).

87 Sambanthamoorthy, K. *et al.* Identification of small molecules inhibiting diguanylate cyclases to control bacterial biofilm development. *Biofouling* **30**, 17-28, doi:10.1080/08927014.2013.832224 (2014).

88 Zheng, Y., Tsuji, G., Opoku-Temeng, C. & Sintim, H. O. Inhibition of P. aeruginosa c-di-GMP phosphodiesterase RocR and swarming motility by a benzoisothiazolinone derivative. *Chemical Science* **7**, 6238-6244, doi:10.1039/C6SC02103D (2016).

89 Zheng, Y., Zhou, J., Sayre, D. A. & Sintim, H. O. Identification of bromophenol thiohydantoin as an inhibitor of DisA, a c-di-AMP synthase, from a 1000 compound library, using the coralyne assay. *Chemical Communications* **50**, 11234-11237, doi:10.1039/c4cc02916j (2014).

90 Opoku-Temeng, C. & Sintim, H. O. Potent inhibition of cyclic diadenylate monophosphate cyclase by the antiparasitic drug, suramin. *Chemical Communications* **52**, 3754-3757, doi:10.1039/c5cc10446g (2016).

91 Opoku-Temeng, C. & Sintim, H. O. Inhibition of cyclic diadenylate cyclase, DisA, by polyphenols. *Scientific Reports* **6**, 25445, doi:10.1038/srep25445 (2016).

92 Opoku-Temeng, C., Dayal, N., Miller, J. & Sintim, H. O. Hydroxybenzylidene-indolinones, c-di-AMP synthase inhibitors, have antibacterial and anti-biofilm activities and also re-sensitize resistant bacteria to methicillin and vancomycin. *RSC Advances* **7**, 8288-8294, doi:10.1039/C6RA28443D (2017).

93 Brown, G. D. *et al.* Hidden Killers: Human Fungal Infections. *Science Translational Medicine* **4**, 165rv113-165rv113, doi:10.1126/scitranslmed.3004404 (2012).

94 Ostrosky-Zeichner, L., Casadevall, A., Galgiani, J. N., Odds, F. C. & Rex, J. H. An insight into the antifungal pipeline: selected new molecules and beyond. *Nature Reviews Drug Discovery* **9**, 719, doi:10.1038/nrd3074 (2010).

95 Groll, A. H., Piscitelli, S. C. & Walsh, T. J. in *Advances in Pharmacology* Vol. 44 (eds J. Thomas August, M. W. Anders, Ferid Murad, & Joseph T. Coyle) 343-500 (Academic Press, 1998).

96 Dutcher, J. D. The Discovery and Development of Amphotericin B. *Diseases of the Chest* **54**, 296-298, doi:https://doi.org/10.1378/chest.54.Supplement_1.296 (1968).

97 Andriole, V. T. Current and future antifungal therapy: new targets for antifungal agents. *Journal of Antimicrobial Chemotherapy* **44**, 151-162, doi:10.1093/jac/44.2.151 (1999).

98 Tassel, D. & Madoff, M. A. Treatment of Candida Sepsis and Cryptococcus Meningitis With 5-Fluorocytosine: A New Antifungal Agent. *JAMA* **206**, 830-832, doi:10.1001/jama.1968.03150040042009 (1968).

99 Gubbins, P. O. & Anaissie, E. J. in *Clinical Mycology (Second Edition)* (eds Elias J. Anaissie, Michael R. McGinnis, & Michael A. Pfaller) 161-195 (Churchill Livingstone, 2009).

100 Sheehan, D. J., Hitchcock, C. A. & Sibley, C. M. Current and Emerging Azole Antifungal Agents. *Clinical Microbiology Reviews* **12**, 40-79, doi:10.1128/cmr.12.1.40 (1999).

101 Maertens, J. A. History of the development of azole derivatives. *Clinical Microbiology and Infection* **10**, 1-10, doi:10.1111/j.1470-9465.2004.00841.x (2004).

102 Aguilar-Zapata, D., Petraitiene, R. & Petraitis, V. Echinocandins: The Expanding Antifungal Armamentarium. *Clinical Infectious Diseases* **61**, S604-S611, doi:10.1093/cid/civ814 (2015).

103 Fairlamb, A. H., Gow, N. A. R., Matthews, K. R. & Waters, A. P. Drug resistance in eukaryotic microorganisms. *Nature Microbiology* **1**, 16092, doi:10.1038/nmicrobiol.2016.92 (2016).

104 Lockhart, S. R. *et al.* Simultaneous Emergence of Multidrug-Resistant Candida auris on 3 Continents Confirmed by Whole-Genome Sequencing and Epidemiological Analyses. *Clinical infectious diseases : an official publication of the Infectious Diseases Society of America* **64**, 134-140, doi:10.1093/cid/ciw691 (2017).

105 Arendrup, M. C. & Patterson, T. F. Multidrug-Resistant Candida: Epidemiology, Molecular Mechanisms, and Treatment. *The Journal of Infectious Diseases* **216**, S445-S451, doi:10.1093/infdis/jix131 (2017).

106 Srinivasan, A., Lopez-Ribot, J. L. & Ramasubramanian, A. K. Overcoming antifungal resistance. *Drug Discov Today Technol* **11**, 65-71, doi:10.1016/j.ddtec.2014.02.005 (2014).

107 Ghannoum, M. A. & Rice, L. B. Antifungal Agents: Mode of Action, Mechanisms of Resistance, and Correlation of These Mechanisms with Bacterial Resistance. *Clinical Microbiology Reviews* **12**, 501-517, doi:10.1128/cmr.12.4.501 (1999).

108 Cowen, L. E., Sanglard, D., Howard, S. J., Rogers, P. D. & Perlin, D. S. Mechanisms of Antifungal Drug Resistance. *Cold Spring Harb Perspect Med* **5**, a019752-a019752, doi:10.1101/cshperspect.a019752 (2014).

109 D'Costa, V. M. *et al.* Antibiotic resistance is ancient. *Nature* **477**, 457, doi:10.1038/nature10388 https://www.nature.com/articles/nature10388#supplementary-information (2011).

110 Ventola, C. L. The antibiotic resistance crisis: part 1: causes and threats. *P T* **40**, 277-283 (2015).

111 Fleming, A. Penicillin. *Nobel Lecture* (1945).

112 Castro-Sánchez, E., Moore, L. S. P., Husson, F. & Holmes, A. H. What are the factors driving antimicrobial resistance? Perspectives from a public event in London, England. *BMC Infect Dis* **16**, 465-465, doi:10.1186/s12879-016-1810-x (2016).

113 Bartlett, J. G., Gilbert, D. N. & Spellberg, B. Seven Ways to Preserve the Miracle of Antibiotics. *Clinical Infectious Diseases* **56**, 1445-1450, doi:10.1093/cid/cit070 (2013).

114 Kraemer, S. A., Ramachandran, A. & Perron, G. G. Antibiotic Pollution in the Environment: From Microbial Ecology to Public Policy. *Microorganisms* **7**, 180, doi:10.3390/microorganisms7060180 (2019).

115 Tosi, M. *et al.* Multidrug resistant bacteria in critically ill patients: a step further antibiotic therapy. *Journal of Emergency and Critical Care Medicine* **2** (2018).

116 Lee, C.-C., Lee, C.-H., Hong, M.-Y., Tang, H.-J. & Ko, W.-C. Timing of appropriate empirical antimicrobial administration and outcome of adults with community-onset bacteremia. *Critical Care* **21**, 119, doi:10.1186/s13054-017-1696-z (2017).

117 Kollef, M., Micek, S., Hampton, N., Doherty, J. A. & Kumar, A. Septic Shock Attributed to Candida Infection: Importance of Empiric Therapy and Source Control. *Clinical Infectious Diseases* **54**, 1739-1746, doi:10.1093/cid/cis305 (2012).

118 Morrell, M., Fraser, V. J. & Kollef, M. H. Delaying the empiric treatment of candida bloodstream infection until positive blood culture results are obtained: a potential risk factor for hospital mortality. *Antimicrobial Agents and Chemotherapy* **49**, 3640-3645, doi:10.1128/aac.49.9.3640-3645.2005 (2005).

119 Mulvey, M. R. & Simor, A. E. Antimicrobial resistance in hospitals: how concerned should we be? *CMAJ* **180**, 408-415, doi:10.1503/cmaj.080239 (2009).

120 Tängdén, T., Cars, O., Melhus, Å. & Löwdin, E. Foreign Travel Is a Major Risk Factor for Colonization with *Escherichia coli* Producing CTX-M-Type Extended-Spectrum β-Lactamases: a Prospective Study with Swedish Volunteers. *Antimicrobial Agents and Chemotherapy* **54**, 3564-3568, doi:10.1128/aac.00220-10 (2010).

121 Schwartz, K. L. & Morris, S. K. Travel and the Spread of Drug-Resistant Bacteria. *Current Infectious Disease Reports* **20**, 29, doi:10.1007/s11908-018-0634-9 (2018).

122 Raman, C. V. & Krishnan, K. S. A New Type of Secondary Radiation. *Nature* **121**, 501-502, doi:10.1038/121501c0 (1928).

123 C V RAMAN, F. R. S. A new radiation* *Indian J. Phys.* **2** 387-398 (1928).

124 American Chemical Society International Historic Chemical Landmarks. The Raman Effect.

125 van Manen, H.-J., Kraan, Y. M., Roos, D. & Otto, C. Single-cell Raman and fluorescence microscopy reveal the association of lipid bodies with phagosomes in leukocytes. *Proc. Natl. Acad. Sci. U. S. A.* **102**, 10159-10164, doi:10.1073/pnas.0502746102 (2005).

126 Slipchenko, M. N., Le, T. T., Chen, H. & Cheng, J.-X. High-Speed Vibrational Imaging and Spectral Analysis of Lipid Bodies by Compound Raman Microscopy. *The Journal of Physical Chemistry B* **113**, 7681-7686, doi:10.1021/jp902231y (2009).

127 Min, W., Freudiger, C. W., Lu, S. & Xie, X. S. Coherent Nonlinear Optical Imaging: Beyond Fluorescence Microscopy. *Annual Review of Physical Chemistry* **62**, 507-530, doi:10.1146/annurev.physchem.012809.103512 (2011).

128 Huffnagle, G. B. & Noverr, M. C. The emerging world of the fungal microbiome. *Trends in Microbiology* **21**, 334-341, doi:https://doi.org/10.1016/j.tim.2013.04.002 (2013).

129 Gow, N., Brown, G. D., Brown, A., Netea, M. & McArdle, K. E. Waging war on fungi - The unknown superbugs. *Microbiology Today* **39**, 208-211 (2012).

130 Wisplinghoff, H. *et al.* Nosocomial Bloodstream Infections in US Hospitals: Analysis of 24,179 Cases from a Prospective Nationwide Surveillance Study. *Clinical Infectious Diseases* **39**, 309-317, doi:10.1086/421946 (2004).

131 Pfaller, M. A. & Diekema, D. J. Epidemiology of Invasive Candidiasis: a Persistent Public Health Problem. *Clinical Microbiology Reviews* **20**, 133-163, doi:10.1128/cmr.00029-06 (2007).

132 Pfaller, M. A. & Diekema, D. J. Epidemiology of Invasive Mycoses in North America. *Critical Reviews in Microbiology* **36**, 1-53, doi:10.3109/10408410903241444 (2010).

133 Sudbery, P. E. Growth of Candida albicans hyphae. *Nature Reviews Microbiology* **9**, 737-748, doi:10.1038/nrmicro2636 (2011).

134 Ene, I. V. *et al.* Host carbon sources modulate cell wall architecture, drug resistance and virulence in a fungal pathogen. *Cellular Microbiology* **14**, 1319-1335, doi:10.1111/j.1462-5822.2012.01813.x (2012).

135 Richardson, M. & Lass-Flörl, C. Changing epidemiology of systemic fungal infections. *Clinical Microbiology and Infection* **14**, 5-24, doi:https://doi.org/10.1111/j.1469-0691.2008.01978.x (2008).

136 Pappas, P. G. *et al.* Clinical Practice Guideline for the Management of Candidiasis: 2016 Update by the Infectious Diseases Society of America. *Clinical Infectious Diseases* **62**, e1-e50, doi:10.1093/cid/civ933 (2015).

137 Debruyne, D. & Ryckelynck, J.-P. Clinical Pharmacokinetics of Fluconazole. *Clinical Pharmacokinetics* **24**, 10-27, doi:10.2165/00003088-199324010-00002 (1993).

138 Perlin, D. S. Antifungal drug resistance: do molecular methods provide a way forward? *Curr Opin Infect Dis* **22**, 568-573, doi:10.1097/qco.0b013e3283321ce5 (2009).

139 Vella, A. *et al.* Rapid Antifungal Susceptibility Testing by Matrix-Assisted Laser Desorption Ionization–Time of Flight Mass Spectrometry Analysis. *Journal of Clinical Microbiology* **51**, 2964-2969, doi:10.1128/jcm.00903-13 (2013).

140 Brown, A. J. P., Brown, G. D., Netea, M. G. & Gow, N. A. R. Metabolism impacts upon Candida immunogenicity and pathogenicity at multiple levels. *Trends in Microbiology* **22**, 614-622, doi:https://doi.org/10.1016/j.tim.2014.07.001 (2014).

141 Fairlamb, A. H., Gow, N. A. R., Matthews, K. R. & Waters, A. P. Drug resistance in eukaryotic microorganisms. *Nature Microbiology* **1**, 16092, doi:10.1038/nmicrobiol.2016.92 (2016).

142 Ward, Patrick S. & Thompson, Craig B. Metabolic Reprogramming: A Cancer Hallmark Even Warburg Did Not Anticipate. *Cancer Cell* **21**, 297-308, doi:https://doi.org/10.1016/j.ccr.2012.02.014 (2012).

143 Beloribi-Djefaflia, S., Vasseur, S. & Guillaumond, F. Lipid metabolic reprogramming in cancer cells. *Oncogenesis* **5**, e189-e189, doi:10.1038/oncsis.2015.49 (2016).

144 Steinhauser, M. L. *et al.* Multi-isotope imaging mass spectrometry quantifies stem cell division and metabolism. *Nature* **481**, 516-519, doi:10.1038/nature10734 (2012).

145 Miura, D. *et al.* Ultrahighly Sensitive in Situ Metabolomic Imaging for Visualizing Spatiotemporal Metabolic Behaviors. *Analytical Chemistry* **82**, 9789-9796, doi:10.1021/ac101998z (2010).

146 Carden, A. & Morris, M. Application of vibrational spectroscopy to the study of mineralized tissues (review). *Journal of Biomedical Optics* **5** (2000).

147 Cheng, J.-X. & Xie, X. S. Vibrational spectroscopic imaging of living systems: An emerging platform for biology and medicine. *Science* **350**, aaa8870, doi:10.1126/science.aaa8870 (2015).

148 Cheng, J.-X. & Xie, X. S. Coherent Anti-Stokes Raman Scattering Microscopy: Instrumentation, Theory, and Applications. *The Journal of Physical Chemistry B* **108**, 827-840, doi:10.1021/jp035693v (2004).

149 Radulovic, M. *et al.* The emergence of lipid droplets in yeast: current status and experimental approaches. *Current Genetics* **59**, 231-242, doi:10.1007/s00294-013-0407-9 (2013).

150 Fu, D. *et al.* In Vivo Metabolic Fingerprinting of Neutral Lipids with Hyperspectral Stimulated Raman Scattering Microscopy. *Journal of the American Chemical Society* **136**, 8820-8828, doi:10.1021/ja504199s (2014).

151 Yue, S. *et al.* Cholesteryl Ester Accumulation Induced by PTEN Loss and PI3K/AKT Activation Underlies Human Prostate Cancer Aggressiveness. *Cell Metabolism* **19**, 393-406, doi:https://doi.org/10.1016/j.cmet.2014.01.019 (2014).

152 Li, J. et al. Lipid Desaturation Is a Metabolic Marker and Therapeutic Target of Ovarian Cancer Stem Cells. Cell Stem Cell 20, 303-314.e305, doi:https://doi.org/10.1016/j.stem.2016.11.004 (2017).

153 Slipchenko, M. N., Oglesbee, R. A., Zhang, D., Wu, W. & Cheng, J.-X. Heterodyne detected nonlinear optical imaging in a lock-in free manner. *Journal of Biophotonics* **5**, 801-807, doi:10.1002/jbio.201200005 (2012).

154 Li, J. & Cheng, J.-X. Direct Visualization of De novo Lipogenesis in Single Living Cells. *Scientific Reports* **4**, 6807, doi:10.1038/srep06807 (2014).

155 Kohli, A., Smriti, N., Mukhopadhyay, K., Rattan, A. & Prasad, R. In Vitro Low-Level Resistance to Azoles in *Candida albicans* Is Associated with Changes in Membrane Lipid Fluidity and Asymmetry. *Antimicrobial Agents and Chemotherapy* **46**, 1046-1052, doi:10.1128/aac.46.4.1046-1052.2002 (2002).

156 Prasad, R. & Kapoor, K. in *International Review of Cytology* Vol. 242 215-248 (Academic Press, 2004).

157 Pasrija, R., Panwar, S. L. & Prasad, R. Multidrug Transporters CaCdr1p and CaMdr1p of *Candida albicans* Display Different Lipid Specificities: both Ergosterol and Sphingolipids Are Essential for Targeting of CaCdr1p to Membrane Rafts. *Antimicrobial Agents and Chemotherapy* **52**, 694-704, doi:10.1128/aac.00861-07 (2008).

158 Madani, S., Hichami, A., Legrand, A., Belleville, J. & Khan, N. A. Implication of acyl chain of diacylglycerols in activation of different isoforms of protein kinase C. *The FASEB Journal* **15**, 2595-2601, doi:10.1096/fj.01-0753int (2001).

159 Newton, A. C. Protein Kinase C: Structure, Function, and Regulation. *Journal of Biological Chemistry* **270**, 28495-28498, doi:10.1074/jbc.270.48.28495 (1995).

160 LaFayette, S. L. *et al.* PKC Signaling Regulates Drug Resistance of the Fungal Pathogen Candida albicans via Circuitry Comprised of Mkc1, Calcineurin, and Hsp90. *PLoS Pathog* **6**, e1001069, doi:10.1371/journal.ppat.1001069 (2010).

161 Hynes, M. J. & Murray, S. L. ATP-Citrate Lyase Is Required for Production of Cytosolic Acetyl Coenzyme A and Development in *Aspergillus nidulans*. *Eukaryotic Cell* **9**, 1039-1048, doi:10.1128/ec.00080-10 (2010).

162 Carman, A. J., Vylkova, S. & Lorenz, M. C. Role of acetyl coenzyme A synthesis and breakdown in alternative carbon source utilization in Candida albicans. *Eukaryotic cell* **7**, 1733-1741, doi:10.1128/ec.00253-08 (2008).

163 Towle, H. C. Glucose as a regulator of eukaryotic gene transcription. *Trends in Endocrinology & Metabolism* **16**, 489-494, doi:https://doi.org/10.1016/j.tem.2005.10.003 (2005).

164 Sandager, L. *et al.* Storage Lipid Synthesis Is Non-essential in Yeast. *Journal of Biological Chemistry* **277**, 6478-6482, doi:10.1074/jbc.M109109200 (2002).

165 Zhong, D. *et al.* The Glycolytic Inhibitor 2-Deoxyglucose Activates Multiple Prosurvival Pathways through IGF1R. *Journal of Biological Chemistry* **284**, 23225-23233, doi:10.1074/jbc.M109.005280 (2009).

166 Zou, C., Wang, Y. & Shen, Z. 2-NBDG as a fluorescent indicator for direct glucose uptake measurement. *Journal of Biochemical and Biophysical Methods* **64**, 207-215, doi:https://doi.org/10.1016/j.jbbm.2005.08.001 (2005).

167 Rodaki, A. *et al.* Glucose Promotes Stress Resistance in the Fungal Pathogen Candida albicans. *Molecular Biology of the Cell* **20**, 4845-4855, doi:10.1091/mbc.e09-01-0002 (2009).

168 Naclerio, G. A. & Sintim, H. O. Multiple ways to kill bacteria via inhibiting novel cell wall or membrane targets. *Future Medicinal Chemistry* **12**, 1253-1279, doi:10.4155/fmc-2020-0046 (2020).

169 Laxminarayan, R. *et al.* The Lancet Infectious Diseases Commission on antimicrobial resistance: 6 years later. *The Lancet. Infectious diseases* **20**, e51-e60, doi:10.1016/s1473-3099(20)30003-7 (2020).

170 Appelbaum, P. C. 2012 and beyond: potential for the start of a second pre-antibiotic era? *The Journal of antimicrobial chemotherapy* **67**, 2062-2068, doi:10.1093/jac/dks213 (2012).

171 Fair, R. J. & Tor, Y. Antibiotics and Bacterial Resistance in the 21st Century. *Perspectives in Medicinal Chemistry* **6**, PMC.S14459, doi:10.4137/pmc.s14459 (2014).

172 Ventola, C. L. The Antibiotic Resistance Crisis: Part 1: Causes and Threats. *Pharmacy and Therapeutics* **40**, 277-283 (2015).

173 Tacconelli, E. *et al.* Discovery, research, and development of new antibiotics: the WHO priority list of antibiotic-resistant bacteria and tuberculosis. *The Lancet Infectious Diseases*, doi:10.1016/s1473-3099(17)30753-3.

174 Fernandes, P. Antibacterial discovery and development—the failure of success? *Nature Biotechnology* **24**, 1497, doi:10.1038/nbt1206-1497 (2006).

175 Fernandes, P. & Martens, E. Antibiotics in late clinical development. *Biochemical Pharmacology* **133**, 152-163, doi:https://doi.org/10.1016/j.bcp.2016.09.025 (2017).

176 Coates, A. R. M., Halls, G. & Hu, Y. Novel classes of antibiotics or more of the same? *British Journal of Pharmacology* **163**, 184-194, doi:10.1111/j.1476-5381.2011.01250.x (2011).

177 Watkins, R. R., Lemonovich, T. L. & File, T. M. An evidence-based review of linezolid for the treatment of methicillin-resistant *Staphylococcus aureus* (MRSA): place in therapy. *Core Evidence* **7**, 131-143, doi:10.2147/ce.s33430 (2012).

178 Gu, B., Kelesidis, T., Tsiodras, S., Hindler, J. & Humphries, R. M. The emerging problem of linezolid-resistant Staphylococcus. *Journal of Antimicrobial Chemotherapy* **68**, 4-11, doi:10.1093/jac/dks354 (2013).

179 Thwaites, G. E. & Gant, V. Are bloodstream leukocytes Trojan Horses for the metastasis of Staphylococcus aureus? *Nature Reviews Microbiology* **9**, 215, doi:10.1038/nrmicro2508 (2011).

180 Sandberg, A., Hessler, J. H. R., Skov, R. L., Blom, J. & Frimodt-Møller, N. Intracellular Activity of Antibiotics against *Staphylococcus aureus* in a Mouse Peritonitis Model. *Antimicrobial Agents and Chemotherapy* **53**, 1874-1883, doi:10.1128/aac.01605-07 (2009).

181 Gresham, H. D. *et al.* Survival of *Staphylococcus aureus* Inside Neutrophils Contributes to Infection. *The Journal of Immunology* **164**, 3713-3722, doi:10.4049/jimmunol.164.7.3713 (2000).

182 Lehar, S. M. *et al.* Novel antibody–antibiotic conjugate eliminates intracellular S. aureus. *Nature* **527**, 323, doi:10.1038/nature16057 (2015).

183 Barcia-Macay, M., Seral, C., Mingeot-Leclercq, M.-P., Tulkens, P. M. & Van Bambeke, F. Pharmacodynamic evaluation of the intracellular activities of antibiotics against Staphylococcus aureus in a model of THP-1 macrophages. *Antimicrobial agents and chemotherapy* **50**, 841-851, doi:10.1128/AAC.50.3.841-851.2006 (2006).

184 Xiong, M.-H. *et al.* Bacteria-Responsive Multifunctional Nanogel for Targeted Antibiotic Delivery. *Advanced Materials* **24**, 6175-6180, doi:doi:10.1002/adma.201202847 (2012).

185 O'Connell, K. M. G. *et al.* Combating Multidrug-Resistant Bacteria: Current Strategies for the Discovery of Novel Antibacterials. *Angewandte Chemie International Edition* **52**, 10706-10733, doi:doi:10.1002/anie.201209979 (2013).

186 Larocque, E. A., Naganna, N., Opoku-Temeng, C., Lambrecht, A. M. & Sintim, H. O. Alkynylnicotinamide-Based Compounds as ABL1 Inhibitors with Potent Activities against Drug-Resistant CML Harboring ABL1(T315I) Mutant Kinase. *ChemMedChem* **13**, 1172-1180, doi:doi:10.1002/cmdc.201700829 (2018).

187 Larocque, E. *et al.* Aminoisoquinoline benzamides, FLT3 and Src-family kinase inhibitors, potently inhibit proliferation of acute myeloid leukemia cell lines. *Future medicinal chemistry* **9**, 1213-1225, doi:10.4155/fmc-2017-0067 (2017).

188 Ma, X. *et al.* Identification of New FLT3 Inhibitors That Potently Inhibit AML Cell Lines via an Azo Click-It/Staple-It Approach. *ACS Medicinal Chemistry Letters* **8**, 492-497, doi:10.1021/acsmedchemlett.6b00468 (2017).

189 Scott, J. D. & Williams, R. M. Chemistry and Biology of the Tetrahydroisoquinoline Antitumor Antibiotics. *Chemical Reviews* **102**, 1669-1730, doi:10.1021/cr010212u (2002).

190 Galán, A. *et al.* Novel isoquinoline derivatives as antimicrobial agents. *Bioorganic & Medicinal Chemistry* **21**, 3221-3230, doi:https://doi.org/10.1016/j.bmc.2013.03.042 (2013).

191 Panchaud, P. *et al.* Discovery and Optimization of Isoquinoline Ethyl Ureas as Antibacterial Agents. *Journal of Medicinal Chemistry* **60**, 3755-3775, doi:10.1021/acs.jmedchem.6b01834 (2017).

192 Wiegand, I., Hilpert, K. & Hancock, R. E. W. Agar and broth dilution methods to determine the minimal inhibitory concentration (MIC) of antimicrobial substances. *Nature Protocols* **3**, 163-175, doi:10.1038/nprot.2007.521 (2008).

193 Elsebaei, M. M. *et al.* Alkynyl-containing phenylthiazoles: Systemically active antibacterial agents effective against methicillin-resistant Staphylococcus aureus (MRSA). *European Journal of Medicinal Chemistry* **148**, 195-209, doi:10.1016/j.ejmech.2018.02.031 (2018).

194 Hagras, M. *et al.* Naphthylthiazoles: Targeting Multidrug-Resistant and Intracellular Staphylococcus aureus with Biofilm Disruption Activity. *ACS Infectious Diseases* **4**, 1679-1691, doi:10.1021/acsinfecdis.8b00172 (2018).

195 Singh, M. P. *et al.* Mannopeptimycins, new cyclic glycopeptide antibiotics produced by Streptomyces hygroscopicus LL-AC98: antibacterial and mechanistic activities. *Antimicrobial agents and chemotherapy* **47**, 62-69, doi:10.1128/aac.47.1.62-69.2003 (2003).

196 Opoku-Temeng, C., Onyedibe, K. I., Aryal, U. K. & Sintim, H. O. Proteomic analysis of bacterial response to a 4-hydroxybenzylidene indolinone compound, which re-sensitizes bacteria to traditional antibiotics. *Journal of Proteomics* **202**, 103368, doi:https://doi.org/10.1016/j.jprot.2019.04.018 (2019).

197 Pérez, A. *et al.* Involvement of the AcrAB-TolC Efflux Pump in the Resistance, Fitness, and Virulence of *Enterobacter cloacae*. *Antimicrobial Agents and Chemotherapy* **56**, 2084-2090, doi:10.1128/aac.05509-11 (2012).

198 Tyagi, P., Singh, M., Kumari, H., Kumari, A. & Mukhopadhyay, K. Bactericidal Activity of Curcumin I Is Associated with Damaging of Bacterial Membrane. *PLoS One* **10**, e0121313, doi:10.1371/journal.pone.0121313 (2015).

199 Silverman, J. A., Perlmutter, N. G. & Shapiro, H. M. Correlation of daptomycin bactericidal activity and membrane depolarization in Staphylococcus aureus. *Antimicrobial agents and chemotherapy* **47**, 2538-2544, doi:10.1128/aac.47.8.2538-2544.2003 (2003).

200 Heeb, S. *et al.* Quinolones: from antibiotics to autoinducers. *Fems Microbiology Reviews* **35**, 247-274, doi:10.1111/j.1574-6976.2010.00247.x (2011).

201 Gade, N. D. & Qazi, M. S. Fluoroquinolone Therapy in Staphylococcus aureus Infections: Where Do We Stand? *Journal of Laboratory Physicians* **5**, 109-112, doi:10.4103/0974-2727.119862 (2013).

202 Joshi, S., Mumtaz, S., Singh, J., Pasha, S. & Mukhopadhyay, K. Novel Miniature Membrane Active Lipopeptidomimetics against Planktonic and Biofilm Embedded Methicillin-Resistant Staphylococcus aureus. *Scientific Reports* **8**, 1021, doi:10.1038/s41598-017-17234-z (2018).

203 Garmory, H. S. & Titball, R. W. ATP-binding cassette transporters are targets for the development of antibacterial vaccines and therapies. *Infection and immunity* **72**, 6757-6763, doi:10.1128/iai.72.12.6757-6763.2004 (2004).

204 Gründling, A. Potassium Uptake Systems in *Staphylococcus aureus*: New Stories about Ancient Systems. *mBio* **4**, e00784-00713, doi:10.1128/mBio.00784-13 (2013).

205 Vermassen, A. *et al.* Cell Wall Hydrolases in Bacteria: Insight on the Diversity of Cell Wall Amidases, Glycosidases and Peptidases Toward Peptidoglycan. *Frontiers in Microbiology* **10**, doi:10.3389/fmicb.2019.00331 (2019).

206 Connelly, J. C., Kirkham, L. A. & Leach, D. R. F. The SbcCD nuclease of *Escherichia coli* is a structural maintenance of chromosomes (SMC) family protein that cleaves hairpin DNA. *Proceedings of the National Academy of Sciences* **95**, 7969-7974, doi:10.1073/pnas.95.14.7969 (1998).

207 Fowler, R. G. & Schaaper, R. M. The role of the mutT gene of Escherichia coli in maintaining replication fidelity. *FEMS Microbiology Reviews* **21**, 43-54, doi:10.1111/j.1574-6976.1997.tb00344.x (1997).

208 Ho, H. N., van Oijen, A. M. & Ghodke, H. The transcription-repair coupling factor Mfd associates with RNA polymerase in the absence of exogenous damage. *Nature Communications* **9**, 1570, doi:10.1038/s41467-018-03790-z (2018).

209 Deaconescu, A. M., Savery, N. & Darst, S. A. The bacterial transcription repair coupling factor. *Current opinion in structural biology* **17**, 96-102, doi:10.1016/j.sbi.2007.01.005 (2007).

210 Gregersen, L. H. & Svejstrup, J. Q. The Cellular Response to Transcription-Blocking DNA Damage. *Trends Biochem Sci* **43**, 327-341, doi:10.1016/j.tibs.2018.02.010 (2018).

211 Elmwall, J. *et al.* Galectin-3 Is a Target for Proteases Involved in the Virulence of *Staphylococcus aureus*. *Infection and Immunity* **85**, e00177-00117, doi:10.1128/IAI.00177-17 (2017).

212 Lee, L. Y. *et al.* The Staphylococcus aureus Map protein is an immunomodulator that interferes with T cell-mediated responses. *J Clin Invest* **110**, 1461-1471, doi:10.1172/JCI16318 (2002).

213 Smagur, J. *et al.* A new pathway of staphylococcal pathogenesis: apoptosis-like death induced by Staphopain B in human neutrophils and monocytes. *J Innate Immun* **1**, 98-108, doi:10.1159/000181014 (2009).

214 Nilsson, I. M., Hartford, O., Foster, T. & Tarkowski, A. Alpha-toxin and gamma-toxin jointly promote Staphylococcus aureus virulence in murine septic arthritis. *Infection and immunity* **67**, 1045-1049, doi:10.1128/IAI.67.3.1045-1049.1999 (1999).

215 Bouza, E. & Muñoz, P. MONOTHERAPY VERSUS COMBINATION THERAPY FOR BACTERIAL INFECTIONS. *Medical Clinics of North America* **84**, 1357-1389, doi:https://doi.org/10.1016/S0025-7125(05)70293-5 (2000).

216 Orhan, G., Bayram, A., Zer, Y. & Balci, I. Synergy Tests by E Test and Checkerboard Methods of Antimicrobial Combinations against Brucella melitensis. *Journal of Clinical Microbiology* **43**, 140-143, doi:10.1128/jcm.43.1.140-143.2005 (2005).

217 Davies, Bryan W., Bogard, Ryan W., Young, Travis S. & Mekalanos, John J. Coordinated Regulation of Accessory Genetic Elements Produces Cyclic Di-Nucleotides for *V. cholerae* Virulence. *Cell* **149**, 358-370, doi:10.1016/j.cell.2012.01.053 (2012).

218 Ablasser, A. *et al.* cGAS produces a 2′-5′-linked cyclic dinucleotide second messenger that activates STING. *Nature* **498**, 380-384, doi:10.1038/nature12306 (2013).

219 Sun, L., Wu, J., Du, F., Chen, X. & Chen, Z. J. Cyclic GMP-AMP Synthase Is a Cytosolic DNA Sensor That Activates the Type I Interferon Pathway. *Science* **339**, 786, doi:10.1126/science.1232458 (2013).

220 Danilchanka, O. & Mekalanos, John J. Cyclic Dinucleotides and the Innate Immune Response. *Cell* **154**, 962-970, doi:10.1016/j.cell.2013.08.014 (2013).

221 Opoku-Temeng, C. & Sintim, H. O. Inhibition of cyclic diadenylate cyclase, DisA, by polyphenols. *Scientific Reports* **6**, 25445, doi:10.1038/srep25445 https://www.nature.com/articles/srep25445#supplementary-information (2016).

222 Corrigan, R. M. *et al.* Systematic identification of conserved bacterial c-di-AMP receptor proteins. *Proc. Natl. Acad. Sci. U. S. A.* **110**, 9084-9089, doi:10.1073/pnas.1300595110 (2013).

223 Quach, D. *et al.* The CiaR Response Regulator in Group B Streptococcus Promotes Intracellular Survival and Resistance to Innate Immune Defenses. *Journal of Bacteriology* **191**, 2023, doi:10.1128/JB.01216-08 (2009).

224 Eaglesham, J. B., Pan, Y., Kupper, T. S. & Kranzusch, P. J. Viral and metazoan poxins are cGAMP-specific nucleases that restrict cGAS–STING signalling. *Nature* **566**, 259-263, doi:10.1038/s41586-019-0928-6 (2019).

225 de Cheffoy de Courcelles, D., de Loore, K., Freyne, E. & Janssen, P. A. Inhibition of human cardiac cyclic AMP-phosphodiesterases by R 80122, a new selective cyclic AMP-phosphodiesterase III inhibitor: a comparison with other cardiotonic compounds. *Journal of Pharmacology and Experimental Therapeutics* **263**, 6 (1992).

226 Man, H.-W. *et al.* Discovery of (S)-N-{2-[1-(3-Ethoxy-4-methoxyphenyl)-2-methanesulfonylethyl]-1,3-dioxo-2,3-dihydro-1H-isoindol-4-yl}acetamide (Apremilast), a Potent and Orally Active Phosphodiesterase 4 and Tumor Necrosis Factor-α Inhibitor. *Journal of Medicinal Chemistry* **52**, 1522-1524, doi:10.1021/jm900210d (2009).

227 Wang, Z. *et al.* The selectivity and potency of the new PDE5 inhibitor TPN729MA. *The journal of sexual medicine* **10**, 2790-2797, doi:10.1111/jsm.12285 (2013).

228 Grauer, S. M. *et al.* Phosphodiesterase 10A Inhibitor Activity in Preclinical Models of the Positive, Cognitive, and Negative Symptoms of Schizophrenia. *Journal of Pharmacology and Experimental Therapeutics* **331**, 574, doi:10.1124/jpet.109.155994 (2009).

229 Kawaguchi, M. *et al.* Development of an ENPP1 Fluorescence Probe for Inhibitor Screening, Cellular Imaging, and Prognostic Assessment of Malignant Breast Cancer. *Journal of Medicinal Chemistry* **62**, 9254-9269, doi:10.1021/acs.jmedchem.9b01213 (2019).

230 *Microbial Cyclic Di-Nucleotide Signaling*. (Springer, 2020).

231 Rao, F. *et al.* YybT is a signaling protein that contains a cyclic dinucleotide phosphodiesterase domain and a GGDEF domain with ATPase activity. *The Journal of biological chemistry* **285**, 473-482, doi:10.1074/jbc.M109.040238 (2010).

232 Rao, F., Yang, Y., Qi, Y. & Liang, Z.-X. Catalytic Mechanism of Cyclic Di-GMP-Specific Phosphodiesterase: a Study of the EAL Domain-Containing RocR from;*Pseudomonas aeruginosa*. *Journal of Bacteriology* **190**, 3622, doi:10.1128/JB.00165-08 (2008).

233 Zhou, J., Sayre, D. A., Zheng, Y., Szmacinski, H. & Sintim, H. O. Unexpected Complex Formation between Coralyne and Cyclic Diadenosine Monophosphate Providing a Simple Fluorescent Turn-on Assay to Detect This Bacterial Second Messenger. *Analytical Chemistry* **86**, 2412-2420, doi:10.1021/ac403203x (2014).

234 Zhang, J.-H., Chung, T. D. Y. & Oldenburg, K. R. A Simple Statistical Parameter for Use in Evaluation and Validation of High Throughput Screening Assays. *Journal of Biomolecular Screening* **4**, 67-73, doi:10.1177/108705719900400206 (1999).

235 Dey, R. J. *et al.* Inhibition of innate immune cytosolic surveillance by an M. tuberculosis phosphodiesterase. *Nature Chemical Biology* **13**, 210, doi:10.1038/nchembio.2254 https://www.nature.com/articles/nchembio.2254#supplementary-information (2016).

236 Yammine, A., Gao, J. & Kwan, A. H. Tryptophan Fluorescence Quenching Assays for Measuring Protein-ligand Binding Affinities: Principles and a Practical Guide. *Bio-protocol* **9**, e3253, doi:10.21769/BioProtoc.3253 (2019).

237 Rao, F. *et al.* YybT Is a Signaling Protein That Contains a Cyclic Dinucleotide Phosphodiesterase Domain and a GGDEF Domain with ATPase Activity. *Journal of Biological Chemistry* **285**, 473-482, doi:10.1074/jbc.M109.040238 (2010).

238 Kulesekara, H. *et al.* Analysis of *Pseudomonas aeruginos*a diguanylate cyclases and phosphodiesterases reveals a role for bis-(3′-5′)-cyclic-GMP in virulence. *Proc. Natl. Acad. Sci. U. S. A.* **103**, 2839-2844, doi:10.1073/pnas.0511090103 (2006).

239 Jenal, U., Reinders, A. & Lori, C. Cyclic di-GMP: second messenger extraordinaire. *Nature Reviews Microbiology* **15**, 271-284, doi:10.1038/nrmicro.2016.190 (2017).

240 Li, T. & Chen, Z. J. The cGAS-cGAMP-STING pathway connects DNA damage to inflammation, senescence, and cancer. *The Journal of experimental medicine* **215**, 1287-1299, doi:10.1084/jem.20180139 (2018).

241 Ishikawa, H. & Barber, G. N. STING is an endoplasmic reticulum adaptor that facilitates innate immune signalling. *Nature* **455**, 674-678, doi:10.1038/nature07317 (2008).

242 Ishikawa, H., Ma, Z. & Barber, G. N. STING regulates intracellular DNA-mediated, type I interferon-dependent innate immunity. *Nature* **461**, 788-792, doi:10.1038/nature08476 (2009).

243 Sintim, H. O., Mikek, C. G., Wang, M. & Sooreshjani, M. A. Interrupting cyclic dinucleotide-cGAS–STING axis with small molecules. *MedChemComm* **10**, 1999-2023, doi:10.1039/C8MD00555A (2019).

244 Morehouse, B. R. *et al.* STING cyclic dinucleotide sensing originated in bacteria. *Nature*, doi:10.1038/s41586-020-2719-5 (2020).

245 Sun, L., Wu, J., Du, F., Chen, X. & Chen, Z. J. Cyclic GMP-AMP synthase is a cytosolic DNA sensor that activates the type I interferon pathway. *Science (New York, N.Y.)* **339**, 786-791, doi:10.1126/science.1232458 (2013).

246 Kato, K., Omura, H., Ishitani, R. & Nureki, O. Cyclic GMP-AMP as an Endogenous Second Messenger in Innate Immune Signaling by Cytosolic DNA. *Annual review of biochemistry* **86**, 541-566, doi:10.1146/annurev-biochem-061516-044813 (2017).

247 Du, M. & Chen, Z. J. DNA-induced liquid phase condensation of cGAS activates innate immune signaling. *Science*, eaat1022, doi:10.1126/science.aat1022 (2018).

248 Gao, P. *et al.* Structure-Function Analysis of STING Activation by c[G(2',5')pA(3',5')p] and Targeting by Antiviral DMXAA. *Cell* **154**, 748-762, doi:10.1016/j.cell.2013.07.023 (2013).

249 Zhang, X. *et al.* Cyclic GMP-AMP containing mixed phosphodiester linkages is an endogenous high-affinity ligand for STING. *Mol Cell* **51**, 226-235, doi:10.1016/j.molcel.2013.05.022 (2013).

250 Shang, G., Zhang, C., Chen, Z. J., Bai, X.-c. & Zhang, X. Cryo-EM structures of STING reveal its mechanism of activation by cyclic GMP–AMP. *Nature* **567**, 389-393, doi:10.1038/s41586-019-0998-5 (2019).

251 Ergun, S. L., Fernandez, D., Weiss, T. M. & Li, L. STING Polymer Structure Reveals Mechanisms for Activation, Hyperactivation, and Inhibition. *Cell* **178**, 290-301.e210, doi:https://doi.org/10.1016/j.cell.2019.05.036 (2019).

252 Tanaka, Y. & Chen, Z. J. STING Specifies IRF3 Phosphorylation by TBK1 in the Cytosolic DNA Signaling Pathway. *Science Signaling* **5**, ra20, doi:10.1126/scisignal.2002521 (2012).

253 Konno, H., Konno, K. & Barber, G. N. Cyclic dinucleotides trigger ULK1 (ATG1) phosphorylation of STING to prevent sustained innate immune signaling. *Cell* **155**, 688-698, doi:10.1016/j.cell.2013.09.049 (2013).

254 Zhang, Y. *et al.* The DNA sensor, cyclic GMP-AMP synthase, is essential for induction of IFN-β during Chlamydia trachomatis infection. *Journal of immunology (Baltimore, Md. : 1950)* **193**, 2394-2404, doi:10.4049/jimmunol.1302718 (2014).

255 Li, X. D. *et al.* Pivotal roles of cGAS-cGAMP signaling in antiviral defense and immune adjuvant effects. *Science* **341**, 1390-1394, doi:10.1126/science.1244040 (2013).

256 Hansen, K. *et al.* Listeria monocytogenes induces IFNβ expression through an IFI16-, cGAS- and STING-dependent pathway. *The EMBO journal* **33**, 1654-1666, doi:10.15252/embj.201488029 (2014).

257 Woo, S.-R. *et al.* STING-Dependent Cytosolic DNA Sensing Mediates Innate Immune Recognition of Immunogenic Tumors. *Immunity* **41**, 830-842, doi:https://doi.org/10.1016/j.immuni.2014.10.017 (2014).

258 Carozza, J. A. *et al.* Extracellular cGAMP is a cancer-cell-produced immunotransmitter involved in radiation-induced anticancer immunity. *Nature Cancer* **1**, 184-196, doi:10.1038/s43018-020-0028-4 (2020).

259 Crow, Y. J. *et al.* Mutations in the gene encoding the 3′-5′ DNA exonuclease TREX1 cause Aicardi-Goutières syndrome at the AGS1 locus. *Nature Genetics* **38**, 917-920, doi:10.1038/ng1845 (2006).

260 Lee-Kirsch, M. A. *et al.* Mutations in the gene encoding the 3′-5′ DNA exonuclease TREX1 are associated with systemic lupus erythematosus. *Nature Genetics* **39**, 1065-1067, doi:10.1038/ng2091 (2007).

261 Wang, M., Sooreshjani, M. A., Mikek, C., Opoku-Temeng, C. & Sintim, H. O. Suramin potently inhibits cGAMP synthase, cGAS, in THP1 cells to modulate IFN-β levels. *Future Med Chem* **10**, 1301-1317, doi:10.4155/fmc-2017-0322 (2018).

262 Lama, L. *et al.* Development of human cGAS-specific small-molecule inhibitors for repression of dsDNA-triggered interferon expression. *Nature Communications* **10**, 2261, doi:10.1038/s41467-019-08620-4 (2019).

263 Kato, K. *et al.* Structural insights into cGAMP degradation by Ecto-nucleotide pyrophosphatase phosphodiesterase 1. *Nature Communications* **9**, 4424, doi:10.1038/s41467-018-06922-7 (2018).

264 Stülke, J. & Krüger, L. Cyclic di-AMP Signaling in Bacteria. *Annual Review of Microbiology* **74**, 159-179, doi:10.1146/annurev-micro-020518-115943 (2020).

265 Sintim, H. O. & Opoku-Temeng, C. in *Microbial Cyclic Di-Nucleotide Signaling* (eds Shan-Ho Chou, Nicolas Guiliani, Vincent T. Lee, & Ute Römling) 577-591 (Springer International Publishing, 2020).

266 Li, L. *et al.* Hydrolysis of 2'3'-cGAMP by ENPP1 and design of nonhydrolyzable analogs. *Nat Chem Biol* **10**, 1043-1048, doi:10.1038/nchembio.1661 (2014).

267 Bose, D., Su, Y., Marcus, A., Raulet, D. H. & Hammond, M. C. An RNA-Based Fluorescent Biosensor for High-Throughput Analysis of the cGAS-cGAMP-STING Pathway. *Cell Chemical Biology* **23**, 1539-1549, doi:https://doi.org/10.1016/j.chembiol.2016.10.014 (2016).

268 Kellenberger, C. A., Wilson, S. C., Sales-Lee, J. & Hammond, M. C. RNA-Based Fluorescent Biosensors for Live Cell Imaging of Second Messengers Cyclic di-GMP and Cyclic AMP-GMP. *Journal of the American Chemical Society* **135**, 4906-4909, doi:10.1021/ja311960g (2013).

269 Nakayama, S., Luo, Y., Zhou, J., Dayie, T. K. & Sintim, H. O. Nanomolar fluorescent detection of c-di-GMP using a modular aptamer strategy. *Chemical Communications* **48**, 9059-9061, doi:10.1039/C2CC34379G (2012).

270 Hooy, R. & Sohn, J. in *Methods in Enzymology* Vol. 625 (ed Jungsan Sohn) 77-86 (Academic Press, 2019).

271 Mardjuki, R. E., Carozza, J. A. & Li, L. Development of cGAMP-Luc, a sensitive and precise coupled enzyme assay to measure cGAMP in complex biological samples. *Journal of Biological Chemistry* (2020).

272 Pollock, A. J., Zaver, S. A. & Woodward, J. J. A STING-based biosensor affords broad cyclic dinucleotide detection within single living eukaryotic cells. *Nature Communications* **11**, 3533, doi:10.1038/s41467-020-17228-y (2020).

273 Nakayama, S. *et al.* Thiazole Orange-Induced c-di-GMP Quadruplex Formation Facilitates a Simple Fluorescent Detection of This Ubiquitous Biofilm Regulating Molecule. *Journal of the American Chemical Society* **133**, 4856-4864, doi:10.1021/ja1091062 (2011).

274 Shu, C., Yi, G., Watts, T., Kao, C. C. & Li, P. Structure of STING bound to cyclic di-GMP reveals the mechanism of cyclic dinucleotide recognition by the immune system. *Nature Structural & Molecular Biology* **19**, 722-724, doi:10.1038/nsmb.2331 (2012).

275 Witte, G., Hartung, S., Büttner, K. & Hopfner, K.-P. Structural Biochemistry of a Bacterial Checkpoint Protein Reveals Diadenylate Cyclase Activity Regulated by DNA Recombination Intermediates. *Mol Cell* **30**, 167-178, doi:10.1016/j.molcel.2008.02.020 (2008).

276 Sultan, S. Z., Pitzer, J. E., Miller, M. R. & Motaleb, M. A. Analysis of a Borrelia burgdorferi phosphodiesterase demonstrates a role for cyclic-di-guanosine monophosphate in motility and virulence. *Molecular Microbiology* **77**, 128-142, doi:10.1111/j.1365-2958.2010.07191.x (2010).

277 Rossi, A. M. & Taylor, C. W. Analysis of protein-ligand interactions by fluorescence polarization. *Nature Protocols* **6**, 365-387, doi:10.1038/nprot.2011.305 (2011).

278 Jameson, D. M. & Mocz, G. in *Protein-Ligand Interactions: Methods and Applications* (ed G. Ulrich Nienhaus) 301-322 (Humana Press, 2005).

279 Moerke, N. J. Fluorescence Polarization (FP) Assays for Monitoring Peptide-Protein or Nucleic Acid-Protein Binding. *Current Protocols in Chemical Biology* **1**, 1-15, doi:10.1002/9780470559277.ch090102 (2009).

280 Hall, J. *et al.* Discovery of PF-06928215 as a high affinity inhibitor of cGAS enabled by a novel fluorescence polarization assay. *PLoS One* **12**, e0184843, doi:10.1371/journal.pone.0184843 (2017).

281 Shi, H., Wu, J., Chen, Z. J. & Chen, C. Molecular basis for the specific recognition of the metazoan cyclic GMP-AMP by the innate immune adaptor protein STING. *Proceedings of the National Academy of Sciences* **112**, 8947, doi:10.1073/pnas.1507317112 (2015).

282 Yin, Q. *et al.* Cyclic di-GMP Sensing via the Innate Immune Signaling Protein STING. *Mol Cell* **46**, 735-745, doi:https://doi.org/10.1016/j.molcel.2012.05.029 (2012).

283 Guo, J. *et al.* Distinct Dynamic and Conformational Features of Human STING in Response to 2'3'-cGAMP and c-di-GMP. *Chembiochem* **20**, 1838-1847, doi:10.1002/cbic.201900051 (2019).

284 Wu, J.-J. *et al.* Targeting STING with cyclic di-GMP greatly augmented immune responses of glycopeptide cancer vaccines. *Chemical Communications* **54**, 9655-9658, doi:10.1039/C8CC04860F (2018).

285 Lakowicz, J. R. in *Principles of Fluorescence Spectroscopy* (ed Joseph R. Lakowicz) 291-319 (Springer US, 1999).

286 Roehrl, M. H. A., Wang, J. Y. & Wagner, G. A General Framework for Development and Data Analysis of Competitive High-Throughput Screens for Small-Molecule Inhibitors of Protein−Protein Interactions by Fluorescence Polarization. *Biochemistry* **43**, 16056-16066, doi:10.1021/bi048233g (2004).

287 Jing, M. & Bowser, M. T. Methods for measuring aptamer-protein equilibria: A review. *Analytica Chimica Acta* **686**, 9-18, doi:https://doi.org/10.1016/j.aca.2010.10.032 (2011).

288 Soller, K. J., Yang, J., Veglia, G. & Bowser, M. T. Reversal of Phospholamban Inhibition of the Sarco(endo)plasmic Reticulum Ca2+-ATPase (SERCA) Using Short, Protein-interacting RNAs and Oligonucleotide Analogs. *Journal of Biological Chemistry* **291**, 21510-21518 (2016).

289 Mao, H. *et al.* The mechanism and regularity of quenching the effect of bases on fluorophores: the base-quenched probe method. *Analyst* **143**, 3292-3301, doi:10.1039/C8AN00116B (2018).

290 Hickman, J. W., Tifrea, D. F. & Harwood, C. S. A chemosensory system that regulates biofilm formation through modulation of cyclic diguanylate levels. *Proc. Natl. Acad. Sci. U. S. A.* **102**, 14422, doi:10.1073/pnas.0507170102 (2005).

291 Kalia, D. *et al.* Nucleotide, c-di-GMP, c-di-AMP, cGMP, cAMP, (p)ppGpp signaling in bacteria and implications in pathogenesis. *Chem Soc Rev* **42**, 305-341, doi:10.1039/c2cs35206k (2013).

292 Kellenberger, C. A., Chen, C., Whiteley, A. T., Portnoy, D. A. & Hammond, M. C. RNA-Based Fluorescent Biosensors for Live Cell Imaging of Second Messenger Cyclic di-AMP. *Journal of the American Chemical Society* **137**, 6432-6435, doi:10.1021/jacs.5b00275 (2015).

293 Roembke, B. T. *et al.* A cyclic dinucleotide containing 2-aminopurine is a general fluorescent sensor for c-di-GMP and 3',3'-cGAMP. *Molecular bioSystems* **10**, 1568-1575, doi:10.1039/c3mb70518h (2014).

294 Tseng, W.-B., Lu, Y.-T., Zhan, S.-W. & Tseng, W.-L. Self-assembly of c-di-GMP, Tb3+, and Ag+ into high-quantum-yield coordination polymer nanoparticles: Mechanism discussion and application as a c-di-GMP sensor. *Sensors and Actuators B: Chemical* **312**, 127960, doi:https://doi.org/10.1016/j.snb.2020.127960 (2020).

295 Inuzuka, S., Matsumura, S. & Ikawa, Y. Optimization of RNA-based c-di-GMP fluorescent sensors through tuning their structural modules. *Journal of Bioscience and Bioengineering* **122**, 183-187, doi:https://doi.org/10.1016/j.jbiosc.2016.01.011 (2016).

296 Kellenberger, C. A. *et al.* A minimalist biosensor: Quantitation of cyclic di-GMP using the conformational change of a riboswitch aptamer. *RNA Biol* **12**, 1189-1197, doi:10.1080/15476286.2015.1062970 (2015).